Technische Universität München

Fakultät für Chemie

Institut für Wasserchemie und Chemische Balneologie

Lehrstuhl für Analytische Chemie und Wasserchemie

Integration of 3D microfluidic platform with gold nanoparticle-catalyzed chemiluminescence analysis system

Yanwei Wang

Vollständiger Abdruck der von der Fakultät für Chemie der Technischen Universität München zu Erlangung des akademischen Grades eines

Doktors der Naturwissenschaften (Dr. rer. nat.)

genehmigten Dissertation.

Vorsitzender:	Prof. Dr. Martin Elsner
Prüfer der Dissertation:	1. Priv.-Doz. Dr. Michael Seidel
	2. Prof. Dr. Angela Casini

Die Dissertation wurde am 12.07.2021 bei der Technischen Universität München eingereicht und durch die Fakultät für Chemie am 13.09.2021 angenommen.

Less is More

Acknowledgments

This thesis is based on research conducted at the Institute of Hydrochemistry, Chair of Analytical Chemistry and Water Chemistry, Technical University of Munich from August 2018 to August 2021, funded by the China Scholarship Council (CSC). I would like to give my gratitude to everyone who helped me during my doctoral project, directly or indirectly. Without their kind help, it would have been impossible to complete this thesis.

First of all, I would like to express my heartfelt thanks to PD. Dr. Michael Seidel for the helpful supervision. This thesis could not be completed without his patient guidance. He gave me great guidance and encouragement in the process of project conceptualization, manuscript review, and experimentation. It is my pleasure to work and study under his supervision.

I would also like to thank all colleagues of the Institute for the kind academic environment. Special thanks to the past and present colleagues of the Bioanalytics and Microanalytical Systems Group. I appreciate Jonas Bemetz for the Matlab programming and building synthesis setup. It offered infrastructure for my project. Many thanks to Katharina Sollweck for her linguistic assistance and helpful suggestions during my manuscripts' preparation, and encouragement during my experiments. Thanks to Julia Neumair and Gerhard Schwaiger for their comments and revision in preparing this thesis. Thanks for valuable discussions on the experiments and data evaluation from my kind colleagues in coffee meetings and institute seminars. Also, thanks for their friendship and patience, which make my life better in Munich. Moreover, special thanks to Roland Hoppe from the workshop for the fabrication of the PMMA carrier and many thanks to Christine Benning for her kindness in scanning electron microscopy characterization.

Finally, I am very grateful to my parents for understanding that I stayed abroad and cannot accompany them. Thanks to my friends who share my anxiety, depression, and happiness. I am also thankful for the kindness of the people around me. Without them, I would not be able to keep fighting for three years.

Publications

Journal papers

Wang, Y.; Seidel, M., Integration of 3D hydrodynamic focused microreactor with microfluidic chemiluminescence sensing for online synthesis and catalytical characterization of gold nanoparticles. *Sensors* 2021, 21 (7). DOI :10.3390/s21072290.

Wang, Y.; Seidel, M., Strategy for fast manufacturing of 3D hydrodynamic focusing multilayer microfluidic chips and its application for flow-based synthesis of gold nanoparticles. *Microfluidics and Nanofluidics* 2021, 25(8). DOI : 10.1007/s10404-021-02463-6.

Wang, Y.; Rink, S.; Baeumner, A.; Seidel, M., 3D microfluidic flow-injection platform with m-carboxy luminol enhanced chemiluminescence for highly sensitive aptamer-based homogeneous assays. *Microchimica Acta* 2021, under review.

Conference papers

Wang, Y.; Seidel, M., Synthesis of gold nanoparticles in a 3D hydrodynamic focused microreactor and their application for online chemiluminescence. *In 3rd European BioSensor Symposium*, Wildau, Germany, 2021.

Table of contents

Summary

Microfluidic platforms have been more and more important in the research field of analytical chemistry. 3D microfluidic chips are usually applied to make microfluidic platforms versatile and solve problems such as fouling and not sufficient space. However, the fabrication of such 3D microfluidic chips is usually costly and tedious. This dissertation aims to develop a microfluidic platform based on laminated layers of microfluidic chips for analytical application, including fabrication of microfluidic chips, online synthesis and characterization, and detection of analytes in the microfluidic chip. To the end (i) a strategy was established for the rapid and effective fabrication of 3D microfluidic chips. The laminated 3D microreactor was successfully applied for the online-synthesis of gold nanoparticles (AuNPs); (ii) the synthesis of AuNPs in a 3D microreactor was directly coupled online with a chemiluminescence (CL) detection system for characterization of their catalytic activity and optimization of the synthesis parameters; (iii) an aptamer-based homogeneous assay was developed in a laminated 3D micromixer for detection of the antibiotic sulfadimethoxine (SDM) by AuNP-catalyzed CL.

3D microfluidic chips were fabricated in a laminated way that pre-cut polymethyl methacrylate (PMMA) layers simply bound together with double-sided pressure-sensitive adhesive (PSA) layers. The channels in each layer were designed as desired with a drawing software and cut by a cutting plotter. Then, the microfluidic chip was manually assembled with gentle pressure. With this easy method, microfluidic chips can be fabricated in a few minutes from the design concept to the working device. Compared with other methods for fabricating microfluidic chips, no expensive equipment such as laser, thermal lamination, and cleanroom was used. Therefore, it offers a possibility to fabricate complex microfluidic chips quickly, cheaply, and efficiently. This method was successfully applied to fabricate a 3D hydrodynamic focusing microreactor to synthesize AuNPs. The fouling of AuNPs was prevented by the application of a defined sheath flow. Different parameters such as flow rate and concentration of reagents were controlled to achieve AuNPs of various sizes.

For further application of the synthesized AuNPs, they should be characterized. AuNPs have drawn big attention in CL analysis systems as enzyme-free catalysts. However, the optimal synthesized AuNPs for a highly efficient CL reaction was still unknown. Therefore, our second

aim was to couple synthesis and CL characterization to get optimal synthesis parameters. The online synthesis of AuNPs with the 3D hydrodynamic focusing microreactor was coupled to a charge-coupled device (CCD) camera with an inset microfluidic CL sensing chip for direct catalytical characterization of AuNPs. All operations were performed automatically with a program controlled by the software Matlab. AuNPs were synthesized through a single-phase reaction at room temperature. The sizes and properties of AuNPs can be modulated by changing the concentration of the reagents to obtain an optimal catalytic activity in the CL system. The catalyst property of the synthesized AuNPs was characterized in the luminol-NaOCl CL system. After optimizing the parameters of synthesis, the CL signal was enhanced to a factor of 171 compared the one without catalyst. Synthesis in a microreactor and direct coupling with a microfluidic CL sensor offers a promising monitoring method to find the best synthesis conditions of AuNPs with excellent catalytic activity.

The stability of the synthesized AuNPs was checked for further offline application, and they were stable for at least one month. In addition, the effect of aggregation and the surface properties of the AuNPs on catalytic activity was also investigated. Aggregated AuNPs can induce higher CL signal by enhanced catalytic activity, and molecules that interact on the surface of AuNPs may reduce the catalytic activity.

A certain amount of salt can cause aggregation of AuNPs with enhancing the CL signal, and aptamers interact with AuNPs leading to inhibition of the aggregation and resulting in a weak CL signal. Based on this mechanism, a homogeneous aptamer-based assay was developed in a microfluidic CL flow-injection platform with AuNPs as the catalyst for analytical application. As efficient mixing of reagents in a microfluidic platform is crucial, a new laminated 3D microfluidic mixer was developed for the platform. The 3D mixer with five layers was applied because 2D mixers cannot manage effective mixing due to limited space and turbulence. The structure of the 3D mixer was optimized for better mixing and recording of CL signals for the CCD camera. The performance of standard luminol and its more hydrophilic derivative *m*-carboxy luminol provided by the Baeumner group was compared in the developed 3D mixer, identifying the hydrophilic derivative to provide a 10-fold signal enhancement with repeatable results. For more sensitive detection, the *m*-carboxy luminol was applied in the microfluidic CL flow-injection platform. Finally, the novel detection platform was developed in a 3D micromixer with an aptamer, AuNPs, and *m*-carboxy luminol, for the homogeneous assay. SDM was measured in the platform as an

example via its aptamer and yielded a broad dynamic range over 5 orders of magnitude (0.01 - 1000 ng/ml) with a limit of detection of 4 pg/ml. This new detection concept can be suggested as a new flow-injection strategy for aptamer-based rapid and cost-efficient analysis in environmental monitoring and food safety.

General introduction

Microfluidic platform in analytical applications

Many classic macroscopic liquid handling systems (such as in a beaker or test tube) have been used for decades to perform analysis and diagnostic assays. Microfluidic platforms compete with these established systems by providing new advantages. Compared to macroscopic systems, the high surface area to volume ratio was the feature of microfluidic platforms [1]. Normal merits of microfluidic platforms include lower cost per test, shorter time to obtain results, higher sensitivity, and portability. Furthermore, the reagent consumption can be significantly reduced by reducing the volume of the assay. In addition, the steps of each test can be reduced through an automatic process.

One of the main application areas of microfluidic platforms is qualitative or quantitative analysis. The analytes can be various molecules, including proteins, nucleic acids, drugs, and metal ions. The materials for the fabrication of microfluidic platforms should be inert to the samples and measurement reagents that may contain organic or inorganic solvents or extreme pH values. Similarly, the sample must not be affected by the microfluidic materials in any way that might affect the analysis results.

High-precision liquid handling and effective mixing strategies are required to obtain accurate quantitative results. Each microfluidic platform should provide a sufficient number of microfluidic units (microfluidic components of a microfluidic platform) so that a specific analytical application with complex protocols can be easily implemented within a given platform [2]. However, this concept does not mean that every microfluidic platform needs to provide a complete set of all units. The more important thing is that different elements are connectable through a well-defined, readily available interconnection and packaging process. Therefore, at least one manufacturing technology is required to realize a complete microfluidic platform with various components.

The pressure-driven laminar flow platform, whose liquid transport mechanism was based on pressure gradient, was widely used in analytical applications [3]. The external or internal pressure sources can be implemented using syringes, pumps, or gas expansion. Samples and reagents can be injected into the microfluidic platform inlet in batch or continuous mode. One of the advantages of this microfluidic platform is the potential for continuous sample processing. By changing the

flow ratio of each reagent, the concentration of reagents can be adjusted accurately. Continuous sample processing is essential for online monitoring of clinical parameters, water quality control, or cell sorting [4].

The main goal of this thesis is to develop a microfluidic platform on the basis of a laminated method for analytical application, including fabrication of microfluidic chips, online synthesis and characterization, and detection of analytes on the microfluidic chip.

In the following, the state of art and the aim are shown.

Target 1: Online syntheses of gold nanoparticles in 3D hydrodynamic focused laminated microfluidic reactors

Microreactors - state of the art

Conventional batch synthesis methods can produce large-scale nanoparticles at once. However, the lack of control of parameters (local temperature, mixing, concentration fluctuations, nucleation, growth, and reagent addition) during the synthesis process often leads to uneven size distributions in different batches. Therefore, these methods are limited when there is a need for highly specific nanoparticles (size, shape, composition, and distribution) for different applications (such as surface-enhanced Raman scattering and catalyst) [5-7].

Many research groups have used microreactors to achieve a rapid and tunable synthesis of monodisperse nanoparticles [6, 8-10]. Compared with traditional batch synthesis, synthesis methods by microfluidic reactors have the advantage of faster reaction rates and narrower size distribution [6]. The other benefits of a microfluidic reactor are that the small channels reduce the amount of reagents used and limit the formation of by-products. Moreover, it can be automated for multi-step synthesis [11]. The weak point is the fouling (the unwanted deposition on surfaces of microfluidic channels), which is related to the higher surface-to-volume ratio.

Microfluidic reactors can be divided into three different types: continuous single-phase laminar flow reactors [6, 12-14], segmented flow reactors [15], and droplet-based reactors [16]. In single-phase reactors, miscible reagent streams are injected into channels or capillaries where the reagents mix and react (**Figure 0.1 a**). To date, most researchers have focused on single-phase reactors because they have a high degree of synthesis flexibility and can tolerate various flow rates and

solvents. However, two problems limit their performance. First of all, the channel wall creates resistance to the flowing liquid, resulting in a parabolic velocity distribution on the entire flow path. The fluid moves the fastest at the center of the channel, which leads to poor residence time distribution in the reactor. Therefore, it results in different size distributions during synthesis. Secondly, the deposition of precursors and products on the walls can cause fouling, affecting the reactor's flow and reducing the service lifetime of reactors [17].

Two-phase reactors overcome the shortcomings of single-phase reactors with an additional immiscible fluid (which can be a gas or a liquid) injecting into the channel [18]. The reaction mixture was divided into a succession of discrete “slugs” or “droplets” (**Figure 0.1 b** and **c**). Both of them pass through the reactor at the same speed and eliminate the velocity dispersion. Part of the reaction mixture can still contact the channel walls in a slug flow. The deposition can be reduced or eliminated with the help of abrasion from the second phase. The immiscible liquid completely isolates the reaction mixture from the wall and prevents the deposition in the droplet flow. However, there are still problems with two-phase reactors. For example, the second phase could have a potential effect on the nucleation and growth kinetics when it was used for synthesis. Therefore, the final crystal structure of nanoparticles and size distribution can be influenced. Moreover, additional purification is required after synthesis, which further complicates the process.

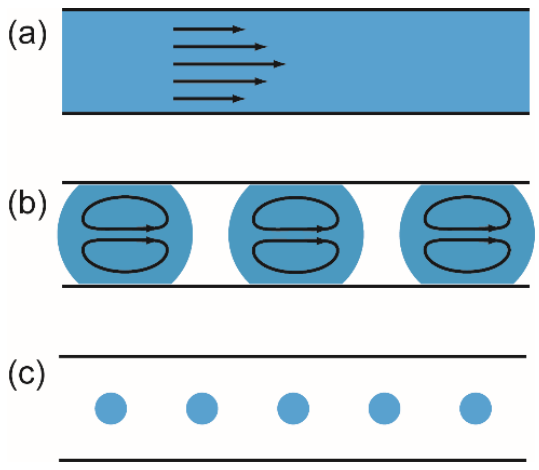

Figure 0.1 Scheme of microfluidic channels with three types of fluid flow: (**a**) single-phase continuous flow with the parabolic velocity of flow; (**b**) segmented flow with discrete units divided by immiscible fluid; (**c**) droplet flow.

Compared to droplet-based technology, hydrodynamic focusing technology, in which the reaction is focused in the center by additional flows, is easy to implement and simulate. The central stream with a lower flow rate is compressed to the center when it flows inside the outer laminar sheath stream with a higher flow rate [19, 20]. This compression can significantly reduce the mixing time, and the required diffusion length can also be reduced [21]. The concentration and ratio of chemical components can be controlled by the relative flow rates, which will determine the nucleation and growth process in the synthesis. When the reaction is focused on the channels' center, the growing nuclei will experience a more uniform reagent concentration. The reason is that the velocity distribution is uniform in the center of the channel, and the reagents can stay in the microchannel for a similar time (**Figure 0.2**). Therefore, due to the uniformity of the fluid velocity, a uniform particle size distribution is produced [22]. In addition, due to the insulation of the sheath solution, fouling is alleviated.

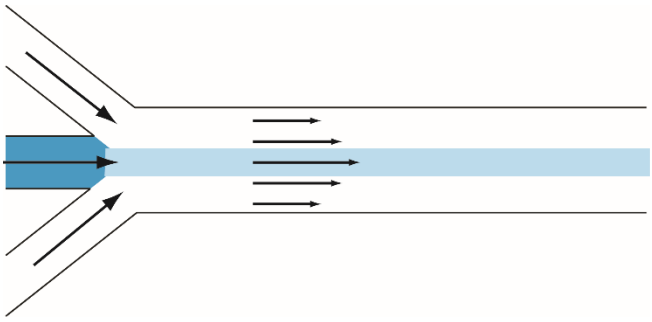

Figure 0.2 Hydrodynamic focusing channel in which the reaction zone is focused to the center of the channel resulting in a more uniform reaction time.

In an ideal fluid focusing device, the central flow should be compressed in both the horizontal and vertical directions, which is called three-dimensional (3D) focusing. The uniform fluid velocity can be obtained on the horizontal and vertical planes. Two reactor types can achieve this effect: a coaxial tube reactor and an on-chip planar reactor. The simplest coaxial tube reactor is a component composed of two concentric tubes. The central flow is injected through the inner capillary tube, and the sheath flow is injected from the outer glass tube (**Figure 0.3 a**) [23]. As there is only one inlet for the sheath flow and one inlet for the central flow, the method can only be applied for two reagents' reactions. Another method to achieve hydrodynamic focusing on the microfluidic system is the use of multiple layers. The middle layer is for the central flow, and the sheath flow can be introduced from the top and bottom or the left and right of the central layer (**Figure 0.3 b**) [20].

The advantage of this method is that different reagents can be used in the sheath solutions as there are usually two inlets for sheath solutions.

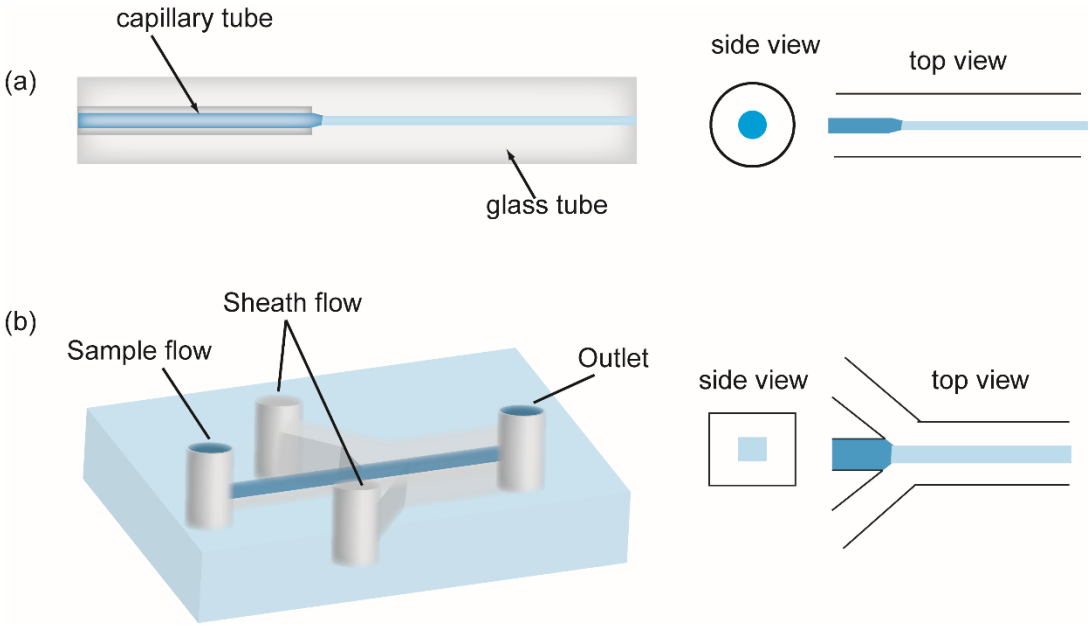

Figure 0.3 (a) Coaxial tube hydrodynamic focusing reactor which is an assembly of two concentric capillary tubes, and **(b)** On-chip planar 3D hydrodynamic focusing devices.

Methods for fabrication of microfluidic chips - state of the art

Glass and silicon wafers were applied as material in the first generation of microfluidic chips with micro-electromechanical technologies. Both materials are fragile and too expensive to be used for disposable devices. Moreover, the fabrication methods are complex and need sophisticated equipment [24]. Most fabrication methods have their limitation for mass production. Therefore, they were mainly used for research applications. The advantage of microfluidic chips with glass and silicon as materials is the high precision of very small microfluidic channels ($\leq$ 100 nm). Moreover, glass and silicon are reliable materials for specific applications under certain extreme test conditions (resistance to organic solvents, high thermostability, resistance to oxidizers) [25]. On the other hand, glass and silicon's hardness also limit their wide application in microfluidic chips as they are not easy to cut and bond. The manufacturing of microfluidic chips involves hazardous chemicals, so protective facilities are required. Also, it is difficult to bind the chips to each other (usually requiring high temperature, high pressure, and ultra-clean environment). The time-consuming experimental manufacturing process, requiring cleanroom facilities and the high

cost of chip manufacturing severely restrict their development. Moreover, since glass or silicon is not gas-permeable and they are difficult to be functionalized by biomolecules, such chips with closed channels are not suitable for cell culture and limit their biological applications.

Polymer-based chips came out a few years after the introduction of silicon/glass chips. A wide variety of polymers with different properties provides more options of suitable materials for microchips. With the advantage of the low-cost, wide range of mechanical and chemical properties, flexibility, and easy processing possibilities, polymers have become attractive microchip materials [26]. Based on their physical properties, polymers can be divided into elastomers, thermosetting plastics, and thermoplastics. The most popular elastomer for the fabrication of microchips is poly(dimethylsiloxane) (PDMS) [27]. The significant advantage of PDMS lies in its ease of processing and low micro-manufacturing costs. The liquid PDMS prepolymer is thermally cured at mild temperatures (40 - 70 °C). Then it is cast in a photoresist template with nanometer resolution. The low surface tension makes it easy to peel off the template after curing. By plasma oxidation of the PDMS surface, it can be easily and irreversibly combined with glass/silicon or another piece of PDMS. Although PDMS is very popular in microfluidic platforms [28, 29], it also has significant limitations. The porous structure of PDMS brings some problems. Small hydrophobic molecules and biomolecules can be absorbed into or on the channel walls, and the concentration of solutions will be changed by water evaporation. Moreover, the incompatibility with organic solvents restricted it in aqueous solutions.

Rather than a microfluidic material, thermosetting materials (such as SU-8) are commonly used as negative photoresists to fabricate photoresist templates [30]. When thermosetting molecules are heated or radiated, they crosslink to form a rigid network that cannot be softened before they decompose. Generally, these materials are resistant to most solvents and stable even at high temperatures. Through appropriate bonding methods, microfluidic chips can be manufactured entirely in thermosetting plastics. The high strength makes it possible to fabricate chips with high aspect ratios and a free-standing structure. Due to the high rigidity of thermosetting plastic, it is not suitable for membrane valve manufacturing. Also, their high cost limits the application in microfluidic chips.

One of the most popular and traditional manufacturing techniques used for microfluidic chips is soft lithography with photoresists and elastomers. SU-8 is usually used to fabricate a mold in which

PDMS is applied to fabricate structures of the microfluidic chips [30]. As shown in **Figure 0.4**, the soft lithography method used for microfluidics is to create a master mold using photolithography technology and then cure the PDMS on top of the master mold. After curing, the PDMS structure was removed from the mold and bonded to a substrate (glass or other parts of PMMA). The photolithography and soft lithography methods are affected by manual and time-consuming processes (pouring, curing, cutting, stamping, and bonding). Special training is required for mold manufacturing and equipment operation. Moreover, it takes a long time, from design to prototyping. These shortcomings limit its commercial potential.

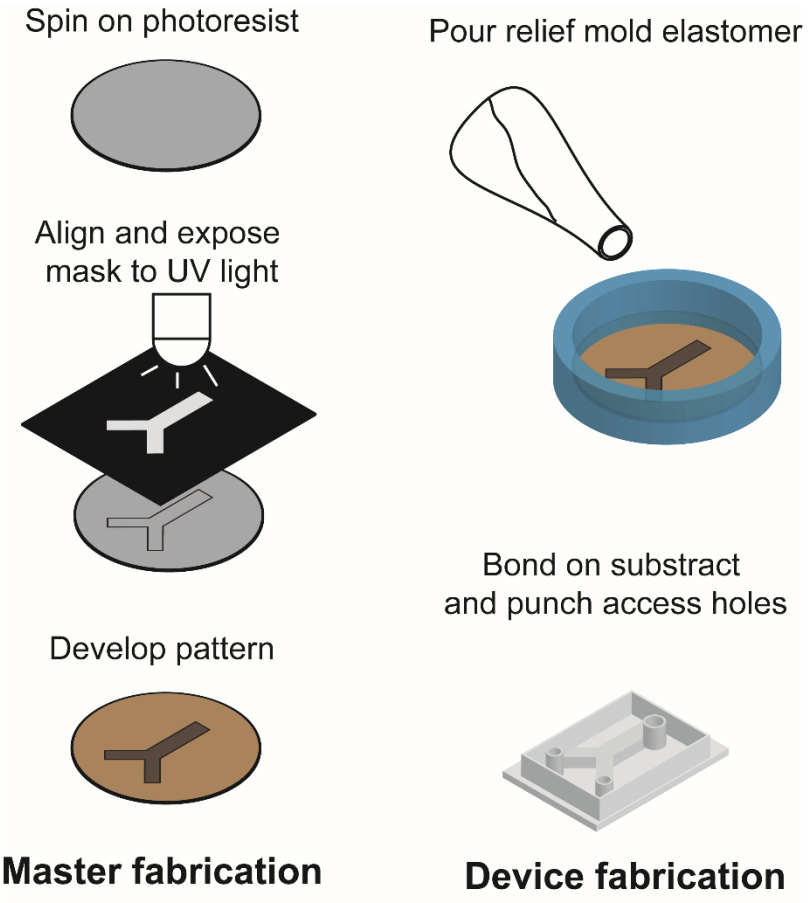

Figure 0.4 Prototyping using soft lithography with photoresists and elastomer.

Unlike thermosetting plastics, thermoplastics can be reshaped after curing. Rich experience in thermoplastics has been accumulated because of their wide application in the industry. Molding and bonding are convenient techniques as they can be reshaped multiple times by reheating. PMMA, polyethylene terephthalate , polystyrene, polyvinyl chloride, and polycarbonate are most

often used as thermoplastics for microfluidic chips applications [31]. Generally, their solvent compatibility is slightly better than PDMS. Unlike elastomers and thermosetting plastics, thermoplastics are usually purchased in solid form and manufactured by thermoforming [31]. Thousands of copies can be produced by thermoforming with high efficiency and low price. However, templates made of metal or silicon are required to be used at high temperatures. They are suitable for commercial production but are uneconomical for prototype use. Therefore, new methods without using templates are developed by assembling and adhere precut sheets by a so named lamination process.

Two simple methods to cut microfluidic channels in thermoplastics are laser cutting and plotter cutting. The advantages of the laser cutting machine are non-contact cutting and higher resolution. However, these advantages came from the high cost of fixed equipment, which on the other side needs to use a vacuum pump to remove debris and smoke, and the potential for burning residues during the cutting process [32, 33]. Rapid cutting by a plotter, also known as Xurography, is a non-lithographic technique using a drag knife printer to generate the master molds or fabricate the micro-devices directly [34]. Cutting plotters are much cheaper, do not require a pumping system, and do not leave burn residues. This method simplifies plastic, paper, and adhesive substrates in the prototyping of microfluidic devices.

The independently pre-cut layers can be bonded together to form channels and microfluidic features known as laminated microfluidic devices [35]. Although the choice of the bonding method inherently depends on the materials used in the manufacturing method, thermal and adhesive bonding are two of the most commonly used bonding methods. Thermal bonding is a simple bonding method usually used in microfluidic devices. In order to promote thermal bonding, the temperature of each layer is raised to a temperature close to the glass transition temperature of one or two materials, and a force is applied to the surface of each layer. When executed correctly, the layers form a solid material that is essentially indistinguishable. The main disadvantage of thermal bonding is that the microchannels may be deformed due to heating or cooling. Some thermal bonding processes also leave air bubbles between the layers. Moreover, thermal bonding is not possible with all materials. When an adhesive is used for bonding, the double-sided tape can be cut and used directly as a flow layer or an adhesive layer between two different sheets. As adhesives can bond most materials together, it greatly increases the types of materials used in microfluidic chips.

Compared with other manufacturing technologies, one of the main advantages of laminated manufacturing is the short time from design to completed microfluidic chips. The design of channels in each layer is in the same routine. Therefore, it is easy to fabricate a 3D microfluidic chip. As the process is simple, no special training is needed, and a person can get the skill in one day. Nonetheless, there still is potential to simplify the process and make it cheaper. We improved the lamination process for multilayer 3D microfluidic systems. Only a cutting plotter was sufficient for the whole process. With the double side adhesive tape no deformation happens in microchannels and transparent PMMA structure makes it possible for flow-based chemiluminescence analysis systems.

The synthesis method of AuNPs - state of the art

Various synthesis methods have been developed for the synthesis of AuNPs. To understand how AuNPs are synthesized using the chemical method and how to control their final properties, it is necessary to understand the nucleation and growth of nanoparticles. The synthesis usually involves the following steps: (1) Reduction of gold salt resulting in the supersaturation for gold atoms. Nuclei formation is induced by the supersaturation of gold atoms. (2) Growth by aggregation or diffusive growth. (3) Slow growth resulting from the constant reduction of gold. (4) Diffusion of atoms/ions onto the surface of nuclei leading to the rapid growth of nuclei and autocatalytic reduction through the electron transfer between the reducing agents [36-38].

Generally, the preparation of AuNPs by chemical reduction involves two main parts: first, using a suitable reducing agent to reduce the gold salt solution and produce Au^0, second stabilizing the obtained AuNPs through a suitable stabilization or capping agent to prevent their aggregation. The synthesis of high-quality AuNPs requires control of shape, size and size distribution, effective stability, and controlled surface functionalization. Therefore, much work has been done to control the synthesis of AuNPs [39-42].

Traditional methods, including the Turkevich-Frens method and the Brust-Schiffrin method, remain the most popular ones. In addition, some new methods (such as the seed-mediated growth method and green synthesis method) have been developed [41].

The Turkevich-Frens method is also known as the sodium citrate reduction method or the classical citrate method, shown in **Figure 0.5**. In this method, sodium citrate is added to a boiling solution of chloroauric acid with sufficient stirring. During the synthesis process, with the formation and

growth of AuNPs, the color changes from yellow to purple or black, and finally to ruby color. The main principle is the reduction of gold ions (Au^{3+}) from chloroauric acid to gold atoms (Au^{0}) through a reducing and capping agent (such as citrate [43]). Several studies have introduced some new methods for the further development of this method. It can be separated into two ways: (1) The size and stability can be changed by controlling the pH value of the reducing agent or the entire mixed reagent [44]; (2) The preparation steps can be simplified by replacing the reducing agent or adding other stabilizers [45]. Usually, this method is very simple because the size can be controlled by changing the molar ratio of gold precursor to reducing agent. However, there are still some shortcomings to overcome: (1) The size of relatively stable AuNPs should bebetween 10 and 50 nm. Outside this range, they will aggregate and become non-spherical; (2) The stability of AuNPs depends to a large extent on stabilizers. Some environmental factors such as pH, salt concentration, and ionic strength will affect the aggregation of AuNPs. Therefore, they are not ideal for further cellular studies. (3) Heating is required in the process, which limits its application. Although it is not yet satisfactory, the Turkevich-Frens method is still one of the most commonly used methods for making AuNPs so far.

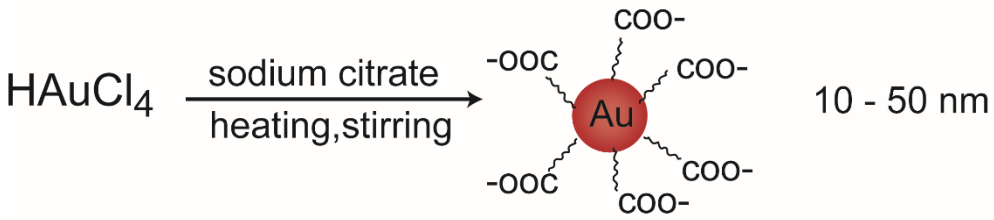

Figure 0.5 Turkevich-Frens method for synthesis of AuNPs by reduction of gold salts in the presence of trisodium citrate.

Brust and Schiffrin reported in 1994 a two-phase reduction method for the preparation of highly stable AuNPs, called the Brust-Schiffrin method [46]. The reaction occurs in a two-phase (water-toluene) system. $HAuCl_4$ was transferred from aqueous-phase to toluene-phase by tetraoctylammonium bromide (TOAB) and then reduced by sodium borohydride ($NaBH_4$), shown in **Figure 0.6**. The size of AuNPs can be adjusted by reaction conditions, such as the thiol/gold ratio, temperature, and reaction rate. The synthesized AuNPs are stabilized by alkanethiol and can dissolve in solvents such as toluene, pentane, and chloroform. These nanoparticles are very stable and can be treated as simple compounds, allowing them to be precipitated, redissolved, stored in

powder form, and chromatographically separated without any significant change in their properties. Moreover, the synthesized AuNPs can be easily subjected to further synthetic operations, such as surface functionalization. With these advantages, the Brust-Schiffrin method is commonly used to conjugate thiol ligands on AuNPs [47].

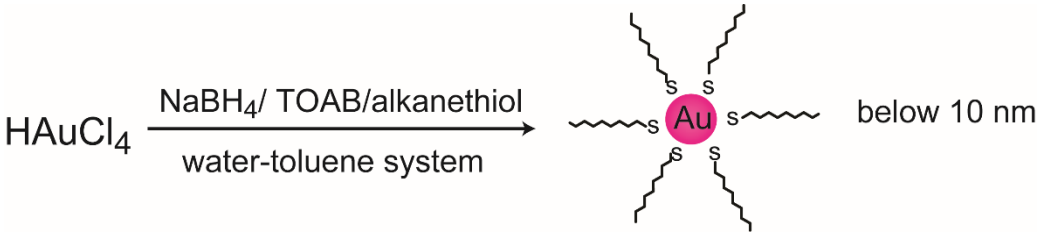

Figure 0.6 Brust-Schiffrin strategy for two-phase fabrication of small-size AuNPs by reduction of gold salts in the presence of external thiol ligands.

The seed-mediated growth method, also known as the step-by-step seed-mediated growth approach, is another commonly used method for controlling the size of AuNPs (**Figure 0.7**). In this method, the seeds (small-sized AuNPs) were firstly prepared by reducing the gold precursor with a strong reducing agent (such as $NaBH_4$ or citrate). Afterward, the small AuNPs were gradually enlarged through growth by adding gold salt solution and a weak reducing agent (such as ascorbic acid). To promote the growth of AuNPs and inhibit new nucleation, a structure-directing agent have to be added [48]. Recently, different reaction conditions have been studied to control the size of synthesized AuNPs. Piella et al. introduced a method to precisely control the size of AuNPs (3.5 - 10 nm) by adjusting the temperature, pH, the concentration of reducing agent, ratio of seed and gold salt [42]. This method shows the merit that the number of synthesized AuNPs can be controlled by adding a controlled number of seeds. As the new nucleation can be prevented, all gold salt was used for the growth. Therefore, the size was controlled.

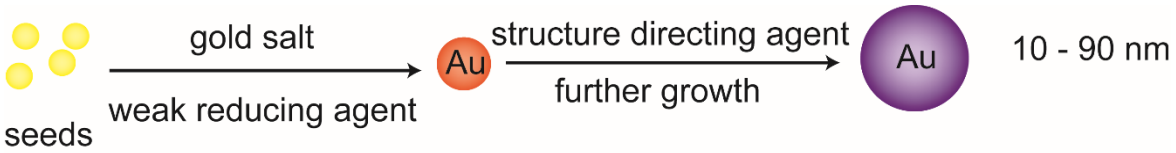

Figure 0.7 Seed-mediated growth method for AuNPs synthesis by the process of nucleation, growth, and stability.

Bare AuNPs are unstable and will gradually aggregate and then precipitate as metallic gold powder. To maintain the original size and the plasmonic properties of AuNPs, a stabilizer must be present throughout the synthesis process (nucleation and growth) [49]. AuNPs can be protected by suitable protective or capping agents to stabilize the nanoparticles and inhibit aggregation. The most commonly used stabilizer involve citrate [50], mercaptan [51], polymers (such as PVP) [52], surfactants [53], and different types of chelating ligands. Charge stabilization and steric stabilization are the two conventional mechanisms for stabilizing nanoparticles. Charge stabilization is accomplished by adsorbing charged ligands (such as citrate) on the surface of the nanoparticles. AuNPs repel each other by the electrostatic charge on the surface and inhibit aggregation. As the surface charge is the main factor, the charge stabilization is sensitive to salt, pH, and other environmental conditions. The steric stabilization is achieved by coating the surface of AuNPs with macromolecules such as polymers as their steric effects can prevent AuNPs from contacting each other and inhibit the aggregation [54]. Apart from stabilizing agents, for certain specific applications the surface of AuNPs has to be selectively functionalized with compounds to achieve the specific process. **Table 0.1** lists a partial summary of the batch synthesis conditions of AuNPs.

Table 0.1 Conditions of batch synthesis of AuNPs.

Reducing agent	Condition	Stabilizer	Size distribution	Ref
Citric acid	Boiling water	Citric acid	6 - 15 nm	[44]
Citric acid / sodium citrate buffer	90 - 100 °C	Citric acid / sodium citrate buffer	14 - 17 nm	[45]
Sodium citrate	Boiling	Sodium citrate and PTS	About 5 nm	[55]
Sodium citrate	Heating	Sodium citrate	Sub - 10 nm	[56]

Reducing agent	Condition	Stabilizer	Size distribution	Ref
$NaBH_4$	Two-phase Liquid-Liquid System	Alkanethiol	1 - 3 nm	[46, 47]
9-BBN	60 °C	ω-functionalized alkylthiols	1.4 - 3.3 nm	[57]
Citrate (seed) ascorbic acid (growth)	35 °C	CTAB	Low polydispersity	[58]
Amino acid	80 °C	Amino acid	Different size and shapes	[59]
PAA	Solar radiation	PAA	-	[60]
Ketyl radicals	UVA light	None	Polydispersity	[61]
DMSO	Ultrasound	DMSO	Hundreds or tens nm polydispersity	[62]
Sodium citrate	Microwave heating	Sodium citrate	Narrower distribution	[63]
Trisodium citrate	Boiling	PVP	-	[64]
Citric acid	UV irradiation	PVP	2 - 10 nm	[13]
Cell-free extracts of fungi	-	-	12 ± 1.5 nm	[65]

Reducing agent	Condition	Stabilizer	Size distribution	Ref
Ascorbic acid	-	Ascorbic acid	7.8 ±1.8 nm 38 ± 18 nm	[66]
PVP	25 - 70 °C or UV	PVP	6 ± 1.5 nm	[67]
KBH_4	-	Polymers with cyano or mercapto groups	2.6 ± 0.4 nm	[52]
Sodium citrate (seed) $NH_2OH \cdot HCl$ (growth)	Seed-mediated growth	mPEG-SH	15 - 170 nm	[68]

Green chemistryhave been developed as alternative synthesis methods because toxic solvents and chemicals can cause problems for biological applications by using AuNPs, and green chemistry is important to achieve sustainability [69]. One solution is to use environmentally friendly reagents for the synthesis of AuNPs. Another solution is to apply natural materials or with the assistance of cells [65, 70]. However, these methods using biological materials are difficult to control, and the mechanism is complicated. Green chemistry methods with cheap and nontoxic reagents could be good ways to be applied in microreactors as no external sources such as heat, light, and microwave are in need during the process. For example, ascorbic acid (AA or AsH_2) is a biomolecule called vitamin C. It can be applied to synthesize AuNPs at room temperature. The following chemical equation shows the synthesis of AuNP using AA as a reducing agent:

$$2AuCl_4^- + 3C_6H_8O_6 \rightarrow 2Au^0 + 3C_6H_6O_6 + 8Cl^- + 6H^+ \quad (1)$$

This oxidation-reduction reaction is complex, involving the reduction of Au^{3+} ions to Au^{1+} and then reducing Au^{1+} to Au^0 [71]. Two hydroxyl groups of AA are deprotonated and be oxidized during the process. The mechanism is shown in **Figure 0.8** [72].

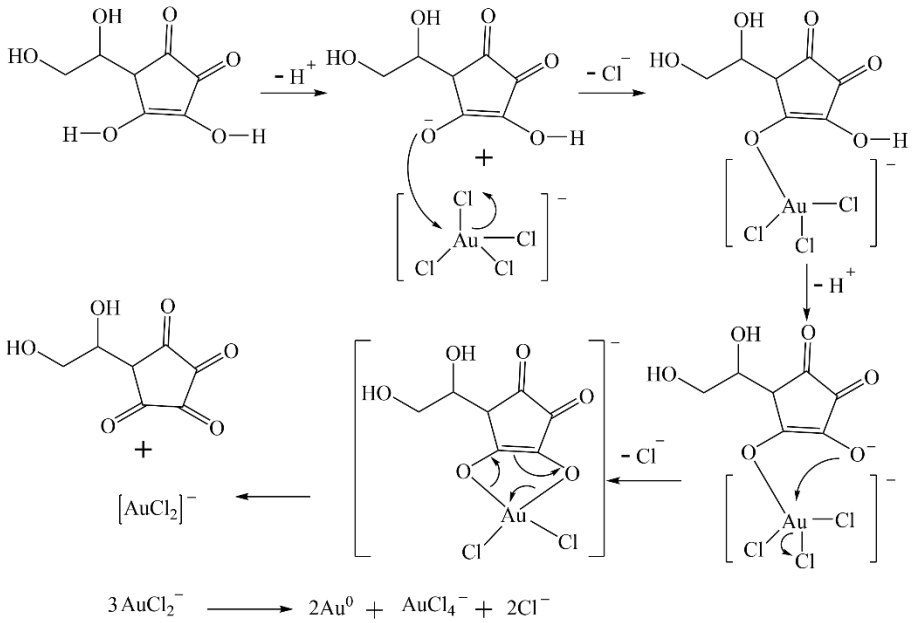

Figure 0.8 The mechanism of AuNPs formation, which is reduced by ascorbic acid [72].

The reduction ability of AA varies due to the presence of three deprotonated species: ascorbic acid (AsH_2), ascorbate monoanion (AsH^-), and ascorbate dianion (As^{2-}), as shown in equation 2 [12, 73]. The three species dominate at different pH values, as shown in **Figure 0.9** [12, 73-75]. Therefore, the size and properties of AuNPs can be adjusted by changing the initial pH value of the AA solution.

$$AsH_2 \overset{K_{a1}}{\Longleftrightarrow} AsH^- + H^+ \overset{K_{a2}}{\Longleftrightarrow} As^{2-} + 2H^+ \qquad (2)$$

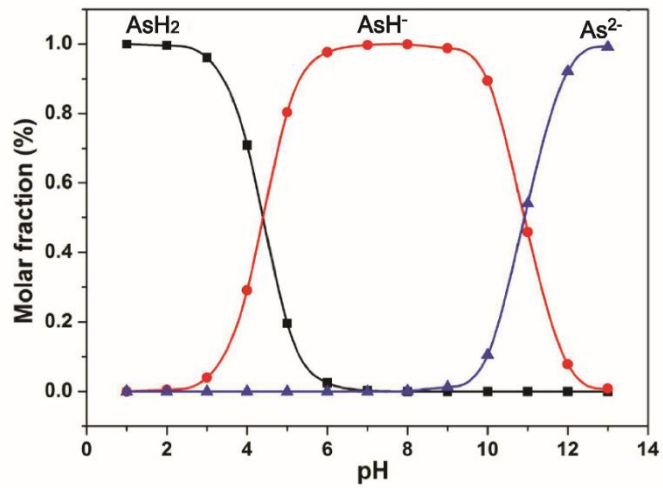

Figure 0.9 Mole fraction of the three absorbate species AsH_2, AsH^- and As^{2-} versus pH [12, 73].

Glucose can act both as a reducing agent for Au^{3+} and as a capping agent to stabilize AuNPs through interaction with hydroxyl groups. Although it is well known that glucose is a reducing sugar, its reducing ability at ambient temperature is limited. However, after adding a small amount of NaOH aqueous solution, glucose can effectively reduce Au^{3+} ions to Au^0 [76]. The alkaline opens the glucose ring through the extraction of protons, thereby promoting the reduction of Au^{3+}. Then, glucose is oxidized to gluconic acid, while Au^{3+} is reduced to Au^0 [77]. The reaction equation is shown in **Figure 0.10**.

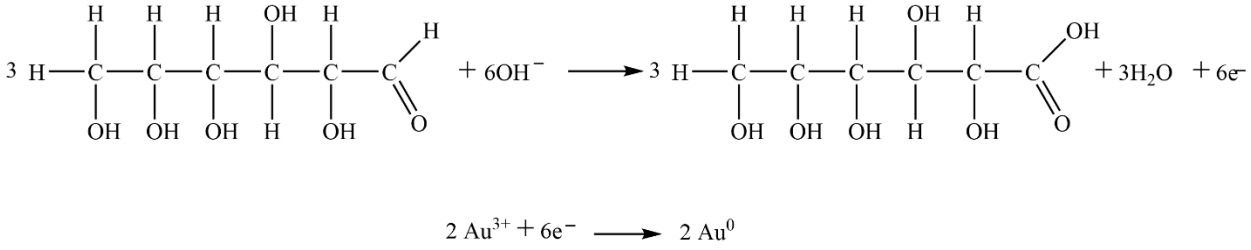

Figure 0.10 The reduction reaction equation for the formation of AuNPs.

It should be mentioned that although glucose in the equation is expressed in open-chain form, most of the structure of glucose in an aqueous solution is in the form of a cyclic chair. On the one hand, glucose acts as an effective reducing agent, rapidly reducing Au^{3+} at room temperature (in the presence of OH^-). On the other hand, it is a stabilizer to passivate the surface of AuNPs and prevent growth. OH^- participates in the reduction reaction. Therefore, the pH environment has a significant impact on the synthesis of AuNPs. High pH (about 6.8 - 10.5) is conducive to the appearance of $Au\text{-}O^-$ groups on the surface of AuNPs, which can interact with the hydroxyl groups of glucose through hydrogen bonds. Therefore, glucose can effectively cover the surface of AuNPs [78].

The classic synthesis methods have the limitation in precisely control the parameters. Green chemistry methods without using heat, light, and microwave could be good ways to be applied in microreactors. The strategy of rapid and effective fabrication of 3D microfluidic chips can be applied to generate a 3D hydrodynamic focusing reactor to synthesize AuNPs. The sheath flow of reducing agents can inhibit the fouling of AuNPs on the microfluidic walls. With the automatic control of programs such as concentrations of reagents and flow rates, the property of synthesized AuNPs can be easily controlled.

Target 2: Online synthesis of AuNPs with 3D microreactor coupled with characterization by chemiluminescence

Properties and applications of AuNPs - state of the art

The surface area to volume ratio of AuNPs with a small size (1 - 100 nm) is exceptionally high, and most of the atoms forming the particle remain on the surface, which is important for applications such as catalysis [79]. AuNPs can provide an excellent three-dimensional scaffold for labeling. Due to the free electrons from the conduction band, functional groups that bind to AuNPs, such as amines and thiols, can be used for the conjugation of proteins and other biomolecules with AuNPs [10, 80]. Therefore, AuNPs have been used in many biomedical applications, such as selective photodynamic therapy [81], carriers for drug delivery and release [80, 82], immunoassay [83, 84], bioanalysis [85, 86], in vitro/in vivo imaging [87, 88].

AuNPs exhibit interesting optical properties, enabling them to be used as functional dyes in different fields (such as sensing and imaging). The solution of AuNPs has a very strong absorption capacity and shows different colors according to the size and shape of the nanoparticles. The color of AuNPs is attributed to the collective oscillation of free conduction electrons caused by the interacting electromagnetic fields. This phenomenon is surface plasmon resonance (SPR) [54], as shown in **Figure 0.11**.

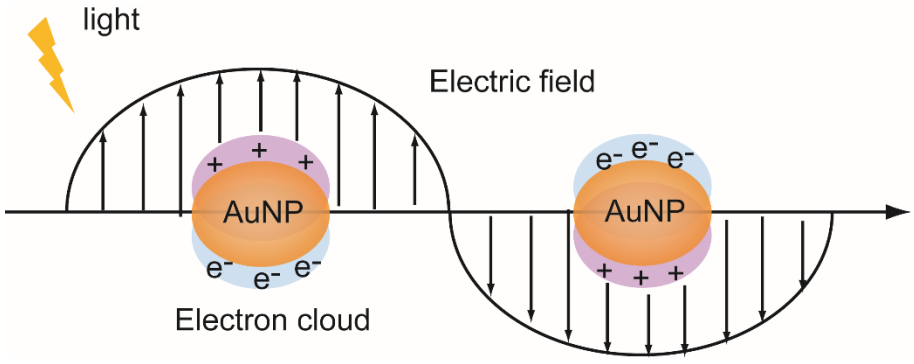

Figure 0.11 Schematic representation of localized surface plasmon resonance of metal nanoparticles by oscillating conduction electrons across the nanosphere in an electromagnetic field.

The surface plasmon absorption frequency and width are related to many factors. The nanoparticles' shape and size, the dielectric constant of the metal, and the surrounding environment

are the most critical factors. The aggregation of AuNPs leads to a significant redshift of the SPR frequency, a widening of the surface plasmon band. And due to the plasmon coupling between the particles, the color of the solution changes from red to blue. This property makes them suitable in colorimetric sensors [89]. When analyte molecules are added, AuNPs will be induced to aggregate or dissociate. When the distance between particles is smaller than the average particle size of AuNPs, the color will change from red to blue, showing aggregation, which can be easily observed with the naked eye [90]. In addition, a UV-Vis spectrophotometer can be used to record the changes. Moreover, when the pH or ionic strength of the AuNPs surface changes, the process of aggregation and redispersion may form a circle [64].

AuNPs in CL analysis systems - state of the art

CL is a phenomenon where energy from chemical reactions generates excited molecules, and they return to the ground state with light emitted. Therefore, there is no need for an excitation source and optical filters in CL-based analytical systems compared with other optical techniques like fluorescence or surface-enhanced Raman spectroscopy. Hence, CL was widely applied in analytical chemistry for sensitive quantification of contaminants in environmental or food samples and diagnostics. The advantages are the creation of simple portable instruments usable for field measurements, low costs, easy to automate the analysis procedure, and high sensitivity [91].

Many different CL analytical systems have been developed, and the main CL reagents include $Ru(bpy)_3^{2+}$, lucigenin, peroxyoxalate derivates, and luminol. Luminol is a low-cost substrate, and it has become the most commonly used reagent in CL reaction since it was first reported in the CL phenomenon in 1928. The CL reaction involves the oxidation of luminol in the presence of a catalyst under alkaline conditions to generate the excited 3-aminophthalate ions. The excited ions emit blue light of 425 nm when they return to the ground state. The mechanism for the CL reaction with luminol has been proposed, which includes three basic reaction steps: (1) deprotonation of luminol and then it is oxidated to the anionic luminol radical ($L^{\bullet-}$); (2) the radical anion is further oxidated to a peroxyketal derivative, the peroxide intermediate; (3) the key intermediate is decomposed to 3-aminophthalate with emission of light [92]. Among them, step 1 was considered to be the rate-determining step of the reaction. The commonly used oxidants include ClO^-, Ce(IV), H_2O_2, IO_4^-, MnO_4^- and Br_2 . NaOCl was one of the first oxidants applied in the luminol CL system. The reaction could emit sufficient light and show visible luminescence in university laboratories

[93]. The oxidation reaction can be catalyzed by enzymes (horseradish peroxidase), metal ions (Fe^{2+}, Fe^{3+}, Co^{2+}, Hg^{2+}, Cu^{2+}, Cr^{2+}, Mn^{4+}, Ni^{2+}) or certain metal complexes (ferrocene, ferricyanide) [94].

In order to improve sensitivity and stability, CL research has expanded from traditional molecular systems to nanoparticle systems. Metal nanoparticles can be used as a catalyst, luminophore, reducing agent, or energy acceptor in the CL reaction, mainly due to the large surface area and special structure of nanomaterials [95]. AuNPs were first reported to be applied in the luminol-based CL system by Cui in 2005 [96]. It was speculated that the enhancement mechanism of AuNPs on luminol-based CL was derived from the catalysis of AuNPs. When AuNPs were added, they facilitated the radical generation. A further electron transfer occurs on the surface of AuNPs between $L^{\bullet-}$ and $O_2^{\bullet-}$ radicals to produce the key intermediate peroxyketal derivatives, which leads to an increase in CL [96]. The possible mechanism of the whole process was shown in **Figure 0.12**.

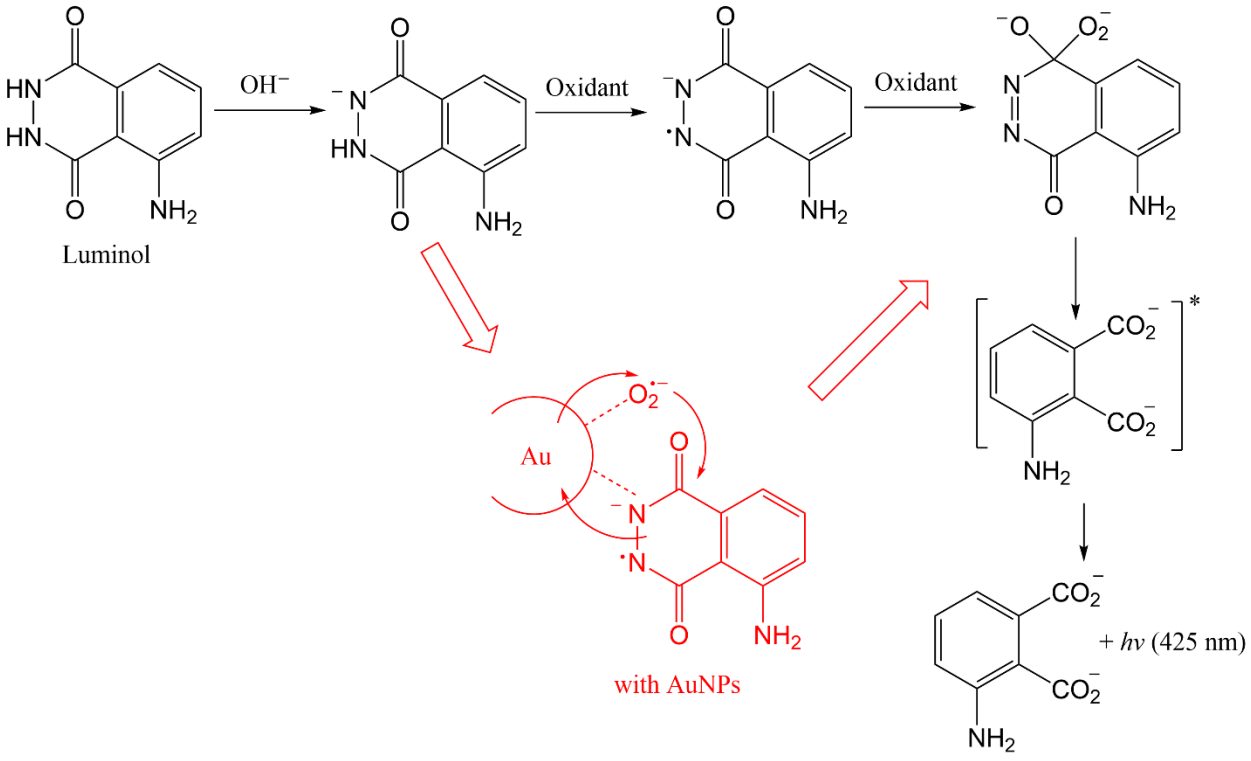

Figure 0.12 Possible mechanism for the CL system with and without AuNPs.

Some researchers have tried to develop an enzyme-free analytical application of the luminol-based CL reaction catalyzed by AuNPs. The CL signal can be inhibited by some organic compounds

which could interact with AuNPs. Thereby the molecules with -OH, -NH_2, and -SH groups can be detected with high sensitivity by this CL inactivation effect. For example, L-cysteine is detected because it can greatly inhibit the CL signal of AuNPs-luminol-H_2O_2 system [97]. AuNPs-Luminol-IO_4^- is applied for the determination of polyphenols by means of the CL quenching effect [98].

In addition to acting as a catalyst, AuNPs can also be used as a label in CL systems. It was reported that $AuCl_4^-$ has a strong catalytic activity when it is anchored on the biomolecules, and the CL signals are proportional to the concentration of $AuCl_4^-$. Therefore, the enlarged AuNPs can be used as probes for biomolecules. When the AuNPs were dissolved by acid, the released Au^{3+} can be detected by CL in the presence of luminol [99].

AuNPs can be the reductant in redox CL reactions. Various reductants could reduce $KMnO_4$ to generate the excited state Mn(II)*, emitting light at approximately 610 - 660 nm when it returns to the ground state. AuNPs smaller than 6.0 nm can quickly reduce $KMnO_4$ in an acidic medium and emit light near 640 nm. AuNPs are oxidized to Au^{3+} in the AuNPs-$KMnO_4$-H_2SO_4 system [100].

AuNPs can absorb a range of light because of the SPR. When the CL spectrum overlaps with the absorption spectrum of AuNPs, there will be a significant decrease in the CL signal, called the CL resonance energy transfer process. Histone was detected by inhibiting the CL resonance energy transfer process in the lucigenin - H_2O_2 system [101].

AuNPs can also be excited by redox reactions. In the presence of the bis(2,4,6-trichlorophenyl) oxalate (TCPO)-H_2O_2, AuNPs with a diameter of 2 to 6 nm were found to show CL at ~415 nm [102]. In the KIO_4-NaOH-Na_2CO_3 system, AuNPs lead to the formation of luminescent intermediate Au^{1+} complexes, carbon dioxide dimers, and singlet oxygen molecular pairs on the surface of AuNPs [103].

In the presence of AuNPs, luminol can react with $AgNO_3$ to produce CL at 425 nm. Under the catalysis of AuNPs, $AgNO_3$ reacts rapidly with luminol to generate Ag and luminol free radicals, which react with dissolved oxygen and emit light. Then, as Ag atoms were immediately deposited on the surface of AuNPs, the catalytic activity decreased, resulting in a sharp drop in CL intensity and slow growth of the core and shell of the nanoparticles [104]. It was reported that dispersed AuNPs could produce weak CL, while aggregated AuNPs can produce strong CL in the luminol-$AgNO_3$ system [105]. This phenomenon was also applicable in the luminol-H_2O_2 analysis systems.

Fibrillar fibrin is detected in the AuNPs CL system because of the interaction between fibrinogen and AuNPs, and the aggregated AuNPs generated strong CL signals [106].

A simple way to cause aggregation of AuNPs is to add some salt to screen the repulsion of AuNPs. Some homogeneous methods have been developed according to this phenomenon. The principle is shown in **Figure 0.13**. Molecules like O-phosphorylethanolamine (PEA) [107], single-strand (ss) DNA [108] can adsorb to the surface of AuNPs and protect them from aggregation in salt [109]. The target molecule should have strong affinity to these protecting molecules. When the target molecule is absent, the protecting molecule will adsorb on the surface of AuNPs and inhibit the aggregation in salt. Therefore, the dispersed AuNPs generate a weak CL signal. If there are some target molecules in the system, they will bind to the protecting molecules. In this case, there are insufficient protecting molecules to stabilize AuNPs in salt, which causes aggregation. Hence, aggregated AuNPs generate a strong CL signal.

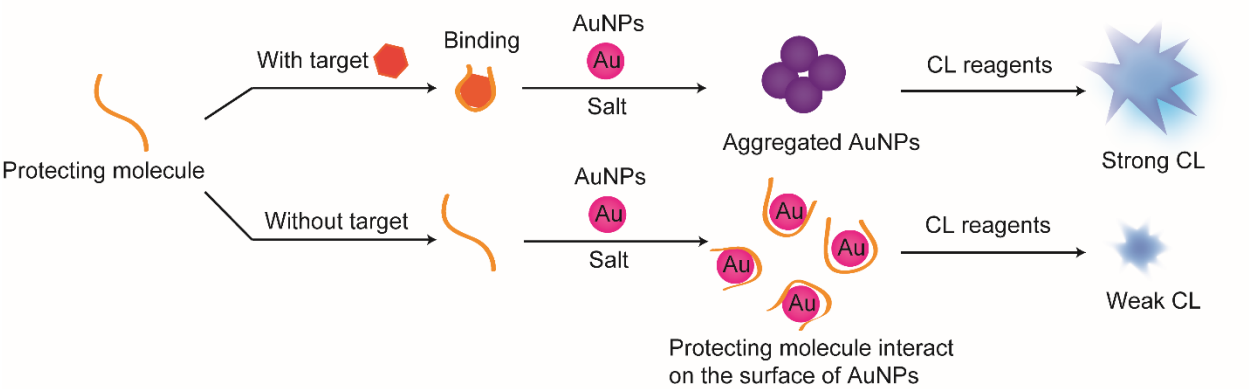

Figure 0.13 Scheme of homogeneous CL assay using AuNPs probe and protecting molecule.

This method was applied for the detection of C - reactive protein (CRP) by PEA [107]. PEA can adhere to the surface of AuNPs and act as protecting molecule to prevent aggregation of AuNPs in salt. Once the CRP - PEA reaction occurs, AuNP will aggregate and show a strong CL signal. An alternative is ssDNA which can also adsorb to the surface of AuNPs and inhibits aggregation. After adding a complementary target DNA, the ssDNA probe will be removed by the hybridization reaction, resulting in the aggregation of AuNP and a stronger CL. Therefore, free ssDNA can be detected [108].

Many studies have demonstrated no positive or negative correlation between CL signals and sizes of AuNPs [96, 98, 104, 110-113]. The ranking of the catalytic properties of AuNPs in different CL

systems were summarized in **Table 0.2**. Additionally, the optimal size of AuNPs depends on different CL systems [96, 98, 104, 110-113]. For example, in the luminol - H_2O_2 system, the 38 nm AuNPs showed the best catalytic performance among the tested AuNPs [96]. However, in luminol-ferricyanide and luminol-hydrazine CL systems, the most intensive CL signal is obtained using 25 nm AuNP and 15 nm AuNP, respectively [110, 111]. Due to the limited number of AuNPs tested and various CL systems, it is difficult to determine the best AuNPs with a specific size.

Table 0.2 The ranking of the catalytic properties of AuNPs in different CL systems.

CL system	Ranking of the catalytic properties of AuNPs	Ref
Luminol-H_2O_2	38 nm > 25 nm > 16 nm > 68 nm > 99 nm > 6 nm	[96]
Luminol-ferricyanide	25 nm> 39 nm > 16 nm > 71 nm > 11 nm	[110]
Luminol-hydrazine	15 nm > 6 nm > 26 nm > 44 nm > 57 nm	[111]
Luminol-$AgNO_3$	8 nm > 16 nm > 25 nm > 38 nm > 68 nm	[104]
Luminol-$NaIO_4$	4 nm > 6 nm > 16 nm	[98]
HCO_4^--eosin Y	50 nm > 33nm > 22 nm > 61nm > 16 nm > 14 nm	[112]

In addition, the morphology of AuNPs affects their catalytic performance in CL reaction. Aggregated AuNPs were found to induce a higher signal in CL reaction with luminol than dispersed ones [108, 109, 114]. Besides the size and shape, AuNPs with different surface charge properties also display various functions in CL reaction [109]. Cationic AuNPs or AuNPs with lower negative charge density have been proved to exhibit higher catalytic activity [107, 109, 114]. Due to all these variables, it is difficult to confirm the optimal AuNPs for a certain CL reaction. According to our knowledge, researchers only buy commercial AuNPs or produce them batch-wise. Only limited kinds of AuNPs were tried in a CL reaction. Therefore, it is crucial to develop an online monitoring system that can easily control the property of AuNPs during synthesis and immediately inspect the catalytic CL activity.

Online synthesis coupled with characterization

In order to characterize AuNPs, many techniques have been developed in the past few decades and used to study optical properties, size, shape, morphology, structure, and surface chemistry of nanoparticles. For example, transmission electron microscopy (TEM) and scanning electron microscopy (SEM) can determine size and morphology. In addition, size exclusion chromatography [115] and gel electrophoresis [116] can provide information about size distributions, while nuclear magnetic resonance spectroscopy [117] can characterize the surface chemistry of nanocrystals. Moreover, optical spectroscopy (such as UV-Vis spectroscopy, fluorescence spectroscopy, Raman spectroscopy, and infrared spectroscopy) can be used to understand the optical properties and surface chemistry of AuNPs. Traditionally, these analysis technologies have been considered offline technologies. However, with the development of new miniaturized systems and the decline in equipment costs, it has become possible to integrate a dedicated analysis system into a flow reactor.

Making full use of microfluidic synthesis procedures requires real-time information about the progress of the reaction. Appropriate changes can be made to the reaction conditions during the synthesis to optimize size distribution or physicochemical properties. Optical technology is particularly easy to integrate with microfluidic chips due to its non-invasive nature, and it can obtain instant information about the properties of AuNPs [118].

Online synthesis within a microreactor and catalytic characterization of AuNPs in a CL analysis system can be a new method for confirming synthesis conditions of optimal AuNPs, and it has never been tried before. The catalytic activity of the synthesized AuNPs can be changed through different synthesis conditions, and can be directly characterized by a CL reaction for further application.

Target 3: Develop a 3D microfluidic flow-injection platform with AuNPs catalyzed CL for aptamer-based homogeneous assays

AuNPs and aptamer in homogeneous assay - state of the art

Aptamers are single-stranded DNA or RNA oligonucleotides that can specifically bind to various target molecules (such as proteins, nucleic acids, metal ions, and other small molecules) with high affinity, selectivity, and sensitivity [119]. Aptamers can be produced in large quantities through chemical synthesis. Compared with antibodies, aptamers have the advantages of high stability, easy synthesis, and low cost. In combination with AuNPs, it provides the possibility for homogeneous CL assays. Compared with CL heterogeneous assays, homogeneous detection has attractive features. It eliminates the complicated separation process. Moreover, the identification and signal output process are faster and more efficient. Furthermore, it can avoid non-specific binding with a low background signal [120].

Due to their excellent properties, AuNPs are the most popular nanomaterials in aptamer-based assays. The combination of aptamers and AuNPs through chemical adsorption or physical adsorption has been well developed [121, 122]. These properties of AuNPs contribute to the construction of simple, efficient, and sensitive aptamer-based sensors (devices used to record the existence or change of something in the environment). Compared with natural receptors (such as antibodies and enzymes), aptamer-based sensors have unique advantages in various applications. The formation of the aptamer-based sensor can be easily regulated by using complementary sequences. After adding the target molecule, the competitive interaction between the aptamer, complementary DNA, and target can easily destroy the aptamer-complementary DNA complex. The easy modification and labeling of aptamer sequences are another advantage. They can be easily immobilized on solid supports. Therefore, aptamer-based analysis can also be applied in a microarray platform [123].

Colorimetric detection is a very attractive method because of its simplicity and low cost, making it particularly suitable for immediate detection. Since the Mirkin's group first reported the use of AuNPs for colorimetric DNA detection [124], AuNPs have been most commonly used to develop colorimetric aptamer-based sensors due to their unique properties. The dispersed AuNPs are red

when observed with naked eyes and purple after aggregation. As the distance between AuNP particles decreases, the formation of a network of AuNPs results in a red to purple color change.

The mentioned property can be applied in sensors with three different strategies. The first strategy is to use two aptamers, which are called the dual aptamer, binding to the different sites of a target, as shown in **Figure 0.14 a.** AuNPs are modified with the dual aptamers and kept in a dispersed state with red color. The target can generate an AuNPs network when combined with dual aptamers. Therefore, the color of AuNPs turns purple. The limitation of this strategy is that only a few dual aptamers have been reported for the target. The second format is based on the interaction between complementary DNA and aptamer to form a network. In the presence of the target, the AuNPs network is destroyed by combining the aptamer and the target, resulting in a purple to red change, as shown in **Figure 0.14 b**. With these two strategies, AuNPs have to be modified with the aptamer beforehand.

Another strategy is based on the aggregation of AuNPs by controlling the surface conditions shown in **Figure 0.14 c**. AuNPs in suspension are usually stabilized by anions adsorbed on their surface. The induced electrostatic repulsion between AuNPs is stronger than the van der Waals attraction between AuNPs. Salt usually induces the aggregation of AuNPs because it reduces the electrostatic repulsion between AuNPs. When aptamers adsorb on the surface of AuNPs, the aggregation of AuNPs can be inhibited under high salt conditions. Compared to the other strategies, this one was much easier. In an analytical application, aptamer concentration must be optimized in case insufficient aptamer cannot protect AuNPs well.

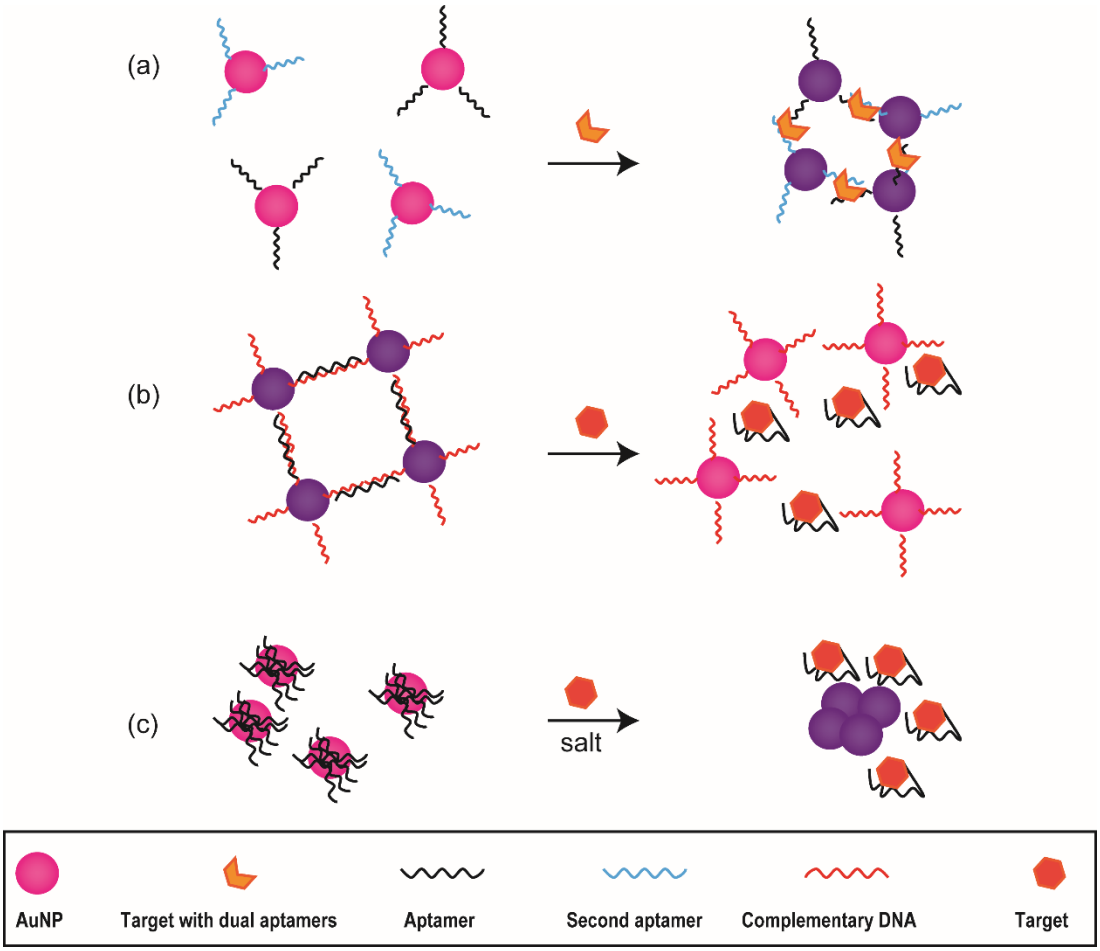

Figure 0.14 Strategies of the aptamer-based homogeneous assays with (**a** and **b**) modified and (**c**) unmodified AuNPs.

Micromixers - state of the art

In the design of microfluidic platforms, mixing is usually a critical issue, especially in homogenous assays. Due to the size of micro-level flow channels and low flow velocities, the fluid movement is laminar, and the mixing mainly depends on diffusion [125]. Therefore, the mixing efficiency of microfluidic platforms is very low. In order to solve this problem, the strategy is to impose interference on the flow field to improve the mixing efficiency. According to how the interference is applied, mixing can be divided into active mixing and passive mixing [126].

Active mixing, which exerts an additional effect on the flow field through external forces, can regularly disturb the flow field to improve the mixing efficiency [127]. All the forces that can affect the flow field can be used as the driving force for active mixing, including magnetic force [128], sound waves [129], microwaves [130], or electric fields [131]. The design of active mixers

that use magnetic force involves magnetic stirring beads with an external rotating magnetic field as a driving force to stir the fluid to be mixed. For a mixer driven by a sound field, ultrasonic waves are often used as a driving force that can drive a vibrating membrane to disturb the flow field and improve mixing efficiency. The principle of a mixer using an electric field is to use a changing direct currency electric field to generate electroosmotic flow in the fluid, which drives and mixes the fluid. Active mixers have the advantages of small size, simple structure, and high mixing efficiency. However, its shortcomings are also obvious. Additional equipment is required to provide driving force, which greatly increases the cost of microfluidic chips. Also, the portability of the chip no longer exists. In addition, the mixing process requires specialized operation and control, which is very difficult for ordinary users and makes the microfluidic chip a product that can only be used in professional laboratories. Moreover, the external driving force will inevitably produce a heating effect on the fluid in the micromixer, which may negatively influence certain chemical reactions and biological activity. All these inherent defects limit the use and development of active mixers in the application field.

The passive mixer improves the mixing efficiency by changing the flow field through the special design of the flow channel shape [132]. When the fluid flows through the local structure, a local pressure loss occurs. This part of the pressure potential energy is converted into kinetic energy, which redistributes the velocity field and plays a role in stirring the fluid. According to the microchannel geometric structure, the passive micromixer can be divided into the branched and non-branched types [133]. Examples of branched and non-branched mixer are shown in **Figure 0.15 a** and **b**.

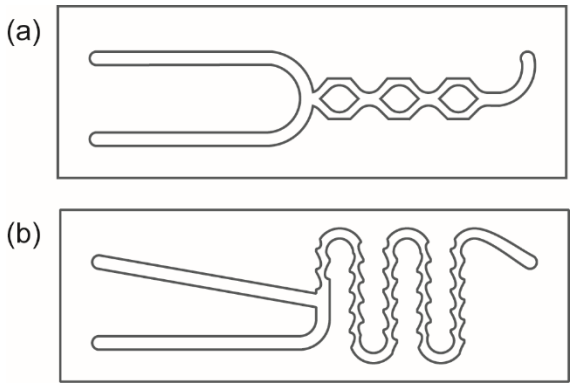

Figure 0.15 Example of (**a**) branched and (**b**) non-branched mixer.

The design strategy of the branched mixer is to split the main channel into two or more channels which will be merged into the main channel to form a mixing unit. Each mixing unit can be designed separately. Finally, a complete micromixer structure is composed of multiple mixing units. The internal fluid is split and reorganized. In this process, the redistribution degree and range of the velocity field have increased, resulting in an increase in mixing efficiency. The geometric feature of the non-branch mixer is that there is only one mixing microchannel. The geometry of the channel is usually designed with sharp corners and obstacles to change the velocity in the flow field, increase the relative movement between fluids, and enhance the diffusion strength of the fluid. As a passive mixer can achieve efficient mixing without additional force, its costs for equipment are much lower than that of the active mixer. In addition, passive mixers require neither very sophisticated operation procedures nor specialized laboratories. Therefore, passive mixers could find their way in microanalytical systems for end user-friendly applications.

The passive mixer can be applied in 2D and 3D microfluidic chips, and 3D micromixers usually have better performance due to the extra mixing space. A 3D passive mixer can be fabricated efficiently using the developed laminated method without expensive instruments. Additionally, a 3D mixer can perfectly fit below the CCD camera and offer a space for a homogeneous assay. AuNPs with optimal catalytic activity can be combined with an aptamer for specific analytic detection. A novel detection platform can be developed in the 3D micromixer with AuNP-catalyzed CL for aptamer-based homogeneous assays.

References

1. Pennathur, S., C.D. Meinhart, and H.T. Soh, *How to exploit the features of microfluidics technology.* Lab Chip, 2008. **8**(1): p. 20-2.
2. Yuen, P.K. and V.N. Goral, *Low-cost rapid prototyping of flexible microfluidic devices using a desktop digital craft cutter.* Lab Chip, 2010. **10**(3): p. 384-7.
3. Huh, D., W. Gu, Y. Kamotani, J.B. Grotberg, and S. Takayama, *Microfluidics for flow cytometric analysis of cells and particles.* Physiol. Meas., 2005. **26**(3): p. R73-98.
4. Mark, D., S. Haeberle, G. Roth, F. von Stetten, and R. Zengerle, *Microfluidic lab-on-a-chip platforms: requirements, characteristics and applications.* Chem. Soc. Rev., 2010. **39**(3): p. 1153-82.

5. Luty-Błocho, M., K. Fitzner, V. Hessel, P. Löb, M. Maskos, D. Metzke, K. Pacławski, and M. Wojnicki, *Synthesis of gold nanoparticles in an interdigital micromixer using ascorbic acid and sodium borohydride as reducers.* Chem. Eng. J., 2011. **171**(1): p. 279-290.

6. Wagner, J. and J.M. Kohler, *Continuous synthesis of gold nanoparticles in a microreactor.* Nano Lett., 2005. **5**(4): p. 685-91.

7. Köhler, J.M., L. Abahmane, J. Wagner, J. Albert, and G. Mayer, *Preparation of metal nanoparticles with varied composition for catalytical applications in microreactors.* Chem. Eng. Sci., 2008. **63**(20): p. 5048-5055.

8. Wagner, J., T. Kirner, G. Mayer, J. Albert, and J.M. Köhler, *Generation of metal nanoparticles in a microchannel reactor.* Chem. Eng. J., 2004. **101**(1-3): p. 251-260.

9. Gomez-de Pedro, S., M. Puyol, and J. Alonso-Chamarro, *Continuous flow synthesis of nanoparticles using ceramic microfluidic devices.* Nanotechnology, 2010. **21**(41): p. 415603.

10. Shalom, D., R.C.R. Wootton, R.F. Winkle, B.F. Cottam, R. Vilar, A.J. deMello, and C.P. Wilde, *Synthesis of thiol functionalized gold nanoparticles using a continuous flow microfluidic reactor.* Mater. Lett., 2007. **61**(4-5): p. 1146-1150.

11. Wang, C.H. and G.B. Lee, *Automatic bio-sampling chips integrated with micro-pumps and micro-valves for disease detection.* Biosens. Bioelectron., 2005. **21**(3): p. 419-25.

12. Bandulasena, M.V., G.T. Vladisavljević, O.G. Odunmbaku, and B. Benyahia, *Continuous synthesis of PVP stabilized biocompatible gold nanoparticles with a controlled size using a 3D glass capillary microfluidic device.* Chem. Eng. Sci., 2017. **171**: p. 233-243.

13. Yang, S., T. Zhang, L. Zhang, S. Wang, Z. Yang, and B. Ding, *Continuous synthesis of gold nanoparticles and nanoplates with controlled size and shape under UV irradiation.* Colloids Surf. Physicochem. Eng. Aspects, 2007. **296**(1-3): p. 37-44.

14. Ishizaka, T., A. Ishigaki, H. Kawanami, A. Suzuki, and T.M. Suzuki, *Dynamic control of gold nanoparticle morphology in a microchannel flow reactor by glucose reduction in aqueous sodium hydroxide solution.* J. Colloid Interface Sci., 2012. **367**(1): p. 135-8.

15. Cabeza, V.S., S. Kuhn, A.A. Kulkarni, and K.F. Jensen, *Size-controlled flow synthesis of gold nanoparticles using a segmented flow microfluidic platform.* Langmuir, 2012. **28**(17): p. 7007-13.

16. Bandulasena, M.V., G.T. Vladisavljević, and B. Benyahia, *Droplet-based microfluidic method for robust preparation of gold nanoparticles in axisymmetric flow focusing device.* Chem. Eng. Sci., 2019. **195**: p. 657-664.

17. Schoenitz, M., L. Grundemann, W. Augustin, and S. Scholl, *Fouling in microstructured devices: a review.* Chem. Commun. (Camb.), 2015. **51**(39): p. 8213-28.

18. Phillips, T.W., I.G. Lignos, R.M. Maceiczyk, A.J. deMello, and J.C. deMello, *Nanocrystal synthesis in microfluidic reactors: where next?* Lab Chip, 2014. **14**(17): p. 3172-80.

19. Simonnet, C. and A. Groisman, *Two-dimensional hydrodynamic focusing in a simple microfluidic device.* Appl. Phys. Lett., 2005. **87**(11).

20. Chiu, Y.J., S.H. Cho, Z. Mei, V. Lien, T.F. Wu, and Y.H. Lo, *Universally applicable three-dimensional hydrodynamic microfluidic flow focusing.* Lab Chip, 2013. **13**(9): p. 1803-9.

21. Lu, M., S. Yang, Y.P. Ho, C.L. Grigsby, K.W. Leong, and T.J. Huang, *Shape-controlled synthesis of hybrid nanomaterials via three-dimensional hydrodynamic focusing.* ACS Nano, 2014. **8**(10): p. 10026-34.

22. Lu, M., A. Ozcelik, C.L. Grigsby, Y. Zhao, F. Guo, K.W. Leong, and T.J. Huang, *Microfluidic Hydrodynamic Focusing for Synthesis of Nanomaterials.* Nano Today, 2016. **11**(6): p. 778-792.

23. Takagi, M., T. Maki, M. Miyahara, and K. Mae, *Production of titania nanoparticles by using a new microreactor assembled with same axle dual pipe.* Chem. Eng. J., 2004. **101**(1-3): p. 269-276.

24. Patel, J.N., B. Kaminska, B.L. Gray, and B.D. Gates, *PDMS as a sacrificial substrate for SU-8-based biomedical and microfluidic applications.* J. Micromech. Microeng., 2008. **18**(9): p. 095028.

25. Ren, K., J. Zhou, and H. Wu, *Materials for microfluidic chip fabrication.* Acc. Chem. Res., 2013. **46**(11): p. 2396-406.

26. Song, S. and K.Y. Lee, *Polymers for Microfluidic Chips.* Macromol. Res., 2006. **14**(2): p. 121-128.

27. McDonald, J.C. and G.M. Whitesides, *Poly(dimethylsiloxane) as a material for fabricating microfluidic devices.* Acc Chem Res, 2002. **35**(7): p. 491-9.

28. Li, B., Y. Qiu, J. Zhang, X. Huang, H. Shi, and H. Yin, *Real-Time Study of Rapid Spread of Antibiotic Resistance Plasmid in Biofilm Using Microfluidics.* Environ. Sci. Technol., 2018. **52**(19): p. 11132-11141.

29. Lu, Y., J. Gao, D.D. Zhang, V. Gau, J.C. Liao, and P.K. Wong, *Single cell antimicrobial susceptibility testing by confined microchannels and electrokinetic loading.* Anal. Chem., 2013. **85**(8): p. 3971-6.

30. Kim, P., *Soft Lithography for Microfluidics: a Review.* Biochip J, 2008. **2**(1): p. 1-11.

31. Becker, H. and C. Gartner, *Polymer microfabrication technologies for microfluidic systems.* Anal. Bioanal. Chem., 2008. **390**(1): p. 89-111.

32. Chen, X., J. Shen, and M. Zhou, *Rapid fabrication of a four-layer PMMA-based microfluidic chip using CO2-laser micromachining and thermal bonding.* J. Micromech. Microeng., 2016. **26**(10): p. 107001.

33. Chen, X., T. Li, and Q.I. Gao, *A Novel Method for Rapid Fabrication of Pmma Microfluidic Chip by Laser Cutting and Sealing Integration.* Surf. Rev. Lett., 2019. **26**(08).

34. Journal of Microelectromechanical SystemsBartholomeusz, D.A.B., R.W.; Andrade, J.D., *Xurography- rapid prototyping of microstructures.* J. Microelectromech. Syst., 2005. **14**(6).

35. Jafek, A.R., S. Harbertson, H. Brady, R. Samuel, and B.K. Gale, *Instrumentation for xPCR Incorporating qPCR and HRMA.* Anal. Chem., 2018. **90**(12): p. 7190-7196.

36. Thanh, N.T., N. Maclean, and S. Mahiddine, *Mechanisms of nucleation and growth of nanoparticles in solution.* Chem. Rev., 2014. **114**(15): p. 7610-30.

37. Rahman, M. and E. Rebrov, *Microreactors for Gold Nanoparticles Synthesis: From Faraday to Flow.* Processes, 2014. **2**(2): p. 466-493.

38. Polte, J., T.T. Ahner, F. Delissen, S. Sokolov, F. Emmerling, A.F. Thunemann, and R. Kraehnert, *Mechanism of gold nanoparticle formation in the classical citrate synthesis method derived from coupled in situ XANES and SAXS evaluation.* J. Am. Chem. Soc., 2010. **132**(4): p. 1296-301.

39. Zhao, P., N. Li, and D. Astruc, *State of the art in gold nanoparticle synthesis.* Coord. Chem. Rev., 2013. **257**(3-4): p. 638-665.

40. Majdalawieh, A., M.C. Kanan, O. El-Kadri, and S.M. Kanan, *Recent Advances in Gold and Silver Nanoparticles: Synthesis and Applications.* J. Nanosci. Nanotechnol., 2014. **14**(7): p. 4757-4780.

41. Qin, L., G. Zeng, C. Lai, D. Huang, P. Xu, C. Zhang, M. Cheng, X. Liu, S. Liu, B. Li, and H. Yi, *"Gold rush" in modern science: Fabrication strategies and typical advanced applications of gold nanoparticles in sensing.* Coord. Chem. Rev., 2018. **359**: p. 1-31.

42. Herizchi, R., E. Abbasi, M. Milani, and A. Akbarzadeh, *Current methods for synthesis of gold nanoparticles.* Artif Cells Nanomed Biotechnol, 2016. **44**(2): p. 596-602.

43. Wuithschick, M., A. Birnbaum, S. Witte, M. Sztucki, U. Vainio, N. Pinna, K. Rademann, F. Emmerling, R. Kraehnert, and J. Polte, *Turkevich in New Robes: Key Questions Answered for the Most Common Gold Nanoparticle Synthesis.* ACS Nano, 2015. **9**(7): p. 7052-71.

44. Shiba, F., *Size control of monodisperse Au nanoparticles synthesized via a citrate reduction process associated with a pH-shifting procedure.* CrystEngComm, 2013. **15**(42).

45. Schulz, F., T. Homolka, N.G. Bastus, V. Puntes, H. Weller, and T. Vossmeyer, *Little adjustments significantly improve the Turkevich synthesis of gold nanoparticles.* Langmuir, 2014. **30**(35): p. 10779-84.

46. Brust, M., M. Walker, D. Bethell, D.J. Schiffrin, and R. Whyman, *Synthesis of thiol-derivatised gold nanoparticles in a two-phase Liquid–Liquid system.* J. Chem. Soc., Chem. Commun., 1994. **0**(7): p. 801-802.

47. Wieckowska, A. and M. Dzwonek, *Ultrasmall Au nanoparticles coated with hexanethiol and anthraquinone/hexanethiol for enzyme-catalyzed oxygen reduction.* Sens. Actuators B Chem., 2016. **224**: p. 514-520.

48. Brown, K.R., D.G. Walter, and M.J. Natan, *Seeding of Colloidal Au Nanoparticle Solutions. 2. Improved Control of Particle Size and Shape.* Chem. Mater., 2000. **12**(2): p. 306-313.

49. Kang, H., J.T. Buchman, R.S. Rodriguez, H.L. Ring, J. He, K.C. Bantz, and C.L. Haynes, *Stabilization of Silver and Gold Nanoparticles: Preservation and Improvement of Plasmonic Functionalities.* Chem. Rev., 2019. **119**(1): p. 664-699.

50. Piella, J., N.G. Bastús, and V. Puntes, *Size-Controlled Synthesis of Sub-10-nanometer Citrate-Stabilized Gold Nanoparticles and Related Optical Properties.* Chem. Mater., 2016. **28**(4): p. 1066-1075.

51. Spampinato, V., M.A. Parracino, R. La Spina, F. Rossi, and G. Ceccone, *Surface Analysis of Gold Nanoparticles Functionalized with Thiol-Modified Glucose SAMs for Biosensor Applications.* Front. Chem., 2016. **4**: p. 8.

52. T. Teranishi, I.K., and M. Miyake,, *Synthesis of Monodisperse Gold Nanoparticles Using Linear Polymers as Protective Agents.* Adv. Mater., 1998.

53. Lyon, L.A., D.J. Peña, and M.J. Natan, *Surface Plasmon Resonance of Au Colloid-Modified Au Films: Particle Size Dependence.* J. Phys. Chem. B, 1999. **103**(28): p. 5826-5831.

54. Alex, S. and A. Tiwari, *Functionalized Gold Nanoparticles: Synthesis, Properties and Applications—A Review.* J. Nanosci. Nanotechnol., 2015. **15**(3): p. 1869-1894.

55. Sanfelice, R.C., A. Pavinatto, V.C. Gonçalves, D.S. Correa, L.H.C. Mattoso, and D.T. Balogh, *Synthesis of a nanocomposite containing a water-soluble polythiophene derivative and gold nanoparticles.* J. Polym. Sci., Part B: Polym. Phys., 2016. **54**(13): p. 1245-1254.

56. Sivaraman, S.K., S. Kumar, and V. Santhanam, *Monodisperse sub-10 nm gold nanoparticles by reversing the order of addition in Turkevich method--the role of chloroauric acid.* J. Colloid Interface Sci., 2011. **361**(2): p. 543-7.

57. Sardar, R. and J.S. Shumaker-Parry, *9-BBN Induced Synthesis of Nearly Monodisperse ω-Functionalized Alkylthiol Stabilized Gold Nanoparticles.* Chem. Mater., 2009. **21**(7): p. 1167-1169.

58. Rodriguez-Fernandez, J., J. Perez-Juste, F.J. Garcia de Abajo, and L.M. Liz-Marzan, *Seeded growth of submicron Au colloids with quadrupole plasmon resonance modes.* Langmuir, 2006. **22**(16): p. 7007-10.

59. Maruyama, T., Y. Fujimoto, and T. Maekawa, *Synthesis of gold nanoparticles using various amino acids.* J. Colloid Interface Sci., 2015. **447**: p. 254-7.

60. Kumar, A., M. Bhatt, G. Vyas, S. Bhatt, and P. Paul, *Sunlight Induced Preparation of Functionalized Gold Nanoparticles as Recyclable Colorimetric Dual Sensor for Aluminum and Fluoride in Water.* ACS Appl. Mater. Interfaces, 2017. **9**(20): p. 17359-17368.

61. McGilvray, K.L., M.R. Decan, D. Wang, and J.C. Scaiano, *Facile photochemical synthesis of unprotected aqueous gold nanoparticles.* J. Am. Chem. Soc., 2006. **128**(50): p. 15980-1.

62. Bhosale, M.A., D.R. Chenna, and B.M. Bhanage, *Ultrasound Assisted Synthesis of Gold Nanoparticles as an Efficient Catalyst for Reduction of Various Nitro Compounds.* ChemistrySelect, 2017. **2**(3): p. 1225-1231.

63. Ngo, V.K.T., D.G. Nguyen, T.P. Huynh, and Q.V. Lam, *A low cost technique for synthesis of gold nanoparticles using microwave heating and its application in signal amplification for detectingEscherichiaColiO157:H7 bacteria.* Adv. Nat. Sci.: Nanosci. Nanotechnol., 2016. **7**(3).

64. Dhumale, V.A., R.K. Gangwar, S.S. Datar, and R.B. Sharma, *Reversible Aggregation Control of Polyvinylpyrrolidone Capped Gold Nanoparticles as a Function of pH.* Mater. Express, 2012. **2**(4): p. 311-318.

65. Vágó, A., G. Szakacs, G. Sáfrán, R. Horvath, B. Pécz, and I. Lagzi, *One-step green synthesis of gold nanoparticles by mesophilic filamentous fungi.* Chem. Phys. Lett., 2016. **645**: p. 1-4.

66. Malassis, L., R. Dreyfus, R.J. Murphy, L.A. Hough, B. Donnio, and C.B. Murray, *One-step green synthesis of gold and silver nanoparticles with ascorbic acid and their versatile surface post-functionalization.* RSC Adv., 2016. **6**(39): p. 33092-33100.

67. Hoppe, C.E., M. Lazzari, I. Pardinas-Blanco, and M.A. Lopez-Quintela, *One-step synthesis of gold and silver hydrosols using poly(N-vinyl-2-pyrrolidone) as a reducing agent.* Langmuir, 2006. **22**(16): p. 7027-34.

68. Rahme, K., L. Chen, R.G. Hobbs, M.A. Morris, C. O'Driscoll, and J.D. Holmes, *PEGylated gold nanoparticles: polymer quantification as a function of PEG lengths and nanoparticle dimensions.* RSC Adv., 2013. **3**(17): p. 6085-6094.

69. Anastas, P. and N. Eghbali, *Green chemistry: principles and practice.* Chem. Soc. Rev., 2010. **39**(1): p. 301-12.

70. Dozie-Nwachukwu, S.O., J.D. Obayemi, Y. Danyo, G. Etuk-Udo, N. Anuku, O.S. Odusanya, K. Malatesta, C. Chi, and W.O. Soboyejo, *Biosynthesis of Gold Nanoparticles with Serratia Marcescens Bacteria.* Adv. Mat. Res., 2015. **1132**: p. 19-35.

71. Luty-Błocho, M., K. Pacławski, M. Wojnicki, and K. Fitzner, *The kinetics of redox reaction of gold(III) chloride complex ions with l-ascorbic acid.* Inorg. Chim. Acta, 2013. **395**: p. 189-196.

72. Annur, S., S.J. Santosa, and N. Hidayat Aprilita, *pH Dependence of Size Control in Gold Nanoparticles Synthesized at Room Temperature.* Orient. J. Chem., 2018. **34**(5): p. 2305-2312.

73. Jun, H., T. Fabienne, M. Florent, P.E. Coulon, M. Nicolas, and S. Olivier, *Understanding of the size control of biocompatible gold nanoparticles in millifluidic channels.* Langmuir, 2012. **28**(45): p. 15966-74.

74. Tyagi, H., A. Kushwaha, A. Kumar, and M. Aslam, *pH-dependent synthesis of stabilized gold nanoparticles using ascorbic acid.* Int. j. nanotechnol. nanosci, 2012. **10**(4): p. 857-860.

75. Mukai, K., M. Nishimura, and S. Kikuchi, *Stopped-flow investigation of the reaction of vitamin C with tocopheroxyl radical in aqueous triton X-100 micellar solutions. The structure-activity relationship of the regeneration reaction of tocopherol by vitamin C.* J. Biol. Chem., 1991. **266**(1): p. 274-8.

76. Liu, J., G. Qin, P. Raveendran, and Y. Ikushima, *Facile "green" synthesis, characterization, and catalytic function of beta-D-glucose-stabilized Au nanocrystals.* Chemistry (Easton), 2006. **12**(8): p. 2131-8.

77. Raveendran, P., J. Fu, and S.L. Wallen, *A simple and "green" method for the synthesis of Au, Ag, and Au–Ag alloy nanoparticles.* Green Chem., 2006. **8**(1): p. 34-38.

78. Sylvestre, J.P., A.V. Kabashin, E. Sacher, M. Meunier, and J.H. Luong, *Stabilization and size control of gold nanoparticles during laser ablation in aqueous cyclodextrins.* J. Am. Chem. Soc., 2004. **126**(23): p. 7176-7.

79. Schauermann, S., N. Nilius, S. Shaikhutdinov, and H.J. Freund, *Nanoparticles for heterogeneous catalysis: new mechanistic insights.* Acc. Chem. Res., 2013. **46**(8): p. 1673-81.

80. Lee, S.H., K.H. Bae, S.H. Kim, K.R. Lee, and T.G. Park, *Amine-functionalized gold nanoparticles as non-cytotoxic and efficient intracellular siRNA delivery carriers.* Int. J. Pharm., 2008. **364**(1): p. 94-101.

81. Hong, E.J., D.G. Choi, and M.S. Shim, *Targeted and effective photodynamic therapy for cancer using functionalized nanomaterials.* Acta Pharm. Sin. B, 2016. **6**(4): p. 297-307.

82. Dreaden, E.C., L.A. Austin, M.A. Mackey, and M.A. El-Sayed, *Size matters: gold nanoparticles in targeted cancer drug delivery.* Ther. Deliv., 2012. **3**(4): p. 457-478.

83. Beloglazova, N.V., I.Y. Goryacheva, R. Niessner, and D. Knopp, *A comparison of horseradish peroxidase, gold nanoparticles and qantum dots as labels in non-instrumental gel-based immunoassay.* Microchim Acta, 2011. **175**(3-4): p. 361-367.

84. Wang, X., R. Niessner, D. Tang, and D. Knopp, *Nanoparticle-based immunosensors and immunoassays for aflatoxins.* Anal. Chim. Acta, 2016. **912**: p. 10-23.

85. Penn, S.G., L. He, and M.J. Natan, *Nanoparticles for bioanalysis.* Curr. Opin. Chem. Biol., 2003. **7**(5): p. 609-15.

86. Tokonami, S., Y. Yamamoto, H. Shiigi, and T. Nagaoka, *Synthesis and bioanalytical applications of specific-shaped metallic nanostructures: a review.* Anal. Chim. Acta, 2012. **716**: p. 76-91.

87. Cai, W., T. Gao, H. Hong, and J. Sun, *Applications of gold nanoparticles in cancer nanotechnology.* Nanotechnol. Sci. Appl., 2008. **1**: p. 17-32.

88. Wilson, R., *The use of gold nanoparticles in diagnostics and detection.* Chem. Soc. Rev., 2008. **37**(9): p. 2028-45.

89. Saha, K., S.S. Agasti, C. Kim, X. Li, and V.M. Rotello, *Gold nanoparticles in chemical and biological sensing.* Chem. Rev., 2012. **112**(5): p. 2739-79.

90. Kreibig, U. and L. Genzel, *Optical absorption of small metallic particles.* Surf. Sci., 1985. **156**: p. 678-700.

91. Li, N., D. Liu, and H. Cui, *Metal-nanoparticle-involved chemiluminescence and its applications in bioassays.* Anal. Bioanal. Chem., 2014. **406**(23): p. 5561-71.

92. Augusto, F.A., G.A. de Souza, S.P. de Souza Junior, M. Khalid, and W.J. Baader, *Efficiency of electron transfer initiated chemiluminescence.* Photochem. Photobiol., 2013. **89**(6): p. 1299-317.

93. Francis, P.S., N.W. Barnett, S.W. Lewis, and K.F. Lim, *Hypohalites and related oxidants as chemiluminescence reagents: a review.* Luminescence, 2004. **19**(2): p. 94-115.

94. Marquette, C.A. and L.J. Blum, *Applications of the luminol chemiluminescent reaction in analytical chemistry.* Anal. Bioanal. Chem., 2006. **385**(3): p. 546-54.

95. Li, Q., L. Zhang, J. Li, and C. Lu, *Nanomaterial-amplified chemiluminescence systems and their applications in bioassays.* TrAC, Trends Anal. Chem., 2011. **30**(2): p. 401-413.

96. Zhang, Z.F., H. Cui, C.Z. Lai, and L.J. Liu, *Gold nanoparticle-catalyzed luminol chemiluminescence and its analytical applications.* Anal. Chem., 2005. **77**(10): p. 3324-9.

97. Liu, W., J. Luo, Y. Guo, J. Kou, B. Li, and Z. Zhang, *Nanoparticle coated paper-based chemiluminescence device for the determination of L-cysteine.* Talanta, 2014. **120**: p. 336-41.

98. Li, S., X. Li, J. Xu, and X. Wei, *Flow-injection chemiluminescence determination of polyphenols using luminol-NaIO4-gold nanoparticles system.* Talanta, 2008. **75**(1): p. 32-7.

99. Fan, A., C. Lau, and J. Lu, *Hydroxylamine-amplified gold nanoparticles for the naked eye and chemiluminescent detection of sequence-specific DNA with notable potential for single-nucleotide polymorphism discrimination.* Analyst, 2009. **134**(3): p. 497-503.

100. Zhang, Z.F., H. Cui, and M.J. Shi, *Chemiluminescence accompanied by the reaction of gold nanoparticles with potassium permanganate.* Phys. Chem. Chem. Phys., 2006. **8**(8): p. 1017-21.

101. He, Y. and H. Cui, *Label free and homogeneous histone sensing based on chemiluminescence resonance energy transfer between lucigenin and gold nanoparticles.* Biosens. Bioelectron., 2013. **47**: p. 313-7.

102. Cui, H., Z.F. Zhang, M.J. Shi, Y. Xu, and Y.L. Wu, *Light emission of gold nanoparticles induced by the reaction of bis(2,4,6-trichlorophenyl) oxalate and hydrogen peroxide.* Anal. Chem., 2005. **77**(19): p. 6402-6.

103. Cui, H., Z.F. Zhang, and M.J. Shi, *Chemiluminescent reactions induced by gold nanoparticles.* J. Phys. Chem. B, 2005. **109**(8): p. 3099-103.

104. Cui, H., J.-Z. Guo, N. Li, and L.-J. Liu, *Gold Nanoparticle Triggered Chemiluminescence between Luminol and AgNO3.* J. Phys. Chem. C, 2008. **112**(30): p. 11319-11323.

105. Luo, J., X. Cui, W. Liu, and B. Li, *Highly sensitive homogenous chemiluminescence immunoassay using gold nanoparticles as label.* Spectrochim. Acta. A Mol. Biomol. Spectrosc., 2014. **131**: p. 243-8.

106. Zhang, Y., J. Liu, T. Liu, H. Li, Q. Xue, R. Li, L. Wang, Q. Yue, and S. Wang, *Label-free, sensitivity detection of fibrillar fibrin using gold nanoparticle-based chemiluminescence system.* Biosens. Bioelectron., 2016. **77**: p. 111-5.

107. Islam, M.S. and S.H. Kang, *Chemiluminescence detection of label-free C-reactive protein based on catalytic activity of gold nanoparticles.* Talanta, 2011. **84**(3): p. 752-8.

108. Qi, Y., B. Li, and Z. Zhang, *Label-free and homogeneous DNA hybridization detection using gold nanoparticles-based chemiluminescence system.* Biosens. Bioelectron., 2009. **24**(12): p. 3581-6.

109. Qi, Y. and B. Li, *A sensitive, label-free, aptamer-based biosensor using a gold nanoparticle-initiated chemiluminescence system.* Chemistry (Easton), 2011. **17**(5): p. 1642-8.

110. Duan, C., H. Cui, Z. Zhang, B. Liu, J. Guo, and W. Wang, *Size-Dependent Inhibition and Enhancement by Gold Nanoparticles of Luminol−Ferricyanide Chemiluminescence.* J. Phys. Chem. C, 2007. **111**(12): p. 4561-4566.

111. Safavi, A., G. Absalan, and F. Bamdad, *Effect of gold nanoparticle as a novel nanocatalyst on luminol-hydrazine chemiluminescence system and its analytical application.* Anal. Chim. Acta, 2008. **610**(2): p. 243-8.

112. Lin, J.M. and M. Liu, *Chemiluminescence from the decomposition of peroxymonocarbonate catalyzed by gold nanoparticles.* J. Phys. Chem. B, 2008. **112**(26): p. 7850-5.

113. Dong, Y.P., T.T. Gao, X.F. Chu, J. Chen, and C.M. Wang, *Flow injection-chemiluminescence determination of ascorbic acid based on luminol–ferricyanide–gold nanoparticles system.* J. Lumin., 2014. **154**: p. 350-355.

114. Qi, Y. and B. Li, *Enhanced effect of aggregated gold nanoparticles on luminol chemiluminescence system and its analytical application.* Spectrochim. Acta. A Mol. Biomol. Spectrosc., 2013. **111**: p. 1-6.

115. Wei, G.T., F.K. Liu, and C.R. Wang, *Shape separation of nanometer gold particles by size-exclusion chromatography.* Anal. Chem., 1999. **71**(11): p. 2085-91.

116. Hanauer, M., S. Pierrat, I. Zins, A. Lotz, and C. Sonnichsen, *Separation of nanoparticles by gel electrophoresis according to size and shape.* Nano Lett., 2007. **7**(9): p. 2881-2885.

117. Hens, Z. and J.C. Martins, *A Solution NMR Toolbox for Characterizing the Surface Chemistry of Colloidal Nanocrystals.* Chem. Mater., 2013. **25**(8): p. 1211-1221.

118. Yue, J., J.C. Schouten, and T.A. Nijhuis, *Integration of Microreactors with Spectroscopic Detection for Online Reaction Monitoring and Catalyst Characterization.* Ind. Eng. Chem. Res., 2012. **51**(45): p. 14583-14609.

119. Mehlhorn, A., P. Rahimi, and Y. Joseph, *Aptamer-Based Biosensors for Antibiotic Detection: A Review.* Biosensors (Basel), 2018. **8**(2).

120. Xia, X., Q. He, Y. Dong, R. Deng, and J. Li, *Aptamer-based Homogeneous Analysis for Food Control.* Curr. Anal. Chem., 2020. **16**(1): p. 4-13.

121. Huang, C.C., Y.F. Huang, Z. Cao, W. Tan, and H.T. Chang, *Aptamer-modified gold nanoparticles for colorimetric determination of platelet-derived growth factors and their receptors.* Anal. Chem., 2005. **77**(17): p. 5735-41.

122. Li, H. and L.J. Rothberg, *Label-free colorimetric detection of specific sequences in genomic DNA amplified by the polymerase chain reaction.* J. Am. Chem. Soc., 2004. **126**(35): p. 10958-61.

123. Kraemer, S., J.D. Vaught, C. Bock, L. Gold, E. Katilius, T.R. Keeney, N. Kim, N.A. Saccomano, S.K. Wilcox, D. Zichi, and G.M. Sanders, *From SOMAmer-based biomarker discovery to diagnostic and clinical applications: a SOMAmer-based, streamlined multiplex proteomic assay.* PLoS One, 2011. **6**(10): p. e26332.

124. Mirkin, C.A., R.L. Letsinger, R.C. Mucic, and J.J. Storhoff, *A DNA-based method for rationally assembling nanoparticles into macroscopic materials.* Nature, 1996. **382**(6592): p. 607-9.

125. Lee, C.Y., C.L. Chang, Y.N. Wang, and L.M. Fu, *Microfluidic mixing: a review.* Int. J. Mol. Sci., 2011. **12**(5): p. 3263-87.

126. Cai, G., L. Xue, H. Zhang, and J. Lin, *A Review on Micromixers.* Micromachines (Basel), 2017. **8**(9).

127. Bayareh, M., M.N. Ashani, and A. Usefian, *Active and passive micromixers: A comprehensive review.* Chem Eng Process, 2020. **147**.

128. Cao, Q., X. Han, and L. Li, *An active microfluidic mixer utilizing a hybrid gradient magnetic field.* Int. J. Appl. Electromagn. Mech., 2015. **47**(3): p. 583-592.

129. Phan, H.V., M.B. Coskun, M. Sesen, G. Pandraud, A. Neild, and T. Alan, *Vibrating membrane with discontinuities for rapid and efficient microfluidic mixing.* Lab Chip, 2015. **15**(21): p. 4206-16.

130. Williams, D.F., F. Ndagijimana, K.A. Remley, J.A. Dunsmore, and S. Hubert, *Scattering-parameter models and representations for microwave mixers.* IEEE Trans. Microwave Theory Tech., 2005. **53**(1): p. 314-321.

131. Wu, Y., Y. Ren, Y. Tao, L. Hou, Q. Hu, and H. Jiang, *A novel micromixer based on the alternating current-flow field effect transistor.* Lab Chip, 2016. **17**(1): p. 186-197.

132. Lee, C.-Y., W.-T. Wang, C.-C. Liu, and L.-M. Fu, *Passive mixers in microfluidic systems: A review.* Chem. Eng. J., 2016. **288**: p. 146-160.

133. Raza, W., S. Hossain, and K.Y. Kim, *A Review of Passive Micromixers with a Comparative Analysis.* Micromachines (Basel), 2020. **11**(5).

Declaration of scientific contribution and summary of “Strategy for fast manufacturing of 3D hydrodynamic focusing multilayer microfluidic chips and its application for flow-based synthesis of gold nanoparticles”

Yanwei Wang [a] and Michael Seidel*[a]

Microfluidics and Nanofluidics 2021. 25(8).
https://doi.org/10.1007/s10404-021-02463-6.

In this publication, the goal of having an easy and cheap method to fabricate a 3D microfluidic chip was proposed by Michael Seidel (MS). Therefore, Yanwei Wang (YW) reviewed the available literature on fabricating method and focused on the laminated method. The application of synthesis of AuNPs was suggested by MS. The structure of the 3D microfluidic chip was designed by YW. YW designed the flow channels with CorelDRAW, cut them out with a cutting plotter, and assembled them to achieve a microreactor. The method for the synthesis of AuNPs was proposed by YW after a literature review. The synthesis was controlled with Matlab, and YW modified the program. There were bubbles and fouling problems during synthesis. MS offered a camera to monitor the synthesis. The camera was interacted with the synthesis by YW. Pictures and videos were obtained, and dye was used to show the flow profile after discussing of MS and YW. The structure of the 3D microreactor was modified, and the problems of fouling and bubbles were solved by YW. YW investigated the repeatability of the synthesis and effect of synthesis parameters. Finally, the novel fabrication method was developed, and the 3D hydrodynamic focusing microreactor was successfully applied to synthesize AuNPs. All results were discussed by MS and YW. YW wrote the manuscript and revised it together with MS.

Chapter: 1

Strategy for fast manufacturing of 3D hydrodynamic focusing multilayer microfluidic chips and its application for flow-based synthesis of gold nanoparticles

Yanwei Wang [a] and Michael Seidel*[a]

Microfluidics and Nanofluidics 2021. 25(8).
https://doi.org/10.1007/s10404-021-02463-6.

[a]Institute of Hydrochemistry, Chair of Analytical Chemistry and Water Chemistry,

Technical University of Munich, Munich, Germany.

*** Correspondence**

Michael Seidel

Michael.Seidel@mytum.de

Abstract

Fabrication of 3D microfluidic devices is normally quite expensive and tedious. A strategy was established to rapidly and effectively produce multilayer 3D microfluidic chips which are made of two layers of poly(methyl methacrylate) (PMMA) sheets and three layers of double-sided pressure sensitive adhesive (PSA) tapes. The channel structures were cut in each layer by cutting plotter before assembly. The structured channels were covered by a PMMA sheet on top and a PMMA carrier which contained threads to connect with tubing. A large variety of PMMA slides and PSA tapes can easily be designed and cut with the help of a cutting plotter. The microfluidic chip was manually assembled by a simple lamination process.The complete fabrication process from device design concept to working device can be completed in minutes without the need of expensive equipment such as laser, thermal lamination, and cleanroom. This rapid frabrication method was applied for design of a 3D hydrodynamic focusing device for synthesis of gold nanoparticles (AuNPs) as proof of concept. The fouling of AuNPs was prevented by means of a sheath flow. Different parameters such as flow rate and concentration of reagents were controlled to achieve AuNPs of various sizes. The sheet-based fabrication method offers a possibility to create complex microfluidic devicesin a rapid, cheap and easy way.

Keywords: 3D hydrodynamic microreactor; cutting plotter; laser and heat free; gold nanoparticles

1.1 Introduction

Microfluidic technology has been developed rapidly in recent decades and offers numerous applications in different scientific and industrial areas. Miniaturized systems offer unique advantages, including high analytical throughput, enhanced sensitivity, reduced reagent volumes and they are easy to couple with analytical instruments [1]. In the early days, microfluidic chips were typically composed of silicon and glass. Although glass and silicon technologies offer high precision, the fabrication methods are complex, time consuming and costly, and cleanroom facilities are required [2]. Additionally, both materials are fragile and too expensive to be used for disposable devices. Therefore, polymers started to be used as an attractive alternative material, due to their low-cost, wide range of mechanical and chemical properties, flexibility and easy processing possibilities [3]. The most popular polymers for microfluidic systems are poly(dimethylsiloxane) (PDMS), poly(methylmethacrylate) (PMMA), high-density polyethylene (HDPE), low density polyethylene (LDPE), polyamide 6 and SU-8. One of the most popular and traditional fabrication techniques used for microfluidic chips is soft lithography with PDMS structures made from SU-8 molds [4]. The basic procedure consists of photolithography, wet-etching and bonding which take a long time from the design to the prototype. Moreover, special training is required for the fabrication of molds and the operation of the equipment. These drawbacks are currently slowing down the development of microchips, especially in research institutions without specialized facilities. Hence, it is crucial to establish rapid prototyping and low-cost alternatives for the fabrication of micro-devices [5]. Non-lithographic fabrication techniques are a potential alternative to produce micro-devices for researchers who have difficulty to access specialized fabrication facilities and equipment. Rapid cutting by a plotter, also known as Xurography, is one of the non-lithographic techniques using a drag knife printer to generate the master molds, or to directly fabricate the micro-devices [6]. Compared with other non-lithographic methods such as LaserJet [7, 8], inkjet printers [9] and 3D printing [10], using a cutting plotter is significantly cheaper, requires no pumping system, and leaves no combustion residues. The independently pre-cut layers can be bonded together to form channels and microfluidic features [11]. Two of the most common and straightforward bonding methods are adhesives and thermal bonding. However, thermal bonding is not possible with all materials. The main disadvantage of thermal bonding is the possible warping of features from the heating or cooling. Except for 3D printing, layered devices are the fastest and easiest way to fabricate microfluidic channels for most

applications. 3D printed microfluidic devices are limited to straight channels and the way to remove the support material could damage the channel [12]. Furthermore, transparent materials can be used in laminated chips for applications such as chemiluminescence and fluorescence, and it is almost impossible to optically observe the inside of a channel for 3D printing. Recently used microfluidic chips manufactured by the lamination method were summarized in **Table 1.1**

Table 1.1 Summary of laminated method for fabrication of microfluidic chips.

Material	**Cutting methods**	**Bonding methods**	**Drawbacks**	**Ref**
Laminating pouches (Scotch TP3854)	Cutting plotter	Thermal lamination machine		[13]
Polyethylene terephthalate (PET) film	Cutting plotter	Thermal lamination machine	Warping of features from the heating or cooling	[14]
Film of fluoropolymers	Cutting plotter	Heat and pressure		[15]
Poly(dimethylsiloxane) (PDMS) membranes	Cutting plotter	Plasma bonding	Time consuming	[16]
Polymethylmethacrylate (PMMA)	CO_2 laser	Double-sided tape		[8]
Acrylic sheets and Hybrislip^{TM} sheets	CO_2 laser	Adhesive transfer tapes	Bulges form around microstructure and the laser leaves significant debris and pyrolysis products	[17]
Polymethylmethacrylate (PMMA)	CO_2 laser	Thermocompressor		[7]

Synthesis of nanoparticles is a popular application for microchips with narrower size distributions and faster reaction rates compared to conventional batch synthesis [18-21]. However, significant fouling of the micro-channels is often observed due to deposition of nanoparticles onto the reactor walls [18]. In an ideal flow focusing device, the central flow should be compressed both horizontally and vertically in order to obtain uniform fluid velocity which is also called three-

dimensional (3D) focusing. In this case, sheath streams can insulate nanoparticles from channel walls and fouling can be avoided [22].

In this work, we propose an easy, cheap, rapid and universal way for the fabrication of laminate PMMA-based 3D flow-focused microreactors. The PMMA sheets and double-sided PSA tape layers were cut using a low-cost cutting plotter. The layers were then assembled with the aid of an alignment tool. 3D microfluidic structure was bonded by a lamination process using mild pressure with a roller. It is a strategy to develop highly flexible plastic microreactors without masks and molds [23] and cleanroom requirements due to the absence of lithographic methods is eliminated. Therefore, this technique is adaptive for research institutions without specialized microsystem engineering of lab-on-chip devices. For proof-of-concept, rapid fabrication technique of microfluidic device is applied to produce 3D hydrodynamic focusing microreactors for synthesis of gold nanoparticles (AuNPs) without fouling. The flow-based reaction was based on the online reduction of Au(III) with ascorbic acid (AA). AuNPs were synthesized at room temperature, unlike with citrate solutions where heating is required [24]. Compared with the strong reducing agent sodium borohydride ($NaBH_4$), AA cannot react with water and therefore, no gas is generated. AuNPs were capped with polyvinylpyrrolidone (PVP) for stability. It could be shown by UV-Vis spectroscopy that reproducible AuNPs were synthesized. The concept of flow-based modulation of size and properties for AuNPs was implemented by the 3D hydrodynamic focusing microreactor [25, 26].

1.2 Materials and methods

1.2.2 Devices and software for fabrication of microchip

The layout of the microreactor was designed with the software CorelDRAW. The CorelDRAW plug-in Cutting Master 3 from Graphtec Corporation (Yokohama, Japan) was used for communication with the cutting plotter. The digital cutting plotter (Graphtec CE6000-40) was supplied by Graphtec Corporation (Yokohama, Japan) to slit chips into sheets. Cutting conditions and settings were executed via the Cutting Master 3. Programmable resolution was 0.025 mm, and the media type was up to 0.25 mm thickness. All sheets were assembled in an alignment tool which was supplied by our in-house workshop.

1.2.1 Materials for the fabrication of microreactor

The microfluidic reactor was constructed out of three layers of PMMA sheets, three layers of double-sided PSA tapes and one PMMA carrier sheet. The PMMA sheets with a thickness of 0.2 mm were supplied by modulor material total (Berlin, Germany). The PSA tape (ARcare 90106) was bought from Adhesive Research (Glen Rock, PA, USA). The carrier sheet with a thickness of 10 mm was fabricated by our in-house workshop. The fabricated PMMA carrier contained threads (1/4" - 28 UNF) to allow the connection with PTFE tubing.

1.2.3 Synthesis of AuNPs

PVP-capped colloidal AuNPs were synthesized by the reduction of tetrachloroaurate (III) ions via AA as described elsewhere [27]. Gold(III) chloride trihydrate ($HAuCl_4 \cdot 3H_2O$)(≥ 99.9% trace metal basis) and reagent grade (≥ 99%) crystalline L-ascorbic acid (AA or AsH_2) were supplied from Sigma Aldrich (USA). The gold precursor stream was 1 mM aqueous $HAuCl_4$ solution containing 1% (w/v) PVP with average MW ~ 29,000 (powder, Sigma Aldrich, Germany) as the capping agent. The reducing agent stream was 20 mM aqueous AA solution with 0.2 M NaOH solution (Sigma-Aldrich, reagent grade, ≥ 98%, pellets). The pH of the solution was measured with a FiveEasy pH meter FP20 (Mettler Toledo, Columbus, OH, USA). This reaction was achieved by a 3D flow focusing the AA sheath streams to the gold precursor stream. Before each synthesis process, the microreactor was flushed twice, first with 0.01% PVP solution to push all bubbles out then the second time with a portion of the reducing reagents to change the pH in the microreactor channel. The syringes then pushed the reagents into the channel at a controlled flow rate ratio (gold precursor: reducing reagents, 1:10). The synthesized AuNPs were then collected in a vial at the outlet of the microreactor. AuNPs were synthesized using reducing agents with different pH by adding different amounts of 0.2 M NaOH. The pH of the original reducing agent was adjusted to 4.30, 5.66, 7.10, 7.61, 10.32, 10.91 by adding 200 µl, 400 µl, 510 µl, 520 µl, 600 µl and 700 µl 0.2 M NaOH to 5 ml 20 mM AA solution, respectively. Various flow rates and concentrations of reagents were also investigated.

Reagents were supplied to the microreactor via three glass syringes (Innovative Labor Systeme GmbH, Germany) connected to a 6-port valve (Cavro Smart Valve, Tecan Group Ltd., Switzerland). One port of each valve was connected to an inlet of the microreactor, one to the waste to clean the syringes, and the remaining four ports were used for the uptake of reagents and

cleaning solution. The glass syringes were operated by three custom made pumps (GWK Präzisionstechnik, Munich, Germany) which were controlled with Matlab (The MathWorks Inc., USA) by a host computer connected via an Ethernet cable. The reaction process was observed and recorded using a microscope camera (1.3 M pixels, 10x, 60x, 100x magnification) (Traveler USB Mikroskop, Supra, Germany). The synthesis and washing processes with different conditions can be controlled and modified in the Matlab program. In this way, all operations could be performed in an automated way. The combined setup is shown in **Figure 1.1**. All waste was collected by a specific company and disposed of in an environmentally friendly way.

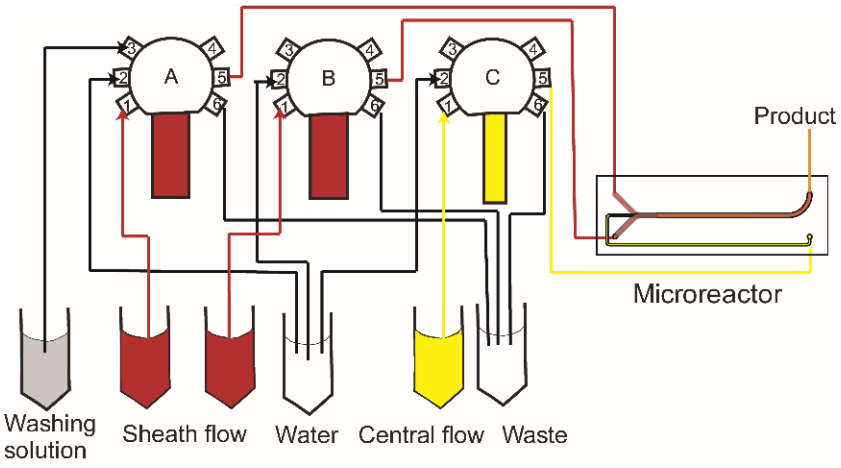

Figure 1.1 Scheme of 3D hydrodynamic focusing microreactor connected to reactant streams. Reagents were supplied to the microreactor via three glass syringes connected to a 6-port valve. One port of each valve was connected to an inlet of the microreactor, and other ports were used for the uptake of reagents, cleaning solution. The setup was controlled automatically by Matlab.

1.2.4 Characterization of AuNPs

A SPECORD 250 PLUS UV/Vis spectrometer (Analytik Jena, Jena, Germany) was used to record the UV-Vis absorption spectra of the gold nanoparticle suspensions. The spectrometer uses a deuterium lamp and a halogen lamp to generate electromagnetic waves of ultraviolet and visible wavelengths. A beam of light with a wavelength ranging from 400 to 900 nm was used for measurement. Disposable polystyrene cuvettes (UV cuvette semi-micro, 1.5 - 3.0 ml, BRAND GMBH, Germany) were used for containing samples and reference. Since all solutions were prepared in ultrapure water, ultrapure water was used as the reference sample. Scanning electron microscopy (SEM) images were acquired on a model Sigma 300 VP microscope (Zeiss Gemini).

The samples were analyzed with an InLens detector using an acceleration voltage of 10 kV, a 30 µm aperture and a working distance of about 1.4 mm.

1.3 Results and discussion

1.3.1 Design and fabrication of a microreactor for the online synthesis of AuNPs

Fouling of nanoparticles by unwanted deposition on surfaces occurs regularly in microstructured devices [28]. The hydrophobization of inner walls of the reactor through silanization is a general method to suppress fouling in glass chips [18, 25]. PMMA is a hydrophobic polymer, easy to handle and process with low cost. Moreover, it can be easily modified into a super-hydrophobic PMMA film [29]. Hydrophobic material suppresses fouling within the inner walls of the reactor due to an increase in slip boundary conditions which reduce wetting and enhance shear rate on the walls [30]. Besides the material itself, the application of a 3D hydrodynamic flow by focusing the central stream with the sheath streams as shown in **Figure 1.2 a** is supposed to prevent fouling in microfluidic devices. A separation between the central stream and the channel walls can be achieved, thereby reducing particle-wall interactions. The microfluidic reactor was constructed of seven layers of alternating PMMA sheets and PSA tapes. **Figure 1.2 b** depicts the scheme of the laminated microfluidic device. The central layer had a channel with a width of 0.7 mm in the first part for the inlet of central flow and then extended to a width of 1.5 mm for the mixing. This layer came from a PSA tape with a thickness of 0.12 mm. Then, the tape was laminated between two PMMA sheets. Afterwards, two PSA tapes with a channel for sheath flow were applied on both sides. The device was closed by a 0.5 mm PMMA sheet on the top and a PMMA carrier with a thickness of 10 mm on the bottom with three inlet and one outlet drill threads holes (1/4” - 28 UNF). The main dimensions were shown in **Figure S1.1**. The difficulty in designing and fabricating 3D hydrodynamic focusing microreactor was solved by the simple assembly process of layering pre-cut PMMA sheets and PSA tapes.

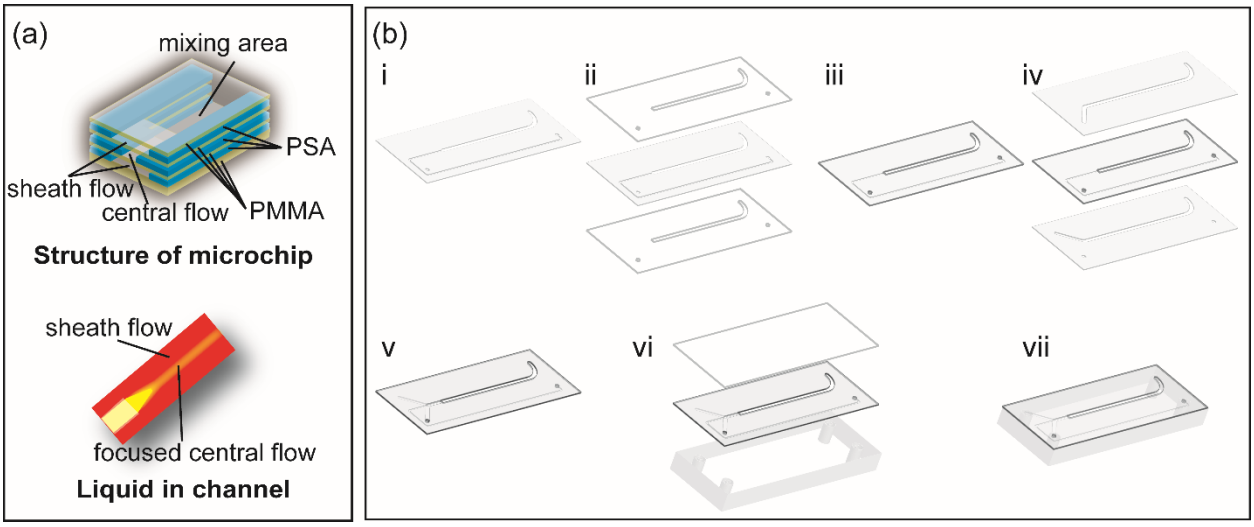

Figure 1.2 (a) Scheme of the 3D microfluidic reactor designed for creation of a central stream by hydrodynamic focusing with a sheath stream. The sheath flow channels were wider, and they were applied on both top and bottom of central flow channel. Therefore, the central flow was focused horizontally and vertically to the center. **(b)** Preparation scheme for the laminated 3D flow focusing device: (i) central layer was cut from PSA tape with digital cutting plotter; (ii-iii) central layer was sandwiched between two PMMA sheets; (iv-v) sheath stream support channels were applied to the top and bottom of the central channel; (vi-vii) cover slide and PMMA carrier with threaded holes for tube connection were applied to yield the final completed device.

One layer of the microfluidic reactor was processed by a cutting plotter as shown in **Figure 1.3 a**. (i) A double-sided PSA tape was adhered onto the repositionable adhesive surface of a reusable cutting mat. (ii) After a customized microfluidic reactor design was generated, the drawing was loaded onto the cutter software. The cutting plotter cut the design out. (iii) While the cut-out double-sided PSA tape was still adhered onto the reusable cutting mat, the cut pattern was carefully removed using tweezers. The PMMA sheets were created using the same method. The sheets were manually assembled together with a mold tool for alignment. The mold had the same size as all the sheets which ensured that the individual layers were aligned correctly. The roll above can be adjusted to exert pressure on the sheets and made sure that the microchip was sealed. The whole process is shown in **Figure 1.3 b**. (i) PSA tape is put in the mold. (ii) The top protective layer of the cut double-sided PSA tape is peeled away revealing the top permanent adhesive surface. (iii) The pre-cut transparent PMMA sheet is applied onto the top of the permanent adhesive surface in the mold. (iv) Pressure is exerted by the roller to bind them together and make sure not to cause any air bubbles or wrinkles in the whole assembly. 3D microfluidic devices can be fabricated by

repeating the above steps. The images of each step for fabrication of microreactor were shown in **Figure 1.3 c**.

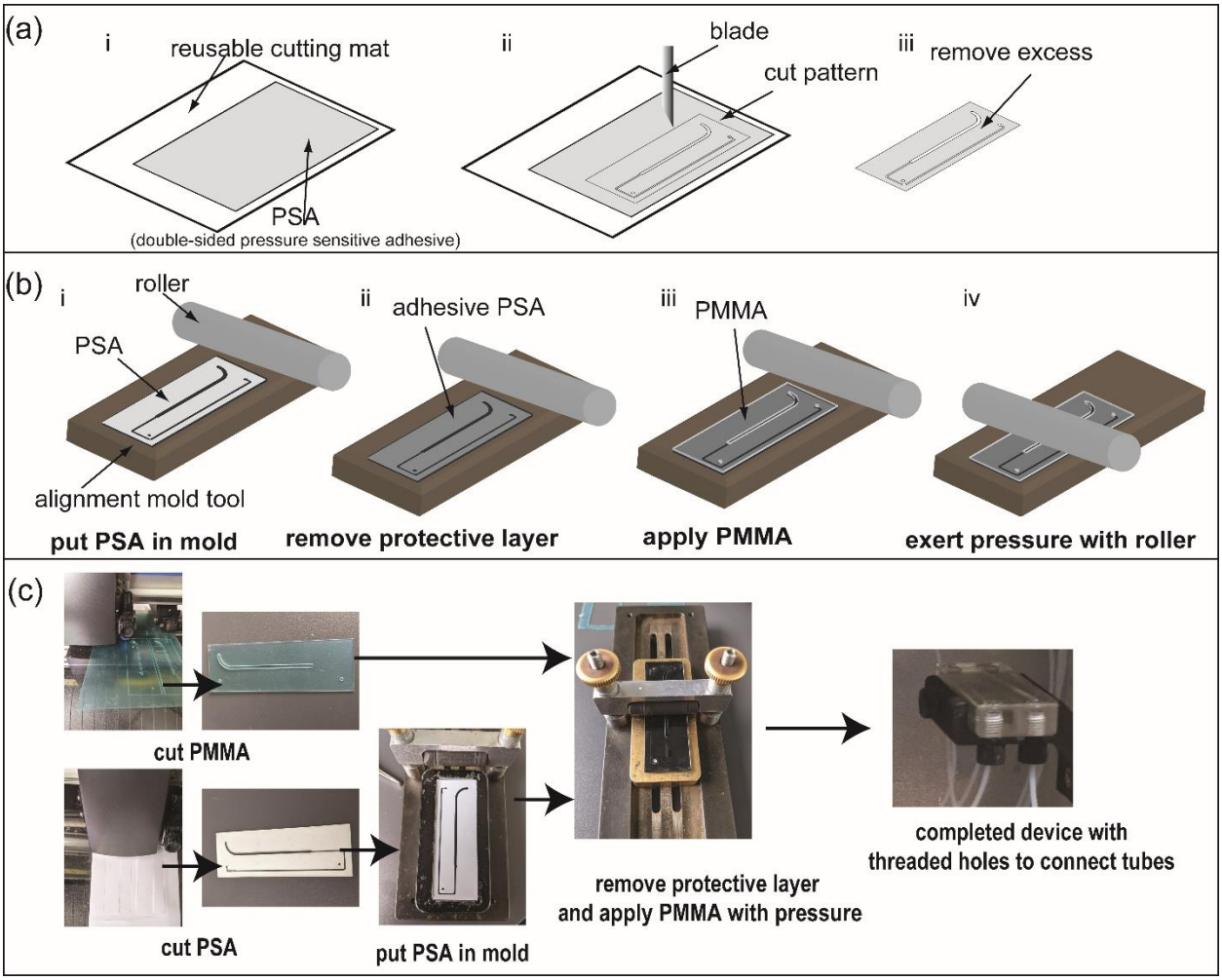

Figure 1.3 (a) Process scheme for cutting one layer of the chip: (i) the PSA attached on a reusable cutting mat, (ii) the pattern was cut out by cutting plotter, (iii) remove excess part and get the final chip layer. **(b)** Process scheme of assembling layers together. (i) PSA tape is put in the mold. (ii) The top protective layer of the PSA tape is peeled away revealing the top permanent adhesive surface. (iii) PMMA sheet is applied onto the top of the permanent adhesive surface in the mold. (iv) Pressure is exerted by the roller to bind them together. **(c)** Process image for cutting layers and assemble them together to get a complete device.

1.3.2 Comparison of 2D and 3D microreactor

Our first flow-based microreactor was designed as depicted in **Figure 1.4 a**. First half of the central PSA layer was used as inlet for the gold precursor and second half for mixing of all the reagents. Reducing agents were pumped through the PSA channel above and below the central layer. However, when it was used for the online synthesis of AuNPs, there were some challenges to be

addressed. First of all, some small bubbles stuck in the interface and then converged into a big one as shown in **Figure 1.4 a**. The big bubble could not be flushed out by liquid. In this case, it interfered with the flow pattern and interrupted the continuous production. Secondly, the central PSA layer was so thin that it did not offer enough space for mixing. Synthesized AuNPs easily fouled on the wall and finally blocked the channel. Additionally, all the reagents were directly mixed together in the interface and the sheath stream was not able to focus the central stream. All these issues indicate that this type of microreactor rather has the properties of a 2D chip even though it technically is defined as 3D. The microreactor was then modified by extending the sheath flow channel to the outlet. The PMMA layer between the central flow layer and sheath flow layer was opened from the interface for mixing as shown in **Figure 1.4 b**. In this case, no bubbles blocked the channel. Additionally, the mixing area was enlarged and offered more space. Also, the corner was changed to a curve which allowed a stable flow and reduced small bubbles. In the 3D microfluidic reactor, the central stream was focused in the centre both vertically and horizontally. As no AuNPs can contact the channel wall, the microreactor was clean all the time as shown in in **Figure 1.4 b**.

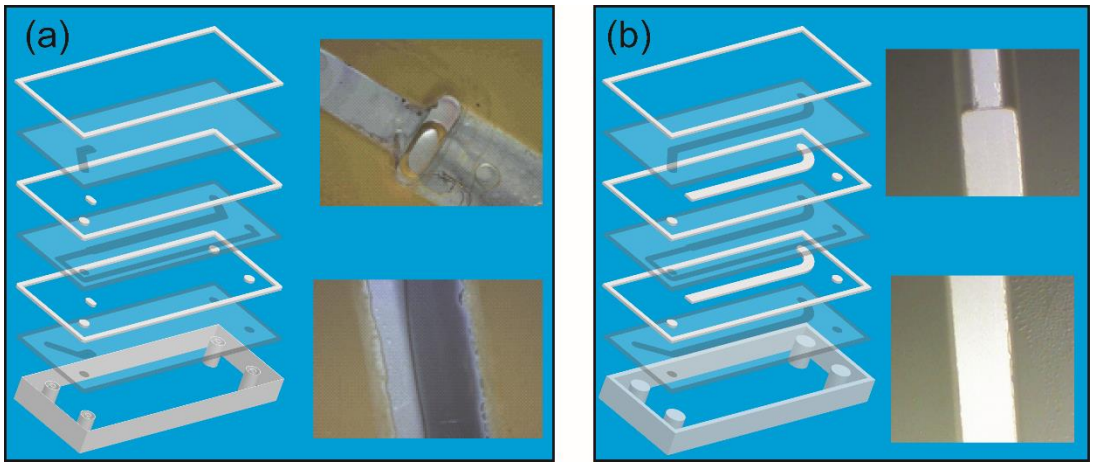

Figure 1.4 Design of microreactors with inserted pictures of interfaces and mixing channels **(a)**2D microfluidic reactor which generated bubbles and fouling**. (b)** 3D microfluidic reactor and image of the flow channels showing no fouling. The reactant stream flow rates ($HAuCl_4$/AA) were 1/10 µl/s. The pH of the reducing agent was 8.

1.3.3 Effect of various interfaces

The interface was defined as the region where the central stream and the sheath streams start to mix (**Figure 1.5 a** and **b**). This is a crucial part, where the reaction begins to take place and is easy

to get fouling. Moreover, some bubbles could accidentally come into the system from liquid or syringes and the flow could be interrupted if they were blocked in the interface. Three different interfaces were compared, semi-circle (**Figure 1.5 c**), bevel (**Figure 1.5 d**) and right angle (**Figure 1.5 e**). It was shown that there was some fouling on the semi-circular interface (**Figure 1.5 c**) because this shape was easy to absorb and converge bubbles. The flow pattern was disturbed there and a portion of reducing agent even flowed back to react with the gold precursor and caused fouling. To reduce dead volume and solve the bubble trapping issue, the bevel interface was designed. However, there was still a problem for the bevel one, a portion of the central gold precursor flowed along the wall in the mixing area and the generated AuNPs have the chance to foul on the wall, as shown in **Figure 1.5 d**. Therefore, the interface was changed to right angle (**Figure 1.5 e**). Small bubbles were easily flushed away because the right angle did not block them. Moreover, the central stream flowed forward and entered the centre of the mixing area without having a chance to touch the mixing wall. How the central stream was focused to the centre with right angle interface was shown in **Figure S1.2**. The effect of flow rates on the focus stream was also investigated in Supplementary Materials.

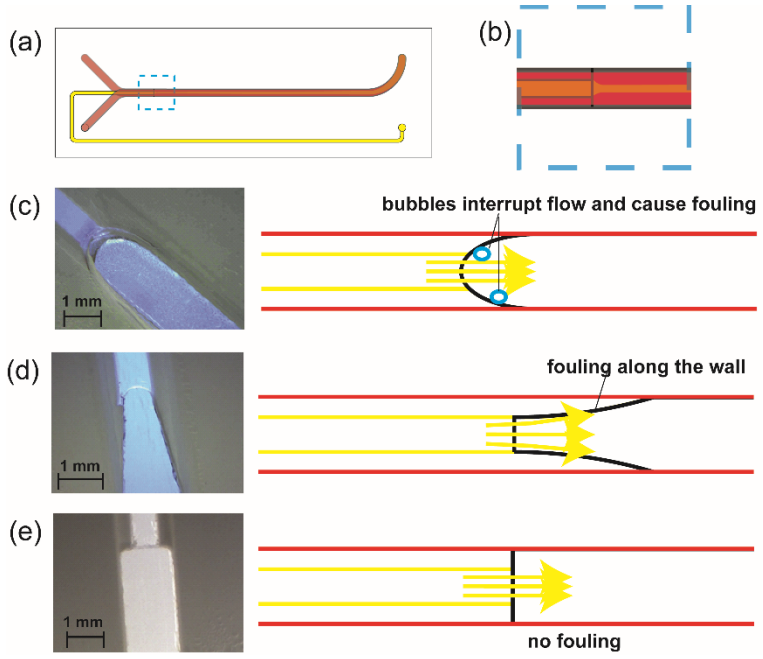

Figure 1.5 (a) Scheme of microreactor with central flow ($HAuCl_4$, yellow) and sheath flow (AA, red) mixing in interface, **(b)** scheme of interface and **(c-e)** images and schemes of different designs of interfaces (yellow line with arrow in schemes represents central stream). The reactant stream flow rates ($HAuCl_4$/AA) were 1/10 µl/s. The pH of the reducing agent was 8.

1.3.4 Online synthesis of AuNPs

The optimized 3D microfluidic reactor was used for online synthesis of PVP capped AuNPs. The synthesis reproducibility was characterized using surface plasmon resonance (SPR) band intensity and shift as indicator parameters by UV-Vis spectra. 5 syntheses were carried out using the same device and same reactant conditions. As shown in **Figure 1.6 a**, the absorbance spectra of these 5 syntheses are almost overlapping each other with a band located about 531 nm and absorbance of 0.26 ± 0.006 a.u. It demonstrated the robustness of the proposed flow system indicating size and shape consistency of the AuNPs. Also, the only peak of the absorbance spectra indicated that particles obtained by the microreactor system exhibit a uniform globular shape and no other shaped gold nanoparticle such as triangles were observed [31]. SEM image showed that the synthesized AuNPs were quasi-spherical with a diameter of 22.09 ± 2.26 nm (**Figure S1.3**).For comparison, syntheses with the same conditions were done using the previous 2D microreactor. As shown in **Figure 1.6 b**, the signal of the first synthesis was lower which means that part of the nanoparticles were fouling in the channel. The second synthesis showed a broad band indicating aggregated AuNPs from the last synthesis which were blocked in the channel. After that, the synthesis was still not repeatable as to be seen by a broad band. The 3D microreactor was then applied for synthesis of AuNPs to investigate the effects of different parameters.

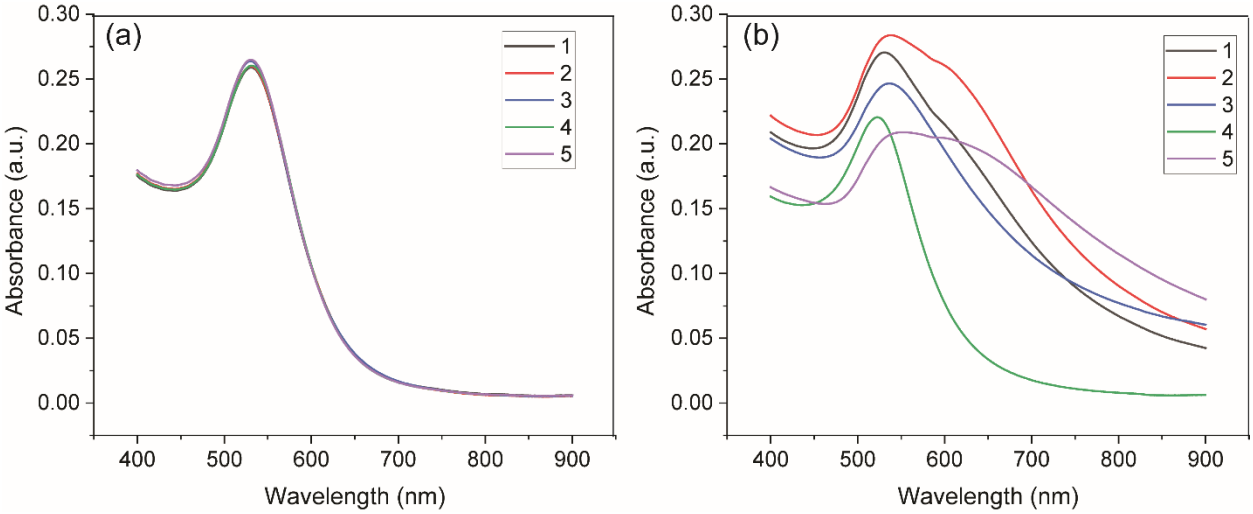

Figure 1.6 UV−Vis spectra of the AuNPs synthesized in the **(a)** 3D microreactor and the **(b)** 2D microreactor. 5 syntheses were carried out using the same device and same reactant conditions and the number in the figures represent the number of synthesis. The reactant stream flow rates ($HAuCl_4$/AA) were 3/30 µl/s. The pH of the reducing agent was 8.46.

Effect of the pH of the reducing agent. The size of the AuNPs mainly depends on the initial pH of the AA solution [18]. AA with higher pH possesses a higher reducing power than with lower pH. In this case, increasing the pH of AA can result in a faster reaction rate and more nucleation sites, and consequently in smaller sizes and higher numbers. The UV-Vis absorbance spectra are shown in **Figure 1.7 a**. From the overall view, there was a shift to a lower wavelength from 563 nm to 517 nm with the increase of the initial pH of the AA solution indicating the decrease in size of the AuNPs. The size distribution can be studied by measuring the fullwidth at half maximum (FWHM) of SPR band [32]. The resulting spectra can be separated into three areas- low pH area (pH 4.30, 5.66), middle pH area (pH 7.10, 7.61) and high pH area (pH 10.32, 10.91). The peaks in the middle pH area were narrowest with FWHM of about 50 nm which meant sizes of AuNPs were more uniform and focused. However, the spectra were wider in low and high pH areas with FWHM of around 90 nm even though they biased to the corresponding position (low pH to high wavelength and high pH to low wavelength). As shown in **Figure S1.4**, the AuNPs synthesized at low pH were large in size. And the size distribution was not uniform at both high and low pH values. Therefore, the medium pH was more suitable for the synthesis of uniform AuNPs.The divergent size distribution of AuNPs may be related to different ion species of AA in a variation of the pH solutions [33]. AsH_2 dominates the solution at lower pH values up to 4, while the percentage of AsH^- increases to reach 100% when the pH is approximately 8. When the pH is 8, AsH_2 reaches its minimum concentration. With increase of pH, the percentage of AsH^- starts to decrease and percentage of As^{2-} ions start to increase. Apparently, the mixture of different species of ascorbic acid affect the growth pattern.

Effect of the reagent concentrations. The concentration of reagents may affect the size of AuNPs. In **Figure 1.7 b**, the increased concentration of AA caused a shift to lower wavelength with higher reducing power. In **Figure 1.7 c**, with an increase of the concentration of gold precursor, the intensity of the absorbance maxima increased as well, which means that more AuNPs were synthesized. At the same time, the spectra were shifted from 540 nm to 529 nm and the FWHM decreased from 97 nm to 64 nm. This implies a smaller size and monodispersity of the nanoparticles. Due to the higher concentration of gold precursor, more nucleation sites are offered. This result also indicates that the amount of AA is sufficient for reducing.

Effect of the flow rate on nanoparticle synthesis. The UV-Vis absorbance spectra using different flow rates are shown in **Figure 1.7 d**. With increase of the flow rate, the spectra are shifted from

530 nm to 518 nm and the maximum absorbance increased by 40.8%, which indicate a smaller size and higher concentration of nanoparticles. The increased flow rate of both regents was likely to increase the diffusion of AA into HAuCl4 solution which in turn could increase the nucleation rate [26]. The more nucleation sites, the higher number of nanoparticles. With the same amount of gold precursor, a smaller size of nanoparticles was generated. Therefore, smaller size and higher number concentration of AuNPs were achieved with higher flow rate. However, when the flow rate was high enough, the effect was not significant compared with other factors, as shown in **Figure S1.5**.

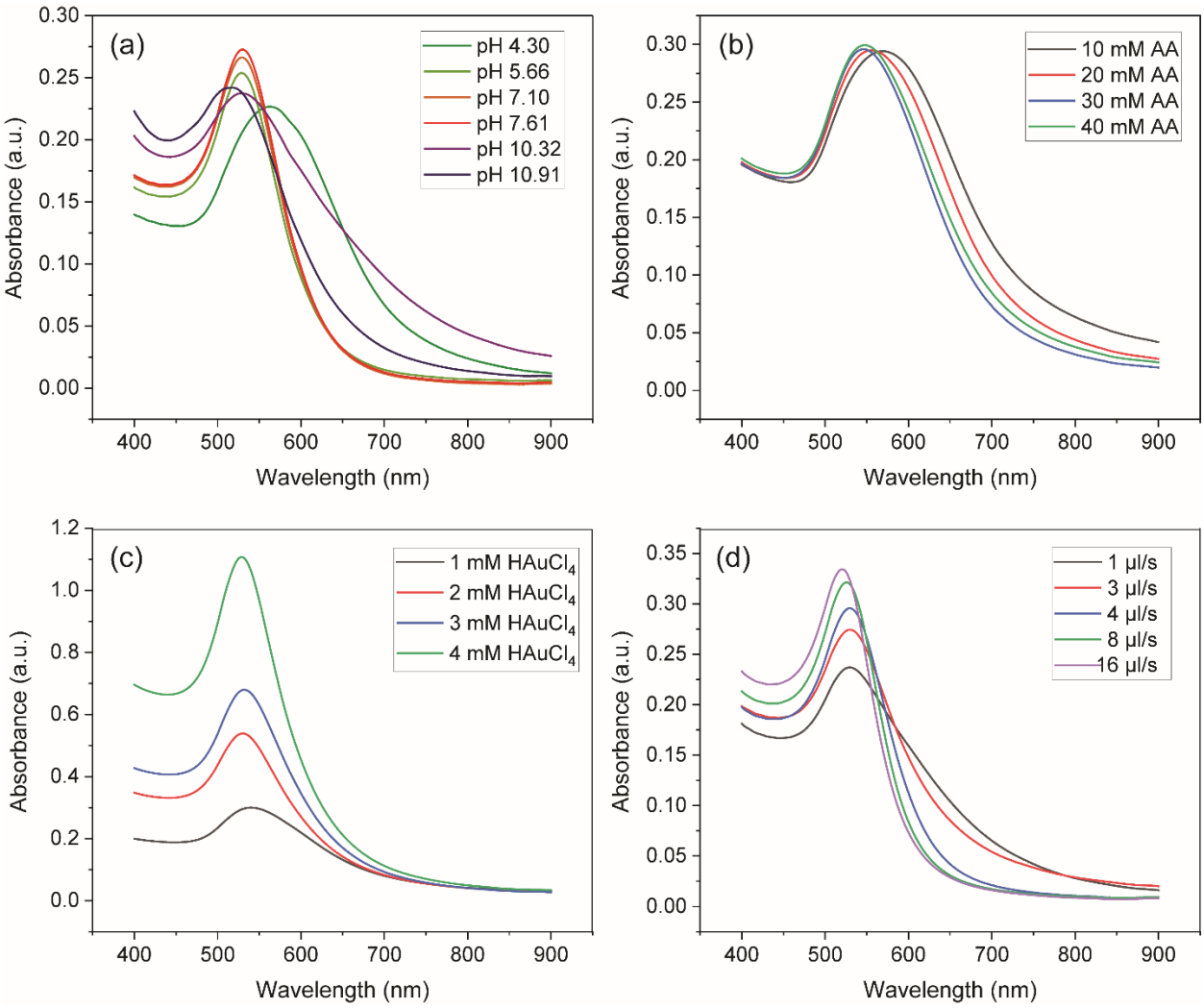

Figure 1.7 UV-Vis spectra of gold nanoparticle suspension prepared by **(a)** keeping flow rate constant at 5 ul/s and changing pH of reducing agent, **(b)** different concentrations of AA, **(c)** different concentrations of gold precursor, **(d)** keeping the flow rate ratio (gold precursor: reducing regents, 1:10) and changing the flow rate of gold precursor.

1.4 Conclusions

A cheap, easy and fast fabrication method for multilayer laminated 3D PMMA-PSA microfluidic chips was presented in this work. Sheet layers were cut by a cutting plotter which allows a fast fabrication of microfluidic structures for different applications. The assembly of the devices was carried out manually with a simple alignment tool. No thermo-compression was required and only a soft compression by a roller was sufficient. The complete fabrication process from device design concept to working device can be completed in minutes without the need of expensive equipment. This fabrication protocol was used for the generation of a 3D microreactor for the reproducible synthesis of AuNPs. Compared with a 2D microreactor, the sheath stream can focus the central flow as well as avoid fouling. The proposed nonlithographic approach offers an alternative for institutes where specialized microfabrication equipment is not available. The results presented in this paper show the successfully reproducible synthesis of spherical colloidal AuNPs without fouling using this 3D hydrodynamic flow-focused, laminated microfluidic device. This was an improvement in comparison to conventional batch reactors where the properties of nanoparticles vary from batch-to-batch. Also, the microfluidic reactor makes it possible to do online synthesis and characterizing or detection [34]. This method of flow-based plastic microfluidic chips construction can be adapted for methods of many different fields, such as pharmaceutical analysis [1], cellomics [35] and flow cytometry [36, 37].

1.5 References

1. Cui, P. and S. Wang, *Application of microfluidic chip technology in pharmaceutical analysis: A review.* J. Pharm. Anal., 2019. **9**(4): p. 238-247.
2. Patel, J.N., B. Kaminska, B.L. Gray, and B.D. Gates, *PDMS as a sacrificial substrate for SU-8-based biomedical and microfluidic applications.* J. Micromech. Microeng., 2008. **18**(9): p. 095028.
3. Song, S. and K.Y. Lee, *Polymers for Microfluidic Chips.* Macromol. Res., 2006. **14**(2): p. 121-128.
4. Kim, P., *Soft Lithography for Microfluidics: a Review.* Biochip J, 2008. **2**(1): p. 1-11.
5. Faustino, V., S.O. Catarino, R. Lima, and G. Minas, *Biomedical microfluidic devices by using low-cost fabrication techniques: A review.* J. Biomech., 2016. **49**(11): p. 2280-2292.

6. Journal of Microelectromechanical SystemsBartholomeusz, D.A.B., R.W.; Andrade, J.D., *Xurography- rapid prototyping of microstructures.* J. Microelectromech. Syst., 2005. **14**(6).

7. Chen, X., J. Shen, and M. Zhou, *Rapid fabrication of a four-layer PMMA-based microfluidic chip using CO2-laser micromachining and thermal bonding.* J. Micromech. Microeng., 2016. **26**(10): p. 107001.

8. Chen, X., T. Li, and Q.I. Gao, *A Novel Method for Rapid Fabrication of Pmma Microfluidic Chip by Laser Cutting and Sealing Integration.* Surf. Rev. Lett., 2019. **26**(08).

9. Vullev, V.I., J. Wan, V. Heinrich, P. Landsman, P.E. Bower, B. Xia, B. Millare, and G. Jones, 2nd, *Nonlithographic fabrication of microfluidic devices.* J. Am. Chem. Soc., 2006. **128**(50): p. 16062-72.

10. Chen, C., B.T. Mehl, A.S. Munshi, A.D. Townsend, D.M. Spence, and R.S. Martin, *3D-printed Microfluidic Devices: Fabrication, Advantages and Limitations-a Mini Review.* Anal. Methods, 2016. **8**(31): p. 6005-6012.

11. Jafek, A.R., S. Harbertson, H. Brady, R. Samuel, and B.K. Gale, *Instrumentation for xPCR Incorporating qPCR and HRMA.* Anal. Chem., 2018. **90**(12): p. 7190-7196.

12. Migneault, S., A. Koubaa, F. Erchiqui, A. Chaala, K. Englund, and M.P. Wolcott, *Effects of processing method and fiber size on the structure and properties of wood–plastic composites.* Compos. Part A Appl. Sci. Manuf., 2009. **40**(1): p. 80-85.

13. Hernández-Rodríguez, J.F., D. Rojas, and A. Escarpa, *Rapid and cost-effective benchtop microfabrication of disposable carbon-based electrochemical microfluidic devices.* Sens. Actuators B Chem., 2020. **324**.

14. Levis, M., N. Kumar, E. Apakian, C. Moreno, U. Hernandez, A. Olivares, F. Ontiveros, and J.J. Zartman, *Microfluidics on the fly: Inexpensive rapid fabrication of thermally laminated microfluidic devices for live imaging and multimodal perturbations of multicellular systems.* Biomicrofluidics, 2019. **13**(2): p. 024111.

15. Hizawa, T., A. Takano, P. Parthiban, P.S. Doyle, E. Iwase, and M. Hashimoto, *Rapid prototyping of fluoropolymer microchannels by xurography for improved solvent resistance.* Biomicrofluidics, 2018. **12**(6): p. 064105.

16. Cosson, S., L.G. Aeberli, N. Brandenberg, and M.P. Lutolf, *Ultra-rapid prototyping of flexible, multi-layered microfluidic devices via razor writing.* Lab Chip, 2015. **15**(1): p. 72-6.

17. Nath, P., D. Fung, Y.A. Kunde, A. Zeytun, B. Branch, and G. Goddard, *Rapid prototyping of robust and versatile microfluidic components using adhesive transfer tapes.* Lab Chip, 2010. **10**(17): p. 2286-91.

18. Wagner, J. and J.M. Kohler, *Continuous synthesis of gold nanoparticles in a microreactor.* Nano Lett., 2005. **5**(4): p. 685-91.

19. Wagner, J., T. Kirner, G. Mayer, J. Albert, and J.M. Köhler, *Generation of metal nanoparticles in a microchannel reactor.* Chem. Eng. J., 2004. **101**(1-3): p. 251-260.

20. Gomez-de Pedro, S., M. Puyol, and J. Alonso-Chamarro, *Continuous flow synthesis of nanoparticles using ceramic microfluidic devices.* Nanotechnology, 2010. **21**(41): p. 415603.

21. Shalom, D., R.C.R. Wootton, R.F. Winkle, B.F. Cottam, R. Vilar, A.J. deMello, and C.P. Wilde, *Synthesis of thiol functionalized gold nanoparticles using a continuous flow microfluidic reactor*. Mater. Lett., 2007. **61**(4-5): p. 1146-1150.

22. Rhee, M., P.M. Valencia, M.I. Rodriguez, R. Langer, O.C. Farokhzad, and R. Karnik, *Synthesis of size-tunable polymeric nanoparticles enabled by 3D hydrodynamic flow focusing in single-layer microchannels.* Adv. Mater., 2011. **23**(12): p. H79-83.

23. Bemetz, J., A. Wegemann, K. Saatchi, A. Haase, U.O. Hafeli, R. Niessner, B. Gleich, and M. Seidel, *Microfluidic-Based Synthesis of Magnetic Nanoparticles Coupled with Miniaturized NMR for Online Relaxation Studies.* Anal. Chem., 2018. **90**(16): p. 9975-9982.

24. Shi, L., E. Buhler, F. Boue, and F. Carn, *How does the size of gold nanoparticles depend on citrate to gold ratio in Turkevich synthesis? Final answer to a debated question.* J. Colloid Interface Sci., 2017. **492**: p. 191-198.

25. Bandulasena, M.V., G.T. Vladisavljević, O.G. Odunmbaku, and B. Benyahia, *Continuous synthesis of PVP stabilized biocompatible gold nanoparticles with a controlled size using a 3D glass capillary microfluidic device.* Chem. Eng. Sci., 2017. **171**: p. 233-243.

26. Jun, H., T. Fabienne, M. Florent, P.E. Coulon, M. Nicolas, and S. Olivier, *Understanding of the size control of biocompatible gold nanoparticles in millifluidic channels.* Langmuir, 2012. **28**(45): p. 15966-74.

27. Luty-Błocho, M., M. Wojnicki, and K. Fitzner, *Gold Nanoparticles Formation via Au(III) Complex Ions Reduction with l-Ascorbic Acid.* Int. J. Chem. Kinet., 2017. **49**(11): p. 789-797.

28. Schoenitz, M., L. Grundemann, W. Augustin, and S. Scholl, *Fouling in microstructured devices: a review.* Chem. Commun. (Camb.), 2015. **51**(39): p. 8213-28.

29. Ma, Y., X. Cao, X. Feng, Y. Ma, and H. Zou, *Fabrication of super-hydrophobic film from PMMA with intrinsic water contact angle below 90°.* Polymer, 2007. **48**(26): p. 7455-7460.

30. Rothstein, J.P., *Slip on Superhydrophobic Surfaces.* Annu. Rev. Fluid Mech., 2010. **42**(1): p. 89-109.

31. Amendola, V., R. Pilot, M. Frasconi, O.M. Marago, and M.A. Iati, *Surface plasmon resonance in gold nanoparticles: a review.* J. Phys. Condens. Matter, 2017. **29**(20): p. 203002.

32. Tran, M., R. DePenning, M. Turner, and S. Padalkar, *Effect of citrate ratio and temperature on gold nanoparticle size and morphology.* Mater. Res. Express., 2016. **3**(10).

33. Mukai, K., M. Nishimura, and S. Kikuchi, *Stopped-flow investigation of the reaction of vitamin C with tocopheroxyl radical in aqueous triton X-100 micellar solutions. The structure-activity relationship of the regeneration reaction of tocopherol by vitamin C.* J. Biol. Chem., 1991. **266**(1): p. 274-8.

34. Pahl, M., M. Mayer, M. Schneider, D. Belder, and K.R. Asmis, *Joining Microfluidics with Infrared Photodissociation: Online Monitoring of Isomeric Flow-Reaction Intermediates.* Anal. Chem., 2019. **91**(5): p. 3199-3203.

35. Andersson, H. and A. van den Berg, *Microfluidic devices for cellomics: a review.* Sens. Actuators B Chem., 2003. **92**(3): p. 315-325.

36. Shrirao, A.B., Z. Fritz, E.M. Novik, G.M. Yarmush, R.S. Schloss, J.D. Zahn, and M.L. Yarmush, *Microfluidic flow cytometry: The role of microfabrication methodologies, performance and functional specification.* Technology (Singap World Sci), 2018. **6**(1): p. 1-23.

37. Ateya, D.A., J.S. Erickson, P.B. Howell, Jr., L.R. Hilliard, J.P. Golden, and F.S. Ligler, *The good, the bad, and the tiny: a review of microflow cytometry.* Anal. Bioanal. Chem., 2008. **391**(5): p. 1485-98.

Declaration of scientific contribution and summary for "Integration of 3D hydrodynamic focused microreactor with microfluidic chemiluminescence sensing for online synthesis and catalytical characterization of gold nanoparticles"

Yanwei Wang [a] and Michael Seidel*[a]

Sensors 2021, 21, 2290.

https://doi.org/10.3390/s21072290

MS suggested applying synthesized AuNPs in the CL system for further application. YW reviewed the available literature and found that the optimal AuNPs in a certain CL reaction was still unknown. Moreover, nothing about the specific synthesis for CL has been found. Therefore, YW proposed coupling synthesis and CL characterization to get the optimal synthesis parameters for further application. The online synthesis of AuNPs with the 3D hydrodynamic focusing microreactor coupling to a charge-coupled device (CCD) camera with an inset microfluidic CL sensing chip was developed by YW. A microfluidic CL sensing chip was designed and fabricated by YW. The method for the synthesis of AuNPs as catalysts was proposed by YW. YW revised the program for synthesis and characterization. The properties of AuNPs were modulated by changing the concentration of reagents by YW to obtain optimal catalytic activity in the CL system. After optimizing the parameters of synthesis, the CL signal was enhanced to a factor of 171. The stability of AuNPs synthesized under optimal conditions was checked by YW for further offline application and found that they were stable for at least one month. In addition, the effect of aggregation and the surface property of AuNPs on catalytic activity was also investigated by YW. All experimental plans and results were discussed by YW and MS. The manuscript was written by YW. MS and YW revised the manuscript.

Chapter: 2

Integration of 3D hydrodynamic focused microreactor with microfluidic chemiluminescence sensing for online synthesis and catalytical characterization of gold nanoparticles

Yanwei Wang [a] and Michael Seidel*[a]

Sensors 2021, 21, 2290.

https://doi.org/10.3390/s21072290

[a]Institute of Hydrochemistry, Chair of Analytical Chemistry and Water Chemistry,

Technical University of Munich, Munich, Germany.

***Correspondence**

Michael Seidel

Michael.Seidel@mytum.de

Abstract

Chemiluminescence assays have shown great advantages compared with other optical techniques. Gold nanoparticles have drawn much attention in chemiluminescence analysis systems as an enzyme-free catalyst. The catalytic activity of gold nanoparticles for chemiluminescence sensing depends on size, shape and the surface charge property, which is hard to characterize in batches. As there is no positive or negative correlation between chemiluminescence signals and sizes of gold nanoparticles, the best way to get optimal gold nanoparticles is to control the reaction conditions via online chemiluminescence sensing systems. Therefore, a new method was developed for online synthesis of gold nanoparticles with a three-dimension hydrodynamic focusing microreactor, directly coupled with a microfluidic chemiluminescence sensing chip, which was coupled to a charge-coupled device camera for direct catalytical characterization of gold nanoparticles. All operations were performed in an automatic way with a program controlled by Matlab. Gold nanoparticles were synthesized through a single-phase reaction using glucose as a reducing agent and stabilizer at room temperature. The property of gold nanoparticles was easily controlled with the three-dimension microreactor during synthesis. The catalyst property of synthesized gold nanoparticles was characterized in a luminol-NaOCl chemiluminescence system. After optimizing parameters of synthesis, the chemiluminescence signal was enhanced to a factor of 171. The gold nanoparticles synthesized under optimal conditions for the luminol-NaOCl system were stable for at least one month. To further investigate the catalytic activity of synthesized gold nanoparticles in various situations, two methods were used to change the property of gold nanoparticles. After adding a certain amount of salt (NaCl), gold nanoparticles aggregated with a changed surface charge property and the catalytic activity was greatly enhanced. Glutathione was used as an example of molecules with thiol groups which interact with gold nanoparticles and reduce the catalytic activity. The chemiluminescence intensity was reduced by 98.9%. Therefore, we could show that using a microreactor for gold nanoparticles synthesis and direct coupling with microfluidic chemiluminescence sensing offers a promising monitoring method to find the best synthesis condition of gold nanoparticles for catalytic activity.

Keywords: gold nanoparticles; online; chemiluminescence; catalyst characterization; microfluidic chip

2.1. Introduction

Chemiluminescence (CL) is a phenomenon in which a specific molecule gets energy from a redox reaction and is excited. The molecule emits light when it returns to a ground state. As there is no need of an excitation source and optical filters, it shows great advantages compared with other optical techniques, such as low cost, simple instrumentation and easy automation [1]. Moreover, the high sensitivity, and wide linear range make CL-based assays applicable in different scientific and industrial areas [2]. Enzymes are used in most CL methods as a catalyst, such as horseradish peroxidase and alkaline phosphatase [3]. However, enzymes have the disadvantages of short lifetime and low stability, which means they are easily denaturalized. Moreover, enzymes are usually expensive with a complex labeling procedure [4]. Recently, precious metal nanomaterials have participated in the CL reaction, which improved performance of the CL system [5]. Among these nanomaterials, gold nanoparticles (AuNPs) have attractive properties, such as easy preparation and modification, stability, large surface area to volume ratio, and good biocompatibility, which have attracted researchers' attention [6]. Some researchers have applied AuNPs as a catalyst in a CL system [7-9]. The catalytic activity of AuNPs with different sizes was systematically investigated in luminol-H_2O_2 CL reactions by Cui's group [10]. It was found that AuNPs with different sizes had different enhancement of the CL signals. However, there is no positive or negative correlation between CL signals and sizes of AuNPs. In other CL systems, studies have also shown that there was no direct relationship between the size of AuNPs and signal intensity [7, 8, 10-14]. Additionally, the optimal size of AuNPs depends on different CL systems [7, 8, 10-14]. For example, in the luminol-H_2O_2 system, the 38 nm AuNPs showed best catalytic performance among the tested AuNPs [10]. However, in luminol-ferricyanide and luminol-hydrazine CL systems, the most intensive CL signal was obtained by using 25 and 15 nm AuNPs, respectively [7, 11]. Due to the limited number of AuNPs tested and various CL systems, it is impossible to determine the best AuNPs with a specific size. In addition, the morphology of AuNPs affects their catalytic performance in CL reactions. Aggregated AuNPs were found to induce a higher signal in CL reactions with luminol than dispersed ones [15-17]. Besides their size and shape, AuNPs with different surface charge properties also display various functions in CL reactions [16]. Cationic AuNPs or AuNPs with lower negative charge density have been proven to exhibit higher catalytic activity [16-18]. Due to all these variables, it is difficult to confirm the optimal AuNPs for a certain CL reaction. Although the most effective AuNPs for a specific CL

reaction have not been determined, AuNPs have been successfully used in many practical applications, as shown in **Table 2.1**. Even though 38 nm AuNPs have been proven to show better catalytic activity in the luminol-H_2O_2 CL system [10], they were not used in any of these applications. According to our knowledge, researchers only buy commercial AuNPs or produce them batch-wise. On the one hand, no one can determine which AuNPs exhibit the best catalytic activity. On the other hand, there is no simple way to control the size of AuNPs during the synthesis process. Therefore, it is crucial to develop an online monitoring system which can easily control the property of AuNPs during synthesis and immediately inspect the catalytic CL activity.

Table 2.1 Practical applications of gold nanoparticles (AuNPs) in different chemiluminescence (CL) systems.

CL system	Size of AuNPs	Application	Ref
Luminol-H_2O_2	13 nm	Detection of L-cysteine in pharmaceutical samples	[19]
Luminol-H_2O_2	12 nm	Detection of fibrillar fibrin in plasma samples	[20]
Luminol-H_2O_2	31 ± 3 nm 27 ± 2 nm	Detection of C-reactive protein in serum samples.	[18]
Luminol-H_2O_2	13 nm	Detection of single-strand DNA in plasma samples	[15]
Lucigenin-H_2O_2	13 ± 3.0 nm	Detection of histone in serum samples	[21]
Luminol-IO_4^-	4 nm	Determination of polyphenols in tap water.	[14]
Luminol-hydrazine	15 nm	Determination of hydrazine in boiler feed water samples.	[11]
Luminol-$AgNO_3$	13 nm	Detection of antigen with antibody functionalized AuNPs in serum samples	[22]

Microreactors have been exploited by many research groups to achieve rapid and tunable synthesis of nanoparticles [23-26], fulfilling the promise of automated systems for reaction optimization [27]. Microfluidic reactors were shown to synthesize products with narrower size distributions and

faster reaction rates compared to conventional batch synthesis [23]. Extremely short mixing times can be achieved in microfluidic reactors due to the thin fluid layer thickness [28]. Moreover, decreased amounts of reagents are used and limited by-products are generated. Microreactors can even be applied for automated multi-step synthesis [29]. A continuous flow microreactor was used for the synthesis of AuNPs by Wagner et al. [23]. Significant fouling of the micro-channels was observed due to deposition of nanoparticles on the reactor walls. Fouling can be relieved by using focusing flow in which sheath streams can insulate nanoparticles from channel walls. Moreover, focusing the reaction flow allows formation of more monodispersed particles due to the uniformity of concentration, residence time and fluid velocity in the center [30]. Recently, our group invented a flow-focused microreactor for synthesis of magnetic nanoparticles [31]. The laminated three-dimension (3D) flow-focused microreactor was further developed for synthesis of AuNPs without fouling [32]. This continuous synthesis method has the potential to couple online with analytical instruments like inductively coupled plasma mass spectrometry (ICP-MS), flow-based UV-Vis spectrometers or sensors. For CL sensing, continuous flow injection improves mixing between the luminol and oxidant, which can result in a higher intensity of CL signal than in a cuvette [9]. Flow-based methods allow a continuous light emission if luminol; oxidants and catalyst are pumped into the microfluidic chip constantly. The CL signal in microchannels can be imaged by a CCD camera for sensing applications.

The principle of online synthesis using a 3D hydrodynamic focused microreactor combined with microfluidic CL sensing was shown for the first time in this work. The catalytical characterization of AuNPs produced continuously through a single-phase reaction were directly measured by CL reactions of luminol and NaOCl in microfluid channels by a CCD camera. NaOCl was one of the first reagents used to demonstrate luminol CL with brilliant blue emission, and is a convenient choice in the classroom [33]. The method can be applied to other CL systems in the same way. AuNPs were synthesized by the reduction of tetrachloroaurate (III) ions with glucose as reducing agent and stabilizer and sodium hydroxide (NaOH) adjusting pH [34]. Synthesizing AuNPs with glucose has never been tried in a 3D microreactor before. Glucose has the advantage that AuNPs can be synthesized at room temperature, unlike with citrate solutions where heating is required [35]. Moreover, compared with the strong reducing agent sodium borohydride (NaBH4), glucose is non-toxic and cannot react with water. The pH value and concentration of glucose has an important effect on the size distribution and stability of the nanoparticles [36]. Therefore, the sizes

and properties of AuNPs were modulated by varying the concentration of reagents to obtain optimal catalytic activity in enhanced CL detection by luminol and NaOCl. The stability of AuNPs synthesized under optimal conditions was checked for one month. The effect of aggregation and the surface property of AuNPs on catalytic activity were also monitored by CL imaging after adding salt and molecules with thiol groups. A possible mechanism for luminol-NaOCl-AuNPs is shown in **Scheme 2.1**. AuNPs show catalytic activity with facilitating radical generation and electron transfer processes on the surface of the AuNPs [10]. AuNPs were stable with negative charged repulsion. When salt was added, the repulsion was screened with decreased density of negative charge which resulted in the aggregation of AuNPs. Therefore, anions can easily interact with the surface of AuNPs and the aggregated AuNPs show better catalytic performance than the dispersed ones [17]. Some organic compounds with -SH groups could strongly interact with AuNPs, and the amount of radical absorbed on the surface of AuNPs might be reduced, which might result in the inhibitive phenomenon [37].

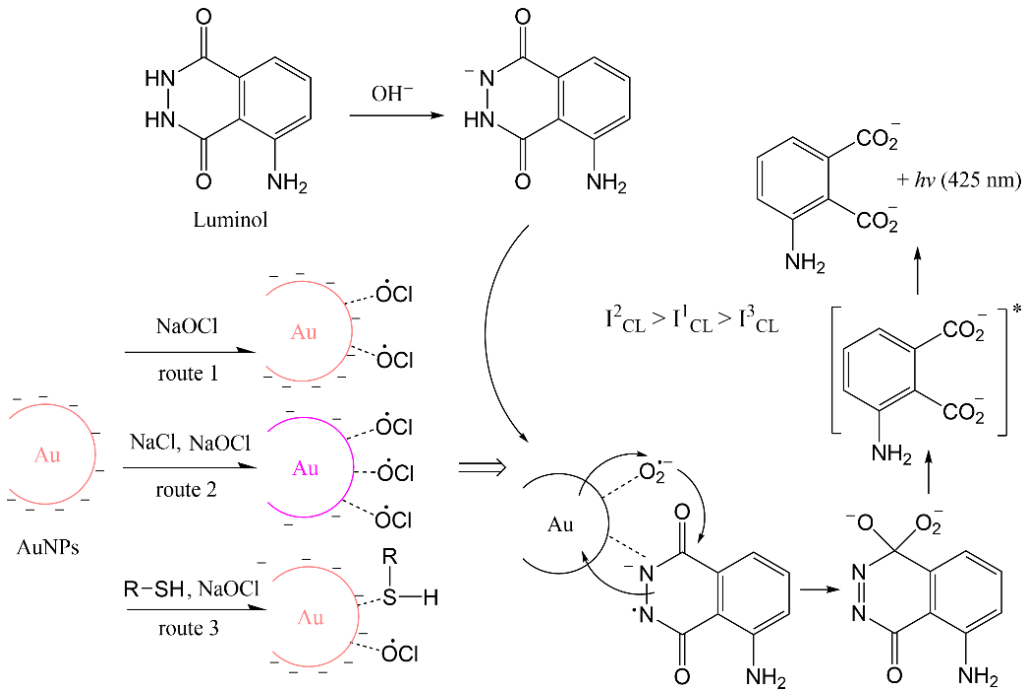

Scheme 2.1 Possible mechanism for luminol-NaOCl-AuNPs CL system.

2.2. Materials and methods

2.2.1. Materials

Gold (III) chloride trihydrate ($HAuCl_4 \cdot 3H_2O$, ≥ 99.9% trace metal basis, Sigma-Aldrich, Munich, Germany) was used as a gold precursor and D-glucose (Sigma-Aldrich, Munich, Germany) was used as a reductant with the aid of sodium hydroxide (NaOH, reagent grade, ≥ 98%, pellets, Sigma-Aldrich, Munich, Germany). Luminol stock solution (4×10^{-2} M) was prepared by dissolving 3-aminophthalhydrazide (luminol, Sigma-Aldrich, Munich, Germany) in 0.10 M NaOH and stored in a fridge for one week before use. The stock solution was diluted with ultrapure water to get the specific concentration. Sodium hypochlorite (NaOCl, 12% Cl) supplied by Carl Roth (Karlsruhe, Germany) was diluted for the working solution. Hydrochloric acid (HCl, Sigma-Aldrich, Munich, Germany, ACS reagent) was used to clean the microreactor after synthesis. Stock solution of glutathione (0.01 M) was prepared by dissolving glutathione (Sigma-Aldrich, Munich, Germany) in ultrapure water, and it was diluted by ultrapure water to make a working solution. Ultrapure water was used to prepare all aqueous solutions. The poly (methyl methacrylate) (PMMA) sheets with a thickness of 0.2 mm were supplied by the company Modulor Material Total (Berlin, Germany). The double-sided pressure-sensitive adhesive (PSA) tape (ARcare 90106) was supplied by Adhesive Research (Glen Rock, PA, USA). The carrier sheet with a thickness of 10 mm was fabricated by our in-house workshop. The fabricated PMMA carrier contained threads (1/4” - 28 UNF) to allow the connection with PTFE tubing.

2.2.2. Synthesis of AuNPs in 3D microreactor

A laminated 3D hydrodynamic flow-focused microreactor was constructed with PSA tape and PMMA. The method eliminated cleanroom requirements due to the absence of lithographic process. The difficulty in designing and fabricating a 3D microreactor was solved by the simple assembly process of layering precut sheets. This 3D microreactor has been proven to synthesize reproducible AuNPs without fouling [32]. The microreactor applied for synthesis of AuNPs was constructed of seven layers of PMMA sheet and PSA tape with 3 inlets for $HAuCl_4$, glucose and NaOH, and one outlet for AuNPs as shown in **Figure 2.1** A series of different concentrations of NaOH (10^{-3} - 1 M) and glucose (3×10^{-4} - 3×10^{-1} M) was tested to see at which concentration AuNPs were generated.

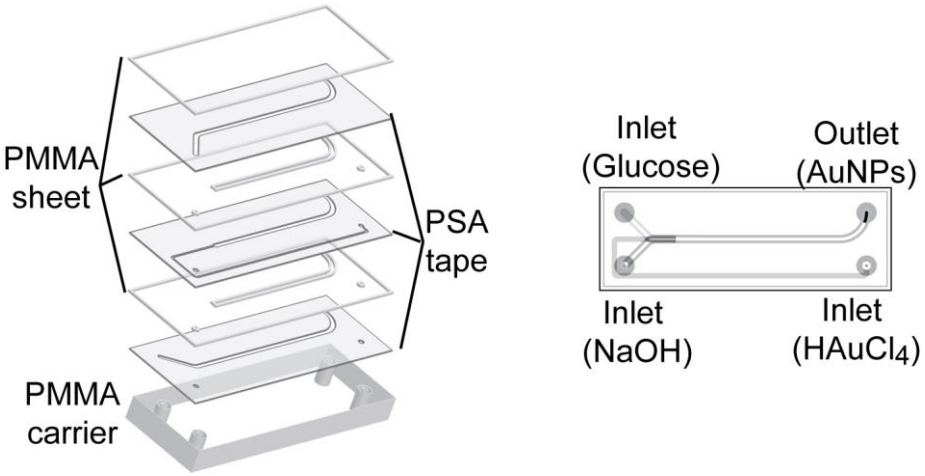

Figure 2.1 Scheme of 3D microreactor for synthesis of AuNPs. The microreactor was constructed of seven layers of alternating PMMA sheets and PSA tapes. The fabricated PMMA carrier contained threads (1/4" - 28 UNF) to allow the connection with PTFE tubing for inlets of $HAuCl_4$, glucose and NaOH, and one outlet for AuNPs.

2.2.3. Procedures for CL measurements

The CL measurements were conducted on CCD camera (16-bit) with a microchip insert for direct online CL imaging as depicted in **Figure 2.2**. The microchip was composed of a transparent glass sheet for coving, one PSA layer and one black plastic sheet with holes for inlets and outlet. The PSA layer with channel offers a place for reagents mixing and CL generation. The glass allows generated light emissions to pass through, and the light is recorded by a sensitive CCD camera with an image. CL intensity is described as the gray intensity of each pixel, ranging from 0 to 65,536 a.u. The background from the dark signal of the CCD was recorded before the measurement, and the background was subtracted from each image before evaluation. ImageJ was used to integrate the signal intensity over the pixels.

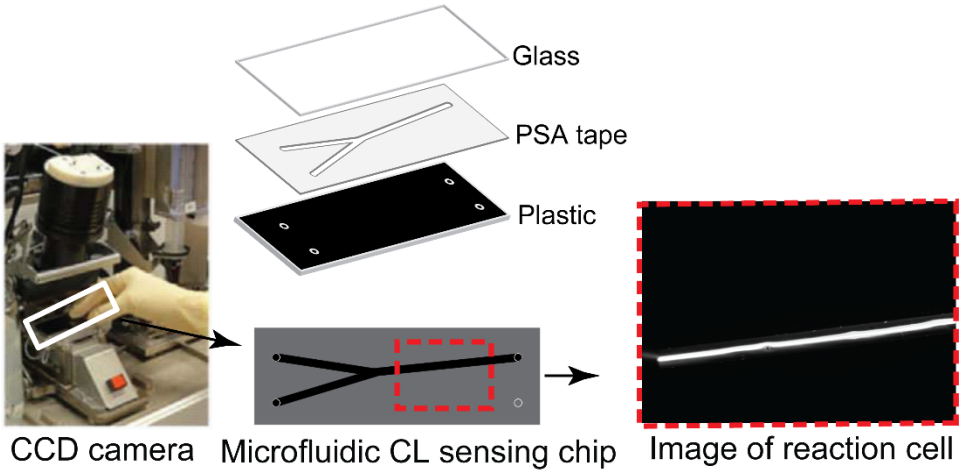

Figure 2.2 Microchip in CCD camera for CL was composed of glass, PSA tape and black plastic with holes for inlets and outlet. Images are taken by CCD camera when reaction occurs in microchip.

2.2.4. Automated synthesis and online CL

The luminol-NaOCl system was coupled with online synthesized AuNPs for catalyst characterization. All operations, including synthesis of AuNPs and CL generation in the coupled CCD camera, were performed in an automatic way. All components were connected using PTFE tube (inner diameter 0.8 mm). The combined setup is shown in **Figure 2.3** Reagents were supplied to the microreactor with three glass syringes (Innovative Laboratory Systems GmbH, Stutzerbach, Germany) connected to a 6-port valve (Cavro Smart Valve, Tecan Group Ltd., Männedorf, Switzerland). The first ports of each valve were used for intake of glucose, NaOH and $HAuCl_4$, which were reagents for synthesis of AuNPs. Then they were transferred to the 5th ports, which were connected to the inlet of the microreactor. The second ports were for injection of water to clean syringes. The 6th ports were for outlet of waste during or after synthesis. The 3rd port of the first valve was for cleaning solution after synthesis. The glass syringes were operated by three custom-made pumps (GWK precision technology, Munich, Germany) which were controlled with Matlab (The MathWorks, Inc., USA) by a host computer connected via an Ethernet cable. The synthesized gold nanoparticles could be directly pumped into a microfluidic CL sensing chip. Another pump was used to deliver reagents for changing the property of AuNPs, luminol and NaOCl, and the flow rates were the same at 1 µL/s. In this paper, NaCl and glutathione were used as two kinds of property-changing reagents. When they were not applied, the syringes for them were blocked. The property-changing reagents were mixed with AuNPs through a three-way valve. The solution from the three-way valve was then mixed with luminol by another three-way valve.

NaOCl was then mixed with the mixture in the microchip inserted in the CCD camera to generate a CL signal. With all reagents pumped into the microchip simultaneously, the signal could be recorded with the CCD camera online.

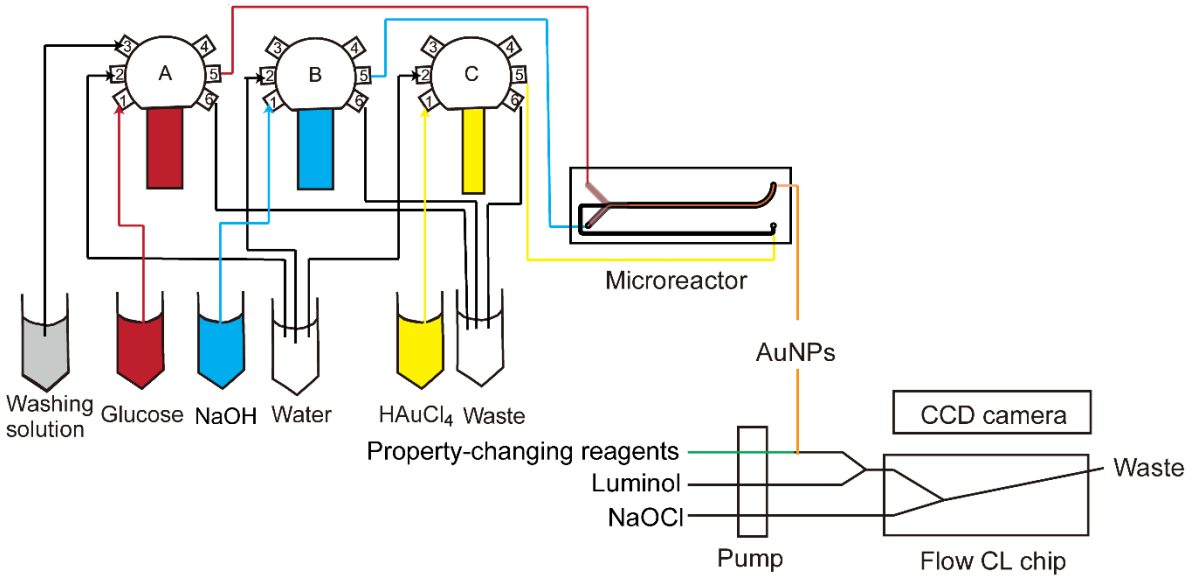

Figure 2.3 Scheme of online synthesis and CL characterization system. The synthesis was controlled automatically by Matlab. Reagents were supplied to the microreactor via three glass syringes connected to a 6-port valve. Synthesized AuNPs were mixed with property-changing reagents, luminol and NaOCl in a microchip to generate a CL signal which was recorded by CCD camera.

2.2.5. Offline characterization of AuNPs

UV-Vis absorbance spectra for gold nanoparticle suspensions were recorded using a SPECORD 250 PLUS UV-Vis spectrometer (Analytik Jena, Jena, Germany). The spectrometer uses deuterium and halogen lamps to produce UV light and a visible range of electromagnetic wavelengths. A beam of light with a wavelength ranging from 400 nm to 900 nm was used for measurement. Disposable polystyrene cuvettes (UV cuvette semi-micro, 1.5 - 3.0 ml, Brand GmbH, Hamburg, Germany) were used for containing samples and reference. Ultrapure water was used as a reference sample as all solutions were prepared in ultrapure water. Scanning electron microscopy (SEM) images were acquired on a model Sigma 300 VP microscope (Zeiss Gemini). The samples were analyzed with an InLens detector using an acceleration voltage of 10 kV, a 30 µm aperture and a working distance of about 1.4 mm.

2.3. Results and discussion

2.3.1. Effects of the reagent concentrations on AuNPs synthesis

The concentration of reagents is an important factor in synthesis of AuNPs. Neither high nor low concentration of NaOH was suitable for synthesis of AuNPs, as shown in **Figure 2.4 a** When the pH was low with 10^{-3} M NaOH, there were no surface plasmon resonance (SPR) absorption bands from 400 to 900 nm, which indicated that no AuNPs were generated [38]. Since OH^- participates in the reduction reaction, the pH environment has a significant impact on the synthesis of AuNPs, and glucose can only act as an effective reducing agent in the presence of OH^- [34]. With high concentration (10^{-1} M and 1 M), there were inconspicuous broad peaks. This implied that AuNPs were aggregated. AuNPs were stabilized with glucose via electrostatic repulsions. High concentration of ions from NaOH may break the electrostatic balance, which can cause aggregation of AuNPs [39]. When the concentration of NaOH rose to 10^{-2} M, the absorbance peak with small full-width at half maximum (FWHM) of the SPR band and high intensity appeared, which indicated narrower size distribution and higher concentration of AuNPs. Therefore, the concentration of NaOH should be around 10^{-2} M. The effect of glucose concentration on the UV-Vis absorption spectra of AuNPs synthesized with 10^{-2} M NaOH is shown in **Figure 2.4 b** For very low concentration of glucose (3×10^{-4} M), limited AuNPs were produced as there was only a small peak around 550 nm. In this case, the amount of glucose was not enough to reduce all Au^{3+} ions in the solution. With higher glucose concentrations from 3×10^{-3} M to 3×10^{-1} M, more AuNPs were produced. The surface-plasmon maximum absorption wavelength (λ_{max}) of AuNPs shifted to a lower value (from 578 nm to 529 nm) with decreasing size of AuNPs. Therefore, it is easy to infer that the higher the glucose concentration, the more effective the reduction function of glucose. There would be more nucleation sites which result in smaller AuNPs and higher number density. To make sure all Au ions can be reduced, concentration of glucose should be higher than 10^{-2} M. The concentration of glucose can be tuned to obtain various sizes of AuNPs.

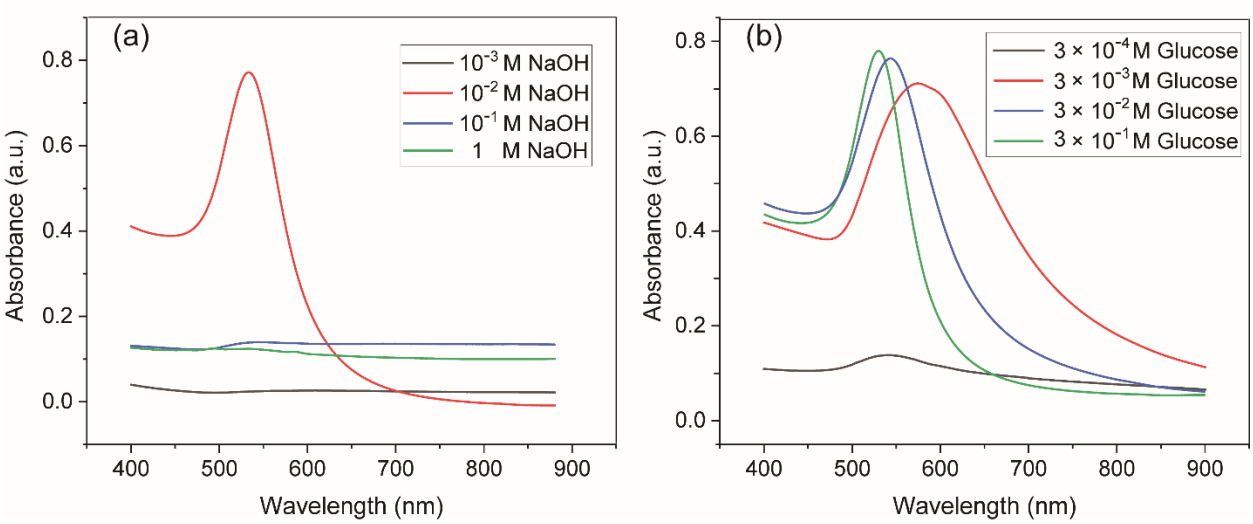

Figure 2.4 UV−Vis spectra of AuNPs synthesized with various reagent concentrations: (**a**) 0.1% $HAuCl_4$, 3×10^{-2} M glucose and various concentrations of NaOH; (**b**) 0.1% $HAuCl_4$, 10^{-2} M NaOH and various concentrations of glucose.

2.3.2. Effect of synthesis parameters on catalytic property of AuNPs

The concentration of glucose and NaOH can affect the size distribution of AuNPs [36]. AuNPs with different sizes can further affect the CL signals with different catalytic activity [10]. As there is no positive or negative correlation between CL signals and sizes of AuNPs, the best way to get optimal AuNPs is to control the reaction conditions via online CL sensing. The properties of AuNPs were easily controlled with the 3D microreactor during synthesis. The parameters for synthesis were optimized for the luminol-NaOCl-AuNPs system to obtain the highest CL signal. To test the catalytic activity of AuNPs, the tube for property-changing reagents was removed and AuNPs were mixed directly with luminol. The effect of NaOH concentration was tested in the range of 0.5 to 10 mM with 0.01% $HAuCl_4$ and 0.3 M glucose (**Figure 2.5 a**). As shown in the figure, the intensity of CL increased with the increase of NaOH concentration in the range of 0.5 - 2 mM. The CL intensity decreased after concentration of NaOH reached 2 mM. After that, the CL signal reach another maximum and then decreased again. There was no linear relationship between NaOH concentration and CL signal; 2 mM NaOH was chosen for further application as it can offer the highest CL signal at these conditions. The effect of glucose concentration on intensity of CL was studied, ranging from 0.2 - 1 M (**Figure 2.5 b**). There was a steady increase of CL intensity as concentration of glucose increased. As glucose solution is almost saturated when the concentration is 1 M, 1 M glucose was used for further application. The effect of $HAuCl_4$

concentration was also investigated as shown in **Figure 2.5 c**. When the concentration of $HAuCl_4$ solution was lower than 0.05%, the intensity of CL increased with the increase of $HAuCl_4$ concentration. The reason could be that more AuNPs were generated with higher concentration of $HAuCl_4$ solution. When the concentration of $HAuCl_4$ solution was higher than 0.05%, the CL intensity decreased because the properties of AuNPs changed. Considering the CL intensity, the ideal conditions for synthesis were as follows: 2 mM NaOH, 1M glucose and 0.05% $HAuCl_4$. Under the optimal conditions, the synthesized AuNPs were quasi-spherical with a diameter of 15.32 ± 1.09 nm, as shown in **Figure S2.1** (Supplementary Materials).

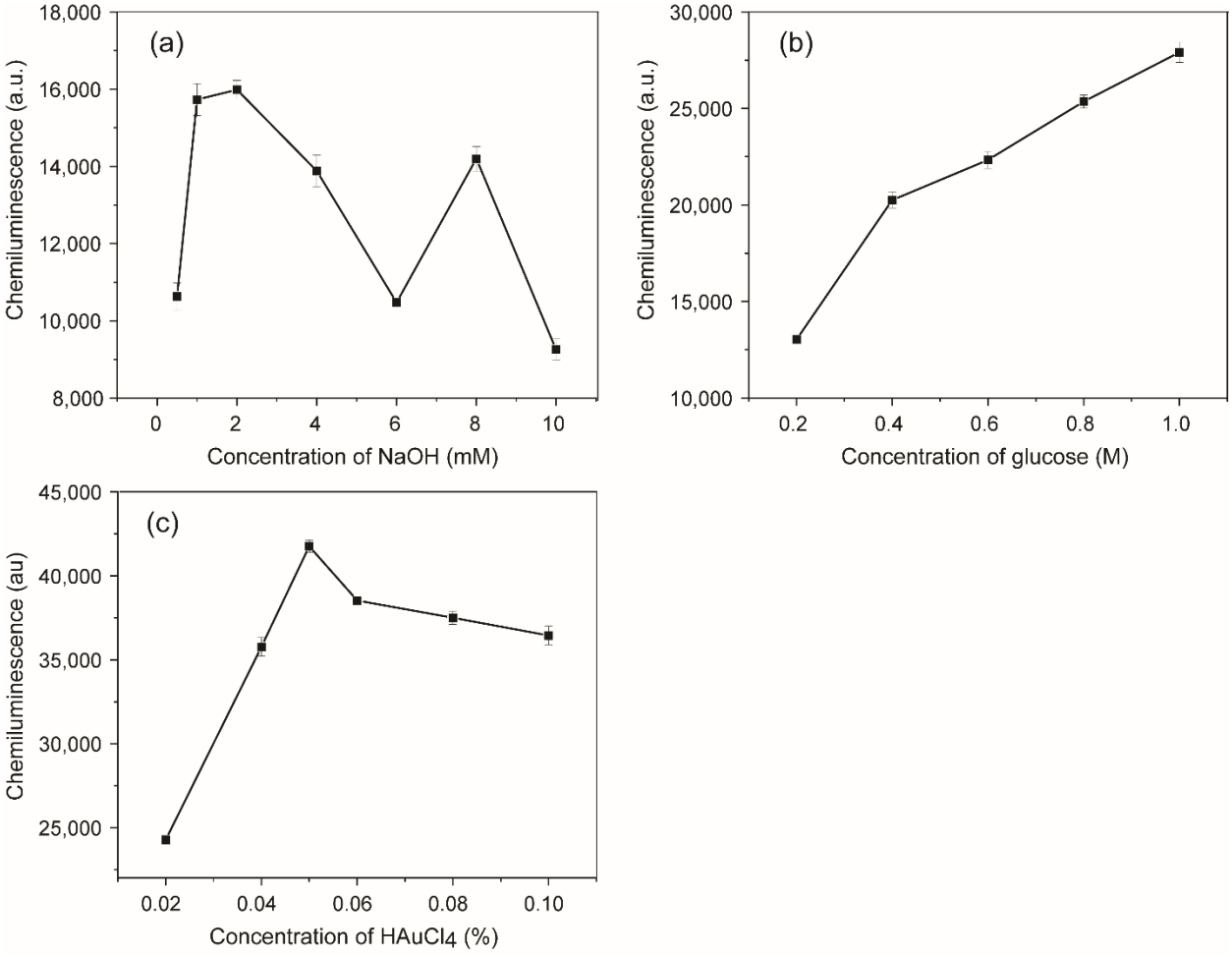

Figure 2.5 Effects of synthesis conditions on the CL intensity: (**a**) 0.01% $HAuCl_4$, 0.3 M glucose and different concentrations of NaOH, 0.5, 1, 2, 4, 6, 8, 10 mM; (**b**) 0.01% $HAuCl_4$, 2 mM NaOH and different concentrations of glucose, 0.2, 0.4, 0.6, 0.8, 1.0 M; (**c**) 2 mM NaOH, 1 M glucose and different concentrations of $HAuCl_4$, 0.02%, 0.04%, 0.05%, 0.06%, 0.08%, 0.1%.

After getting the optimized conditions for synthesis of AuNPs, it was still not clear if the synthesized AuNPs or the reagents for synthesis acted as catalysts. The comparison of CL signals from background and all blanks were done as shown in **Figure 2.6**. The background was from the totally dark signal without luminol-NaOCl. Since the background signal was subtracted from each image before the evaluation, the signal for background was 0 (**Figure 2.6 a**). When luminol and NaOCl were mixed in the chip and only water was added instead of AuNPs, a gray line was shown in the image with a signal of 235 ± 2 a.u., as shown in **Figure 2.6 b**. The most intensive CL signal was obtained for synthesized AuNPs with a signal of 40,378 ± 367 and there was a bright line as shown in **Figure 2.6 c**. The enhancement was 171 times. Blank experiments were also carried out, including with NaOH, glucose and $HAuCl_4$ solutions with the same concentrations for synthesis. As shown in **Figure 2.6**, there was no significant enhancement of CL signal when $HAuCl_4$ was used and the signal reach 245 ± 10 as the concentration was too low, whereas NaOH and glucose could enhance the luminol CL signal slightly to 575 ± 7 as pH was changed. This effect is described elsewhere, too [10]. The concentration of unreacted NaOH and glucose in gold colloids was too low to make a contribution to the enhancement of CL intensity. Thus, the catalytic activity of gold colloid was attributed to AuNPs rather than due to NaOH, glucose or $HAuCl_4$.

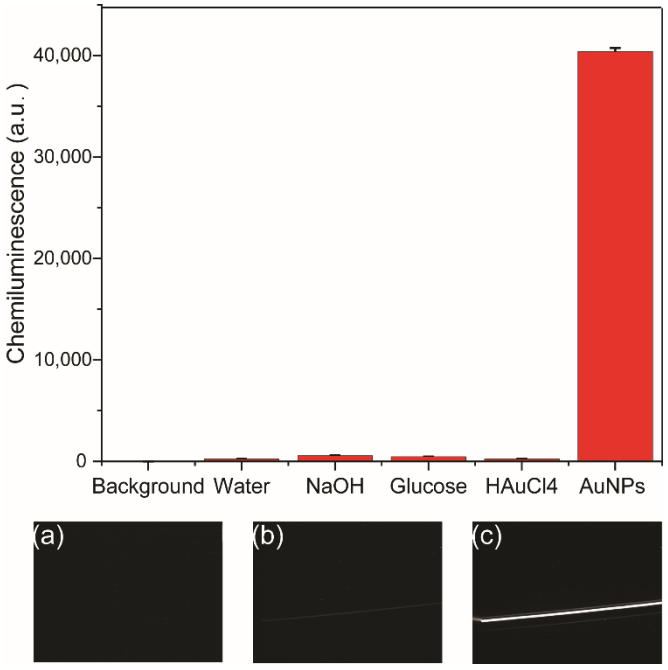

Figure 2.6 Comparison of CL signals generated from background and luminol-NaOCl mixed with four blank solutions: water, 2 mM NaOH, 1M glucose and 0.05% $HAuCl_4$, and synthesized AuNPs. Inset (**a - c**) were images recorded by CCD camera of background, water blank and AuNPs, respectively.

2.3.3. Stability of synthesized AuNPs

The stability of AuNPs can be estimated by observing the color of colloid solution, which did not change with time. The stability of the synthesized AuNPs was carefully investigated over one month by UV−Vis spectroscopy. **Figure 2.7** shows the UV-Vis spectra of AuNPs on day 1 (right after the synthesis), day 3, day 6 and day 31. There was only a slight shift of the SPR band (from 552 to 554 nm) from day 1 to day 3 with a decreased absorbance from 0.95 to 0.93. After that, the SPR band did not change until day 31. The size of AuNPs was maintained and aggregation did not take place.

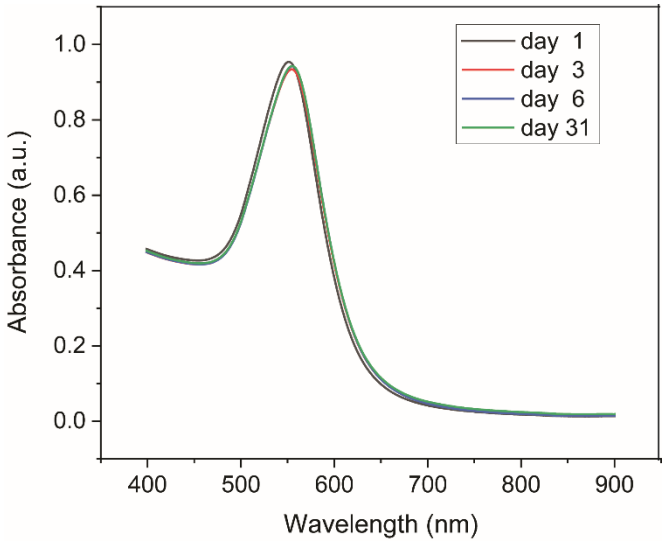

Figure 2.7 UV−Vis spectra of synthesized AuNPs recorded on day1, day 3, day 6 and day 31.

2.3.4. Effect of property-changing reagents on catalytic property of AuNPs

Although the synthesized AuNPs were stable, aggregation could be caused by adding salt. The aggregation of AuNPs can change the CL intensity in a luminol system and many analytical methods were developed according to this principle [17, 20, 40, 41]. Here, different concentrations of NaCl were added to AuNPs to change the property and CL signals were recorded to monitor the catalytic activity as shown in **Figure 2.8 a** With increased concentration of NaCl, the CL signal was enhanced significantly. UV-Vis absorption spectra analysis was carried out to inspect the property change after adding salt. As shown in **Figure 2.8 b**, without salt addition, the absorption

was high and SPR band of AuNPs was narrow, indicating the AuNPs were highly dispersed. As the salt concentration increased, the intensity of SPR decreased with a lower number concentration of AuNPs. Moreover, the absorption spectra were broader and shifted to a high value, indicating a bigger size of AuNPs caused by aggregation. With enough salt, the negative charged repulsion between AuNPs was screened and AuNPs aggregated [17]. Luminol-NaOCl CL reaction occurred in alkaline solution and the main molecules in the reaction were hypochlorite ion (OCl^-) and luminol anion. The anionic molecules would not easily interact with the AuNPs because of a negative charge on the surface. The aggregated AuNPs with lower negative charge density caused by adding salt would be favorable for adsorption and electron transfer. Therefore, the catalytic activity of aggregated AuNPs caused by salt is better than that of dispersed AuNPs.

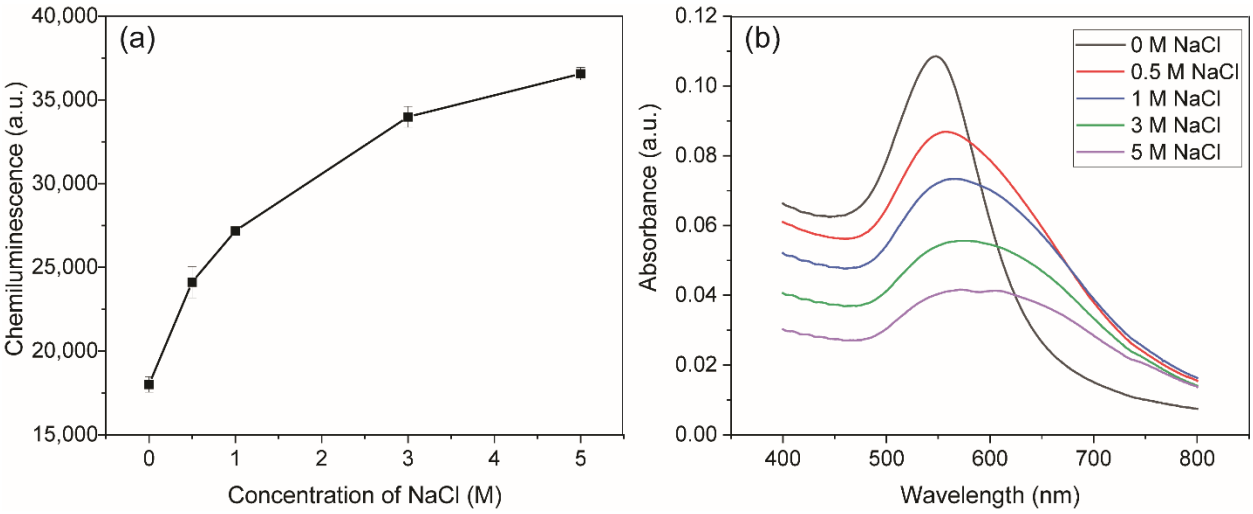

Figure 2.8 (**a**) Effects of NaCl concentration on the CL intensity; (**b**) UV−Vis spectra of the AuNPs with different concentration of NaCl.

There are some organic compounds containing -OH, $-NH_2$ or -SH groups which were reported to easily interact with AuNPs and change the surface property [40]. Glutathione was used as one example of a property-changing reagent with -SH groups. The CL signal was significantly inhibited with glutathione, indicating the decreased catalytic activity of AuNPs, and the degree of inhibition was related to the concentration of glutathione, as shown in **Figure 2.9** With a concentration of 1 mM, glutathione can inhibit 98.9% of the CL signal, from 19,977 to 211. In the luminol-NaOCl-AuNPs system, there are some oxygen intermediates. A decrease of CL intensity can be caused by the competition between reducing groups of -SH and luminol for active

intermediate radicals [17]. The surface of AuNPs was occupied by the compounds and this interrupts reactions occurring on the surface of AuNPs [37]. Therefore, the catalytic activity was decreased when organic molecules bound on the surface of AuNPs.

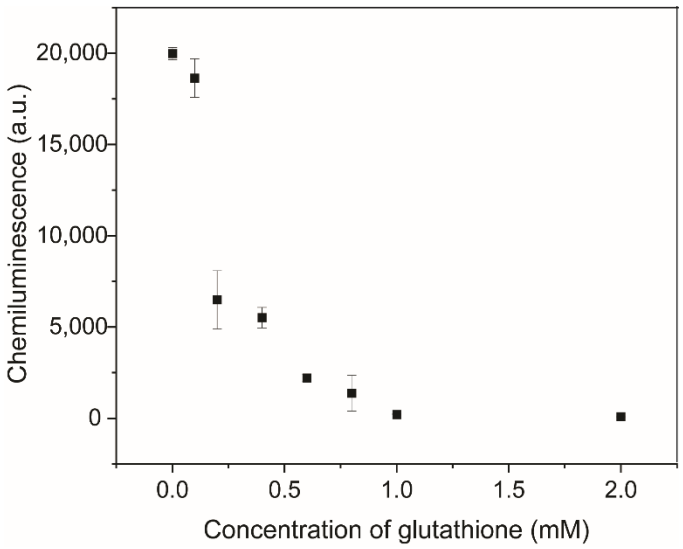

Figure 2.9 CL signals of luminol-NaOCl mixed with AuNPs and different concentration of glutathione (0.01, 0.1, 0.2, 0.4, 0.6, 0.8, 1.0, 2.0 mM).

2.4. Conclusions

A new online CL sensing method was proposed for online synthesis of AuNPs with a 3D hydrodynamic focusing microreactor and direct characterization of the catalytic activity in the flow. AuNPs were synthesized through a single-phase reaction using glucose as reducing agent and stabilizer at room temperature. The property of AuNPs was easily controlled by tuning concentration of reagents in a 3D microreactor during synthesis. The catalyst property of synthesized AuNPs was characterized by microfluidic CL sensing of luminol and NaOCl. With optimized parameters of synthesis, the CL signal was enhanced 171 times. Without adding another stabilizer, AuNPs were stable for more than one month. Two kinds of reagents were used to change the property of AuNPs and to investigate their effect on catalytic activity. The addition of salt could cause aggregation of synthesized AuNPs and the CL signal for the luminol-NaOCl-AuNPs sensing system was greatly enhanced because of the change of surface charge property. Glutathione was applied as an example of a molecule which binds on the surface of AuNPs. The catalytic activity of AuNPs was decreased and the extent of inhibition was related to the

concentration of glutathione. This method offers a good way to confirm optimal synthesis condition of AuNPs for a certain CL sensing application. Researchers can use their own synthesis methods and CL systems according to specific applications. The synthesized AuNPs with good catalyst property can be applied in flow-based CL microarrays instead of enzymes [41, 42]. Another potential application is labeling AuNPs with luminol for ultrasensitive CL-based chemical analyses [43]. The quenching effect can also be utilized to detect molecules with special functional groups [44]. For specific detection, AuNPs can bind with antibodies or aptamers [45, 46].

Supplementary Materials: The following are available online. Figure S2.1: SEM images of synthesized AuNPs with optimal synthesis conditions. Histograms with the respective particle size distributions and the percentage are included as inset.

Author Contributions: Conceptualization, Y.W. and M.S.; methodology, Y.W.; software, Y.W.; validation,Y.W.; formal analysis, Y.W.; investigation, Y.W. and M.S.; data curation, Y.W.; writing—original draft preparation, Y.W.; writing—review and editing, M.S. and Y.W.; supervision, M.S.; project administration, M.S.; funding acquisition, Y.W. and M.S.. All authors have read and agreed to the published version of the manuscript.

Funding: This research was funded by the China Scholarship Council (CSC) with number 201706210083

Institutional Review Board Statement: Not applicable.

Informed Consent Statement: Not applicable.

Data Availability Statement: Not applicable.

Acknowledgments: We gratefully thank Jonas Bemetz for helping with the Matlab program and building the automatic synthesis setup. We also thank Roland Hopper from the workshop for the fabrication of the PMMA carrier. Many tanks to Christine Benning for SEM measurement.

Conflicts of Interest: The authors declare no conflict of interest.

2.5 References

1. Li, N., D. Liu, and H. Cui, *Metal-nanoparticle-involved chemiluminescence and its applications in bioassays.* Anal. Bioanal. Chem., 2014. **406**(23): p. 5561-71.
2. Sun, Y. and J. Lu, *Chemiluminescence-based aptasensors for various target analytes.* Luminescence, 2018. **33**(8): p. 1298-1305.
3. Chen, G., M. Jin, P. Du, C. Zhang, X. Cui, Y. Zhang, J. Wang, F. Jin, Y. She, H. Shao, S. Wang, and L. Zheng, *A review of enhancers for chemiluminescence enzyme immunoassay.* Food Agric. Immunol., 2017. **28**(2): p. 315-327.
4. Chen, W., B. Li, C. Xu, and L. Wang, *Chemiluminescence flow biosensor for hydrogen peroxide using DNAzyme immobilized on eggshell membrane as a thermally stable biocatalyst.* Biosens. Bioelectron., 2009. **24**(8): p. 2534-40.
5. Aslan, K. and C.D. Geddes, *Metal-enhanced chemiluminescence: advanced chemiluminescence concepts for the 21st century.* Chem. Soc. Rev., 2009. **38**(9): p. 2556-64.
6. Yeh, Y.-C., B. Creran, and V.M. Rotello, *Gold nanoparticles: preparation, properties, and applications in bionanotechnology.* Nanoscale, 2012. **4**(6): p. 1871-1880.
7. Duan, C., H. Cui, Z. Zhang, B. Liu, J. Guo, and W. Wang, *Size-Dependent Inhibition and Enhancement by Gold Nanoparticles of Luminol−Ferricyanide Chemiluminescence.* J. Phys. Chem. C, 2007. **111**(12): p. 4561-4566.
8. Cui, H., J.-Z. Guo, N. Li, and L.-J. Liu, *Gold Nanoparticle Triggered Chemiluminescence between Luminol and AgNO3.* J. Phys. Chem. C, 2008. **112**(30): p. 11319-11323.
9. Karabchevsky, A., A. Mosayyebi, and A.V. Kavokin, *Tuning the chemiluminescence of a luminol flow using plasmonic nanoparticles.* Light Sci. Appl., 2016. **5**(11): p. e16164-e16164.
10. Zhang, Z.F., H. Cui, C.Z. Lai, and L.J. Liu, *Gold nanoparticle-catalyzed luminol chemiluminescence and its analytical applications.* Anal. Chem., 2005. **77**(10): p. 3324-9.
11. Safavi, A., G. Absalan, and F. Bamdad, *Effect of gold nanoparticle as a novel nanocatalyst on luminol-hydrazine chemiluminescence system and its analytical application.* Anal. Chim. Acta, 2008. **610**(2): p. 243-8.
12. Lin, J.M. and M. Liu, *Chemiluminescence from the decomposition of peroxymonocarbonate catalyzed by gold nanoparticles.* J. Phys. Chem. B, 2008. **112**(26): p. 7850-5.
13. Dong, Y.P., T.T. Gao, X.F. Chu, J. Chen, and C.M. Wang, *Flow injection-chemiluminescence determination of ascorbic acid based on luminol–ferricyanide–gold nanoparticles system.* J. Lumin., 2014. **154**: p. 350-355.
14. Li, S., X. Li, J. Xu, and X. Wei, *Flow-injection chemiluminescence determination of polyphenols using luminol-NaIO4-gold nanoparticles system.* Talanta, 2008. **75**(1): p. 32-7.
15. Qi, Y., B. Li, and Z. Zhang, *Label-free and homogeneous DNA hybridization detection using gold nanoparticles-based chemiluminescence system.* Biosens. Bioelectron., 2009. **24**(12): p. 3581-6.

16. Qi, Y. and B. Li, *A sensitive, label-free, aptamer-based biosensor using a gold nanoparticle-initiated chemiluminescence system.* Chemistry (Easton), 2011. **17**(5): p. 1642-8.

17. Qi, Y. and B. Li, *Enhanced effect of aggregated gold nanoparticles on luminol chemiluminescence system and its analytical application.* Spectrochim. Acta. A Mol. Biomol. Spectrosc., 2013. **111**: p. 1-6.

18. Islam, M.S. and S.H. Kang, *Chemiluminescence detection of label-free C-reactive protein based on catalytic activity of gold nanoparticles.* Talanta, 2011. **84**(3): p. 752-8.

19. Liu, W., J. Luo, Y. Guo, J. Kou, B. Li, and Z. Zhang, *Nanoparticle coated paper-based chemiluminescence device for the determination of L-cysteine.* Talanta, 2014. **120**: p. 336-41.

20. Zhang, Y., J. Liu, T. Liu, H. Li, Q. Xue, R. Li, L. Wang, Q. Yue, and S. Wang, *Label-free, sensitivity detection of fibrillar fibrin using gold nanoparticle-based chemiluminescence system.* Biosens. Bioelectron., 2016. **77**: p. 111-5.

21. He, Y. and H. Cui, *Label free and homogeneous histone sensing based on chemiluminescence resonance energy transfer between lucigenin and gold nanoparticles.* Biosens. Bioelectron., 2013. **47**: p. 313-7.

22. Luo, J., X. Cui, W. Liu, and B. Li, *Highly sensitive homogenous chemiluminescence immunoassay using gold nanoparticles as label.* Spectrochim. Acta. A Mol. Biomol. Spectrosc., 2014. **131**: p. 243-8.

23. Wagner, J. and J.M. Kohler, *Continuous synthesis of gold nanoparticles in a microreactor.* Nano Lett., 2005. **5**(4): p. 685-91.

24. Wagner, J., T. Kirner, G. Mayer, J. Albert, and J.M. Köhler, *Generation of metal nanoparticles in a microchannel reactor.* Chem. Eng. J., 2004. **101**(1-3): p. 251-260.

25. Gomez-de Pedro, S., M. Puyol, and J. Alonso-Chamarro, *Continuous flow synthesis of nanoparticles using ceramic microfluidic devices.* Nanotechnology, 2010. **21**(41): p. 415603.

26. Shalom, D., R.C.R. Wootton, R.F. Winkle, B.F. Cottam, R. Vilar, A.J. deMello, and C.P. Wilde, *Synthesis of thiol functionalized gold nanoparticles using a continuous flow microfluidic reactor.* Mater. Lett., 2007. **61**(4-5): p. 1146-1150.

27. Reizman, B.J. and K.F. Jensen, *Feedback in Flow for Accelerated Reaction Development.* Acc. Chem. Res., 2016. **49**(9): p. 1786-96.

28. Chang, C.-H., B.K. Paul, V.T. Remcho, S. Atre, and J.E. Hutchison, *Synthesis and post-processing of nanomaterials using microreaction technology.* J. Nanopart. Res., 2008. **10**(6): p. 965-980.

29. Wang, C.H. and G.B. Lee, *Automatic bio-sampling chips integrated with micro-pumps and micro-valves for disease detection.* Biosens. Bioelectron., 2005. **21**(3): p. 419-25.

30. Lu, M., A. Ozcelik, C.L. Grigsby, Y. Zhao, F. Guo, K.W. Leong, and T.J. Huang, *Microfluidic Hydrodynamic Focusing for Synthesis of Nanomaterials.* Nano Today, 2016. **11**(6): p. 778-792.

31. Bemetz, J., A. Wegemann, K. Saatchi, A. Haase, U.O. Hafeli, R. Niessner, B. Gleich, and M. Seidel, *Microfluidic-Based Synthesis of Magnetic Nanoparticles Coupled with Miniaturized NMR for Online Relaxation Studies.* Anal. Chem., 2018. **90**(16): p. 9975-9982.

32. Wang, Y. and M. Seidel, *Strategy for fast manufacturing of 3D hydrodynamic focusing multilayer microfluidic chips and its application for flow-based synthesis of gold nanoparticles.* Microfluid. Nanofluid., 2021. **25**(8).

33. Francis, P.S., N.W. Barnett, S.W. Lewis, and K.F. Lim, *Hypohalites and related oxidants as chemiluminescence reagents: a review.* Luminescence, 2004. **19**(2): p. 94-115.

34. Liu, J., G. Qin, P. Raveendran, and Y. Ikushima, *Facile "green" synthesis, characterization, and catalytic function of beta-D-glucose-stabilized Au nanocrystals.* Chemistry (Easton), 2006. **12**(8): p. 2131-8.

35. Shi, L., E. Buhler, F. Boue, and F. Carn, *How does the size of gold nanoparticles depend on citrate to gold ratio in Turkevich synthesis? Final answer to a debated question.* J. Colloid Interface Sci., 2017. **492**: p. 191-198.

36. Xu, L., X.C. Wu, and J.J. Zhu, *Green preparation and catalytic application of Pd nanoparticles.* Nanotechnology, 2008. **19**(30): p. 305603.

37. Yang, P., Y. Chen, Q. Zhu, F. Wang, L. Wang, and Y. Li, *Sensitive chemiluminescence method for the determination of glutathione, l-cysteine and 6-mercaptopurine.* Microchim Acta, 2008. **163**(3-4): p. 263-269.

38. Thanh, N.T., N. Maclean, and S. Mahiddine, *Mechanisms of nucleation and growth of nanoparticles in solution.* Chem. Rev., 2014. **114**(15): p. 7610-30.

39. Kang, H., J.T. Buchman, R.S. Rodriguez, H.L. Ring, J. He, K.C. Bantz, and C.L. Haynes, *Stabilization of Silver and Gold Nanoparticles: Preservation and Improvement of Plasmonic Functionalities.* Chem. Rev., 2019. **119**(1): p. 664-699.

40. Sujit Kumar Ghosh, S.N., Subrata Kundu, Kunio Esumi,† and Tarasankar Pal*, *Solvent and Ligand Effects on the Localized Surface Plasmon Resonance (LSPR) of Gold Colloids.* J. Phys. Chem. B, 2004. **108**(37): p. 13963-13971.

41. Gopfert, L., M. Elsner, and M. Seidel, *Isothermal haRPA detection of blaCTX-M in bacterial isolates from water samples and comparison with qPCR.* Anal. Methods, 2021. **13**(4): p. 552-557.

42. Meyer, V.K., C.V. Chatelle, W. Weber, R. Niessner, and M. Seidel, *Flow-based regenerable chemiluminescence receptor assay for the detection of tetracyclines.* Anal. Bioanal. Chem., 2020. **412**(14): p. 3467-3476.

43. Syed, L.U., L.Z. Swisher, H. Huff, C. Rochford, F. Wang, J. Liu, J. Wu, M. Richter, S. Balivada, D. Troyer, and J. Li, *Luminol-labeled gold nanoparticles for ultrasensitive chemiluminescence-based chemical analyses.* Analyst, 2013. **138**(19): p. 5600-9.

44. Yang, D., Y. He, Y. Sui, and F. Chen, *Determination of catechol in water based on gold nanoclusters-catalyzed chemiluminescence.* J. Lumin., 2017. **187**: p. 186-192.

45. Huang, Y., L. Gao, and H. Cui, *Assembly of Multifunctionalized Gold Nanoparticles with Chemiluminescent, Catalytic, and Immune Activity for Label-Free Immunoassays.* ACS Appl. Mater. Interfaces, 2018. **10**(20): p. 17040-17046.

46. Yao, L.-Y., X.-Q. Yu, Y.-J. Zhao, and A.-P. Fan, *An aptamer-based chemiluminescence method for ultrasensitive detection of platelet-derived growth factor by cascade amplification combining rolling circle amplification with hydroxylamine-enlarged gold nanoparticles.* Anal. Methods, 2015. **7**(20): p. 8786-8792.

Declaration of scientific contribution and summary for "3D microfluidic flow-injection platform with *m*-carboxy luminol enhanced chemiluminescence for highly sensitive aptamer-based homogeneous assays"

Yanwei Wang [1], Simone Rink[2], Antje J. Baeumner[2] and Michael Seidel[1*]

Microchimica Acta, 2021, under review

YW had the literature review and found that aptamers interact with AuNPs inhibiting the aggregation AuNPs, which could be applied in the CL system. After the first evaluation by YW, there is a big standard deviation that could not be applied in quantification. Therefore, YW developed the microfluidic CL sensor chip into a micromixer. Different mixing patterns were investigated in the 2D mixer, and the 3D mixer with five layers was finally applied because 2D mixers cannot manage effective mixing due to the limited space and turbulence. MS proposed to use another more sensitive luminol to get stable signals. The hydrophilic derivative *m*-carboxy luminol was synthesized and provided by Simone Rink (SR) and Anje J. Baeumner (AJB). SR gave suggestions for prepare the working solution of *m*-carboxy luminol. Comercial luminol and *m*-carboxy luminol were compared in the developed 3D mixer by YW, identifying the hydrophilic derivative to provide 10-fold more signal enhancement with repeatable results. Finally, the novel detection platform was developed in a 3D micromixer with aptamer, AuNPs, and *m*-carboxy luminol, for the homogeneous assay. Sulfadimethoxine was measured in the platform by YW and yielded a stunning dynamic range over 5 orders of magnitude (0.01 - 1000 ng/ml) and a limit of detection of 4 pg/ml. All experimental plans and results were discussed by YW and MS. YW wrote the manuscript. All authors have contributed to the final version of the manuscript.

Chapter: 3

3D microfluidic flow-injection platform with *m*-carboxy luminol enhanced chemiluminescence for highly sensitive aptamer-based homogeneous assays

Yanwei Wang [1], Simone Rink[2], Antje J. Baeumner[2] and Michael Seidel[1*]

Microchimica Acta, 2021, under review

[1]Institute of Hydrochemistry, Chair of Analytical Chemistry and Water Chemistry,

Technical University of Munich, Munich, Germany.

[2]Institute of Analytical Chemistry, Chemo- and Biosensors,

University of Regensburg, Regensburg, Germany.

*** Correspondence**

Michael Seidel

Michael.Seidel@mytum.de

Abstract

Gold nanoparticles-catalyzed chemiluminescence (CL) of luminol is an attractive alternative to strategies relying on enzymes, as their aggregation leads to significantly enhanced CL signals. Consequently, analytes disturbing such aggregation will lead to an easy-to-quantify weakening of the signal. Based on this concept a homogeneous aptamer-based assay for the detection of sulfadimethoxine (SDM) is developed as a microfluidic CL flow-injection platform. Here, the efficient mixing of gold nanoparticles, aptamers and analyte in short channel distances is of utmost importance, and 2D and 3D mixer designs made via Xurography were studied. In the end, since 2D designs could not provide sufficient mixing, a laminated 3D 5-layer microfluidic mixer was developed and optimized with respect to mixing capability and observation by the CCD camera. Furthermore, the performance of standard luminol and its more hydrophilic derivative *m*-carboxy luminol was studied identifying the hydrophilic derivative to provide 10-fold more signal enhancement and reliable results. Finally, the novel detection platform was used for the specific detection of SDM via its aptamer and yielded a stunning dynamic range over 5 orders of magnitude (0.01 - 1000 ng/ml) and a limit of detection of 4 pg/ml. This new detection concept not only outperforms other methods for SDM detection, but can be suggested as a new flow-injection strategy for aptamer-based rapid and cost efficient analysis in environmental monitoring and food safety.

Keywords: 3D mixer; chemiluminescence; *m*-carboxy luminol; AuNPs; aptamer; sulfadimethoxine

3.1 Introduction

Sulfadimethoxine (SDM) is one of the antibacterial drugs which plays a significant role in preventing and treating diseases caused by bacterial infections [1]. However, SDM residues have been found in food and environmental water samples, which not only harm human health through the food chain, but also lead to antibiotic resistance and increase the difficulty of using antibiotics. Therefore, the maximum SDM residue in food stuffs have been proposed as 100 ng/ml by many countries [2]. Conventional methods for determination of SDM involve high performance liquid chromatography (HPLC), gas chromatography-mass spectrometry (GC-MS) and enzyme-linked immunosorbent assay (ELISA) [3-5]. Although these methods are reliable and sensitive, the complex operation, high cost, or tedious treatment process limited their application of convenient and rapid detection.

Chemiluminescence (CL) is a luminescence emission mechanism produced by a chemical reaction without the use of external light source or optical filters. The significant advantages of CL analysis (such as low detection limit, wide linear range, simple instrument, low cost and fast response speed) make CL as a simple, sensitive and cost-effective analysis technique [6]. Recently, some researchers have applied gold nanoparticles (AuNPs) as catalyst in CL systems [7-9]. Compared with enzymes, they have the advantages of easy preparation and modification, large surface area to volume ratio and stability [10]. In our recent work, the synthesis parameter for glucose reduced AuNPs were optimized as good catalyst for luminol-NaOCl-based CL measurements [11]. Luminol is one of the most applied CL reagents. However, applications are limited by its insolubility under physiological conditions. A water-soluble *m*-carboxy luminol was investigated by the Baeumner group and exhibited higher CL signal compared to commercial luminol [12].

In modern analytical instruments, manual handling of solutions has been replaced by flow-based injection, which is compatible with computers and can be automatically processed under strict control of reaction conditions. The combination of CL method and flow-injection analysis reduces the analysis time, and obtains high precision and high sensitivity [13]. For CL sensing, continuous flow-injection improves mixing between the luminol and oxidant, which can result in a higher intensity of CL signal than in a cuvette [9]. If luminol, oxidizer and catalyst are continuously pumped into the microfluidic chip, the flow-based method can emit light continuously. On a microfluidic platform, effective fluid mixing is an essential process, during nanomaterials

synthesis, drug delivery, bioreactors, and sample analysis [14]. Mixing can be easily achieved by turbulence of fluid in a macro system. However, in microfluidic system, mixing is a time-consuming process. Due to the size of the micro-channel and the low flow rate, the fluid movement is laminar, and the mixing mainly depends on molecular diffusion [15]. Therefore, micromixers are an important part in the microfluidic system. Active mixing which apply an additional effect (such as electric fields, sound waves, and magnetic fields) on the flow field through external equipment, can periodically disturb the flow field to improve mixing efficiency [16]. Hence, it takes a short time to complete the mixing. However, complex structures were the bottleneck in the design and manufacture of these mixers. Moreover, additional equipment is required to provide driving force, which greatly increases the cost of the microfluidic chip. The passive mixers involve no external energy and they change the flow field through geometrical modifications (such as a specially designed flow channel shape), thereby improving the mixing efficiency [17, 18]. Based on their specific structures, a variety of passive mixing methods have been developed, such as spiral micromixers [19], zigzag-shaped channels [20, 21], floor-grooved channels [22], split and recombine (SAR) mixers [23, 24] obstacle-based mixers [25], herringbone mixers [26], T-shaped mixers [27], and convergent-divergent walls [28]. All the above designs can be used in 2D and 3D devices. 3D passive micromixers usually benefit from the spatial structure to produce more effective vortices. However, the fabrication of 3D devices is generally more complicated and more expensive than 2D devices. Xurography is a rapid alternative for conventional microfluidic device fabrication methods. This method attracted attention during the last decade for cheap and rapid prototyping of microfluidic devices without using a cleanroom [29]. The 3D multilayer micromixer using Xurography is an option to fabricate effective mixer.

The CL signal in microchannels can be imaged by a CCD camera for sensing applications. The possible limitation of these methods is the lack of selectivity. Antibody-based immunoassays have good sensitivity and selectivity, however, the poor stability of antibodies can result in false negative results [30]. Furthermore, animals are needed for the development or production of polyclonal and monoclonal antibodies. To overcome the above limitations for rapid test systems applicable in the field, aptamers have emerged as new promising recognition biomolecules for analytical applications. Aptamers are single-stranded DNA or RNA oligonucleotides that can specifically bind various target molecules (such as nucleic acids, proteins, metal ions, and other small molecules) with high affinity, selectivity and sensitivity [31]. Aptamers can be routinely

produced in large quantities at low cost by chemical synthesis, avoiding the use of animals for antibody production, and they can be easily modified with different functional groups for labelling or immobilization. Moreover, they are chemically stable, and their shelf life is prolonged. Given all these attractive features, various aptamer-based analytical CL systems have been developed [32, 33]. However, to our knowledge, there is no homogeneous aptamer assay developed for SDM detection by CL. In the present paper, a microfluidic CL measurement system with AuNPs as catalyst and *m*-carboxy luminol as CL reagent was applied. Synthesized AuNPs aggregated in PBS with an enhanced CL signal and aptamer can inhibit the aggregation. To achieve efficient mixing in limited space, a novel 3D mixer was developed with five layers according to the optimal mixing pattern. The 3D mixer was fabricated by a rapid and low-cost Xurography method. The combination of 3D microfluidic flow-injection with *m*-carboxy luminol and gold nanoparticles as miniaturized chemiluminescence analysis system yielded in a stunning dynamic range of 5 orders of magnitude and a very low limit of detection. This method could by applied for continuous monitoring of antibiotics in food or environmental samples.

3.2 Experimental

3.2.1 Reagents and materials

All reagents were purchased from Sigma-Aldrich (www.sigmaaldrich.com) unless stated otherwise. Poly (methyl methacrylate) (PMMA) sheets (thickness of 0.2 mm) were purchased from modulor material total (Berlin, Germany, www.modulor.de). Double-sided pressure-sensitive adhesive (PSA) tapes (ARcare 90106) were supplied by Adhesive Research (Glen Rock, PA, USA, www.adhesivesresearch.com). The black PMMA carrier sheets with a thickness of 2 mm were fabricated in our in-house workshop. Erythrosin extra bluish and Fast Green FCF were used to show flow profile. Commercial luminol stock solution (4×10^{-2} M) was prepared by dissolving 3-aminophthalhydrazide in 0.10 M sodium hydroxide (NaOH, reagent grade, $\geqslant$98%, pellets). *m*-carboxy luminol was provided by the Baeumner group [12] and the stock solution (1 mM) was prepared in carbonate buffer. Carbonate buffer (pH 9.6, 1 L) was prepared by adding 5.76 g of sodium bicarbonate ($NaHCO_3$, ACS reagent) and 3.33 g of sodium carbonate (Na_2CO_3, anhydrous, ACS reagent) to water. Working solutions of luminol were prepared by diluting the stock solution with carbonate buffer. Working solutions of sodium hypochlorite (NaOCl) were prepared freshly from NaOCl (12% Cl) purchased from Carl Roth (Karlsruhe, Germany, www.carlroth.com). Gold

(III) chloride trihydrate ($HAuCl_4 \cdot 3H_2O$) (≥ 99.9%, trace metal basis) and *D*-glucose were used for synthesis of gold nanoparticles (AuNPs). Sulfadimethoxine (SDM) was prepared in water. The sequence of SDM binding aptamer (SBA) 5'-GAGGGCAACGAGTGTTTATAGA-3'[34] was synthesized by Eurofins Genomics (Ebersberg, Germany, www.eurofinsgenomics.eu) and SBA was prepared in phosphate buffered saline (PBS, pH 7.4).

3.2.2 Devices and software

The layout of the mixer was designed with the software CorelDRAW(www.coreldraw.com). The digital cutting plotter (Graphtec CE6000-40) was provided by Graphtec Corporation (Yokohama, Japan, www.graphteccorp.com) to cut sheet into designed layers. Cutting conditions and settings were executed via the Cutting Master 3 from Graphtec Corporation (Yokohama, Japan, www.graphteccorp.com). The pH of solutions was measured with a FiveEasy pH meter FP20 (Mettler Toledo, Columbus, OH, USA, www.mt.com). The CCD camera (16-bit, Model SXV-H9C) was from the Starlight Express Ltd (www.sxccd.com). ImageJ (www.imagej.net) was used to analyse pixel values of pictures taken by the camera. A pump (pump 11, www.harvardapparatus.com) was used to inject the reagents. UV-Vis absorbance spectra for gold nanoparticle suspensions were recorded using a SPECORD 250 PLUS UV/Vis spectrometer (Analytik Jena, Jena, Germany, www.analytik-jena.com). A beam of light with a wavelength ranging from 400 to 900 nm was used for measurement. Disposable polystyrene cuvettes (UV cuvette semi-micro, 1.5 - 3.0 ml, BRAND GMBH, Germany, www.sigmaaldrich.com) were used for containing samples and reference.

3.2.3 Chemiluminescence in mixers

CL measurement was performed with a CCD camera, equipped with a microfluidic mixer. The chip had two inlets for injecting fluids (luminophore and NaOCl) to the main mixing channel, an observation zone for CCD camera and one outlet, as shown in **Figure 3.1 a**. The light generated by luminol-NaOCl reaction was recorded by the CCD camera. The CL intensity was the gray value of each pixel, ranging from 0 to 65,536 a.u.. The microchip was composed by transparent PMMA layers, PSA layers and one black PMMA carrier with holes for inlets and outlet. The 2D micromixer was composed of three layers (**Figure 3.1 b**). The transparent PMMA cover allows generated light to pass through. The middle PSA layer with different channels offers a place for reagents mixing and CL generation. The black PMMA carrier can shield the light from the

environment and offers a dark blank. For 3D mixer (**Figure 3.1 c**), additional PMMA and PSA layers were added to provide more mixing space and cause turbulence. The *m*-carboxy luminol and commercial luminol from Sigma-Aldrich were compared by flow injection method in the 3D mixer. The concentration of luminophore was 0.5 mM and the pH was adjusted by carbonate buffer to 9.6. Luminophore was mixed with 1% NaOCl in 3D mixer by a pump with a flow rate of 10 ml/h. The signal was recorded by a CCD camera with an exposure time of 30 s and repeated 25-times.

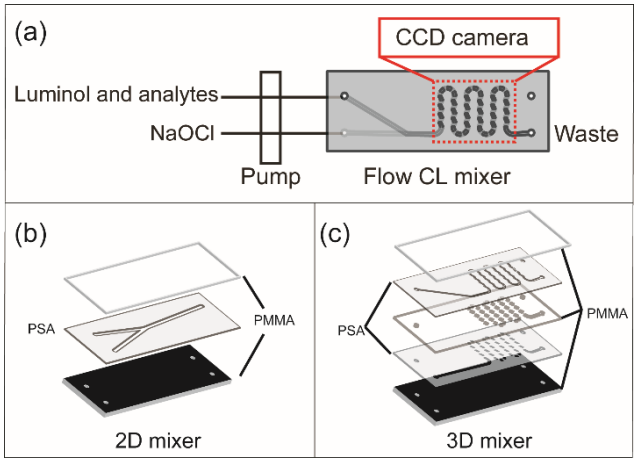

Figure 3.1 (a) Scheme of chemiluminescence (CL) measurement system: the reagents were pumped into mixer to generate CL signal which was recorded by a CCD camera (the observation area was marked by red dashed lines); **(b)** scheme of 2D mixer structure with 3 layers; **(c)** scheme of 3D mixer structure with 5 layers.

3.2.4 Homogeneous detection of sulfadimethoxine

AuNPs were synthesized in an automatic way through a single-phase reaction using glucose as reducing agent. The synthesized AuNPs were used as catalyst in luminol-NaOCl system and the synthesis parameter had been optimized by our group [11]. Briefly, 0.05% $HAuCl_4$, 2 mM NaOH and 1 M glucose were mixed in a 3D microreactor in a flow rate of 0.5 µl/s, 2.5 µl/s and 2.5 µl/s, respectively. The synthesized AuNPs were quasi-spherical with a diameter of 15.32 ± 1.09 nm and aggregated AuNPs caused by salt can enhance the CL signal [11]. The principle for homogeneous detection of SDM was shown in **Figure 3.2**. The SBA can protect AuNPs from aggregation in PBS. When there is SDM in the system, it will bind with SBA with a strong affinity. In this case, there will not be enough SBA to stabilize the AuNPs causing aggregation and thus a stronger CL signal. If SDM is absent, SBA will adsorb on the surface of AuNPs and inhibit the aggregation.

Therefore, the dispersed AuNPs generate a weak CL signal. 100 µl 1 µM aptamer (in PBS) was mixed with 100 µl SDM at different concentrations. Then, 200 µl synthesized AuNPs were added to the mixture and incubated for 5 min. Subsequently, 200 µl 0.1 mM *m*-carboxy luminol was added to the solution and incubated for 30 min. The mixture was mixed with 0.2% NaOCl in 3D mixer by a pump with a flow rate of 20 ml/h. The signal was recorded by a CCD camera with an exposure time of 10 s and repeated 3-times.

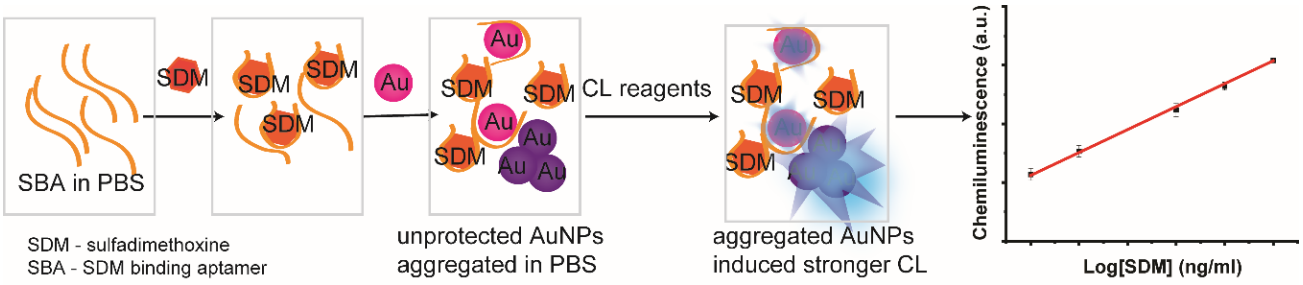

Figure 3.2 Schematic illustration of homogeneous chemiluminescence detection of SDM using AuNPs probe.

3.3 Results and discussion

3.3.1 Design of 2D mixers

For realization of better mixing, seven geometrical structures were applied and comparative analysis for these different micromixers have been done. The reagents can only mix in the middle of the channel for line pattern (LP) mixer and the mixing was not efficient (**Figure 3.3 a)**. Tesla pattern (TP) mixer was recommended considering high mixing performance and easy fabrication due to the planar structure [17]. However, the mixing liquid did not fill the complete channel structure as half of the channel remained dark. (**Figure 3.3 b)**. Similar was observed when the split and recombine pattern (SAR) mixer was applied (**Figure 3.3 c)**. This is probably due to the two channel which merge and separate again, which generates an inhomogeneous pressure distribution guiding the mixing liquid along the path of least resistance. Therefore, mixers with only one channel were designed. For the convergent-divergent pattern (CD) mixer, the channel was symmetrical, only half of the channel showed bright light generation (**Figure 3.3 d)**. Other designs such as the zigzag pattern (ZP) and the obstacle-based pattern (OB) favored small bubble entrapment (**Figure 3.3 e** and **f)**. The mixer with wavy line pattern (WL) showed a better result as

most of the channel lighted up and no bubbles were trapped (**Figure 3.3 g)**. To confirm the efficiency of 2D mixing, the same design (WL) was applied to a transparent chip with dyes to illustrate the flow profile. The chip had two inlet channels for directing the dyes (green and pink) to the main WL mixing channel. As shown in **Figure S3.1** (Supplementary material), the dye flow of green and pink went along the channel separately and only the interface of the two dyes changed the color to purple. Although the mixing channel was prolonged 2-times, no complete mixing was achieved.

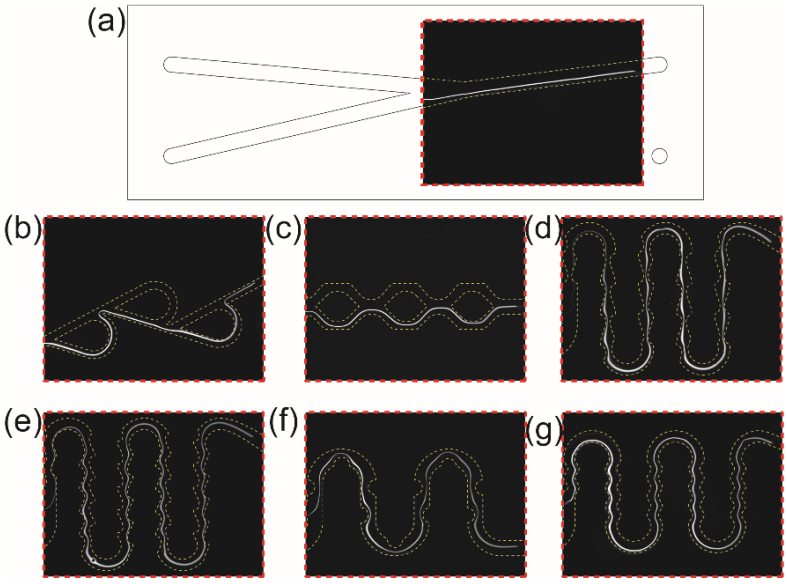

Figure 3.3 Different designs of 2D micromixer (yellow dash line) and images recorded by a CCD camera (black area with bright light): **(a)** design of central PSA layer with two inlets and one outlet with line pattern (LP), the area with red dash line can be recorded by a CCD camera; **(b)** Tesla pattern (TP); **(c)** Split and recombine pattern (SAR); **(d)** Convergent-divergent pattern (CD); **(e)** Zigzag pattern (ZP); **(f)** Obstacle-based pattern (OB) and **(g)** Wavy line pattern (WL).

3.3.2 Design of 3D mixers

As 2D mixers cannot manage the efficient mixing according to the limited space, a 3D mixer was designed with WL for better mixing performance. The structure is shown in **Figure S3.2**. This 3D mixer was composed of two pressure-sensitive adhesive tape (PSA) layers and three PMMA layers. The two PSA layers with an inlet channel for injection and a WL mixing channel were designed for mixing. A PMMA layer with holes was laminated between two PSA layers to expand the mixing space. Various designs of these three layers were compared afterwards. Then, these

channels were closed by a transparent PMMA cover and a black PMMA carrier. The thickness of the central PMMA layer was optimized in transparent 3D mixers using dyes to show the flow profile. For better comparison, the mixing channel was 2-times longer of the length of the CL chip channel. Different thickness of 0.08 mm, 0.17 mm and 0.25 mm were compared. The thicker layer with holes offers more space for mixing, hence the mixing performance was better as shown in **Figure S3.3**. Due to the limitation of the cutting plotter, much thicker PMMA layer cannot be applied, and the thickness was chosen as 0.25 mm.

Three different structures were compared in transparent 3D mixers, and the sectional view schemes and top view images were shown in **Figure 3.4**. For the first design, the layers with injection channels for two kinds of dyes were WL pattern without obstacle. In this case, liquid can be mixed in the central PMMA layer. However, both flows prefer to run parallel along the channel and show no motivation to mix causing inefficient mixing at the end of channel (**Figure 3.4 a**). For the second design, both injection channels were blocked alternately. The two dyes were forced to flow up and down along the channel barriers improving the overall mixing. As shown in **Figure 3.4 b**, mixing was achieved, and the color changed to purple already in the middle of the channel. Unfavorable for this design was small bubble entrapment in the upper channel blocked behind the obstacle which were not easy to be flushed out. Moreover, the slight opacity of the PSA layer would hinder the recording of CL light. Therefore, a third design without obstacles in the upper layer channel, blocking only the lower injection layer, was applied. As the image shows, the mixing was finished earlier with more obstacles (**Figure 3.4 c**). Different flow rates were applied in the optimal designed 3D mixer. As shown in **Figure S3.4**, with a lower flow rate of 5 ml/h, the mixing was efficient in the mixer. Increasing the flow rate, increases the mixing abilities and for a flow rate of 40 ml/h the mixing was finished even with one fifth of the mixing channel length.

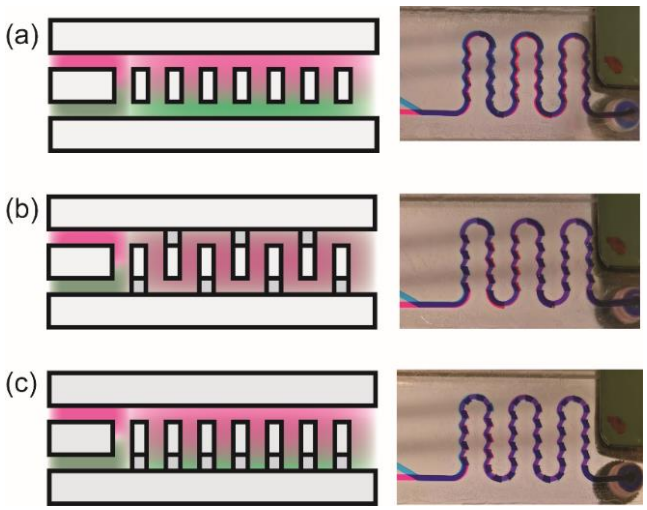

Figure 3.4 Different designs of 3D structure of micromixer and images recorded with dyes showing flow profile (sectional view schemes on the left and top view images on the right).

The design was then transferred to the CL chip. The CL signal obtained with the WL pattern in the 2D and 3D chip were compared. For the 2D chip, the signal only emerged in the center of the mixing channel. The signal was low at the beginning and increased along the channel. The signal was still high at the end of the channel (**Figure 3.5 a**). This can be explained with inefficient mixing taking place only at the interface of both liquid streams. With progression of the liquid flow along the channel, mixing becomes more effective and a higher CL signal was obtained as shown in **Figure 3.5 b.** In contrast, with the 3D chip the generated light filled the complete mixing channel and higher signals were obtained at the beginning (**Figure 3.5 c**). Afterwards, the signal decreased and then almost disappeared at the end indicating the mixing was well and all the reagents were consumed. As shown in **Figure 3.5 d**, the mixing occurs across the whole channel and it was efficient.

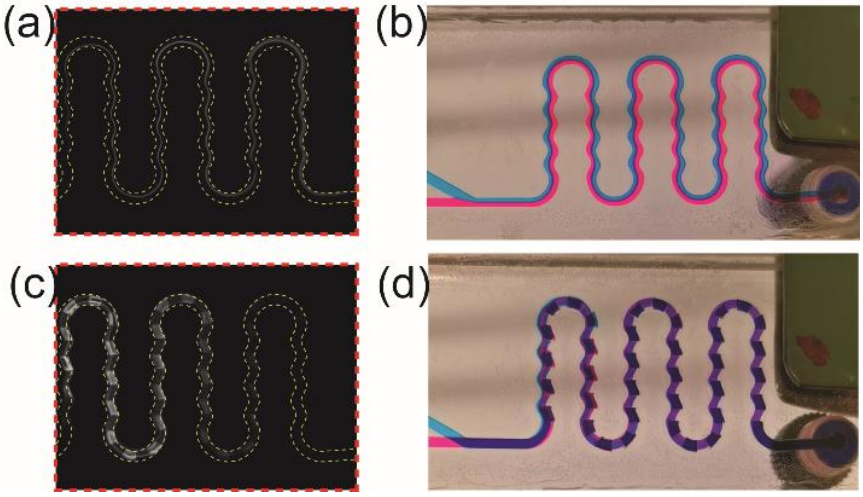

Figure 3.5 Images of chemiluminescence reaction in (**a**) 2D and (**c**) 3D mixer. (**b**) and (**d**) show the mixing profile of 2D and 3D mixer which have the same structure as (**a**) and (**c**), respectively.

3.3.3 Comparison of luminol and *m*-carboxy luminol in 3D mixer

The commercial luminol and *m*-carboxy luminol were injected in a 3D mixer to react with NaOCl and the result was shown in **Figure S3.5**. With commercial luminol, the mean signal was 3787 a.u. with standard deviation of 852 a.u.. When commercial luminol was substituted by *m*-carboxy luminol, the CL signal was increased more than 10-times to 55914 a.u.. Moreover, the signal was more stable with a standard deviation of 303 a.u.

3.3.4 Homogeneous detection of sulfadimethoxine

The synthesized AuNPs were stable in water and have a strong plasmon absorption at 548 nm. After adding PBS, the absorption spectrum of AuNPs was broad and featureless, indicating that AuNPs aggregated as shown in **Figure 3.6 a.** After the aptamer was introduced, the absorption spectrum was restored close to that of AuNPs in water which indicated that aptamers can protect AuNPs from aggregation [35]. The amount of aptamer was investigated. Aptamers at low concentration do not adequately stabilize AuNPs in PBS. However, if the aptamer concentration is too high, SDM could bind with extra aptamer and the detection is not sensitive. Experimental results showed that the optimal concentration of aptamer was 1 μM. UV-Vis absorption spectrum analysis was performed to check whether the SDM was bound to the aptamer in the system. As shown in **Figure 3.6 b,** without SDM, the absorption of AuNPs was high and narrow, indicating the dispersion of AuNPs. As the concentration of SDM increased, the intensity of plasmon

absorption decreased. Moreover, the absorption spectra were broader and shifted to a high value, indicating aggregation of AuNPs. This phenomenon can be explained by the binding of SDM and aptamer, and the remaining SBA was not enough to stabilize AuNPs in PBS.

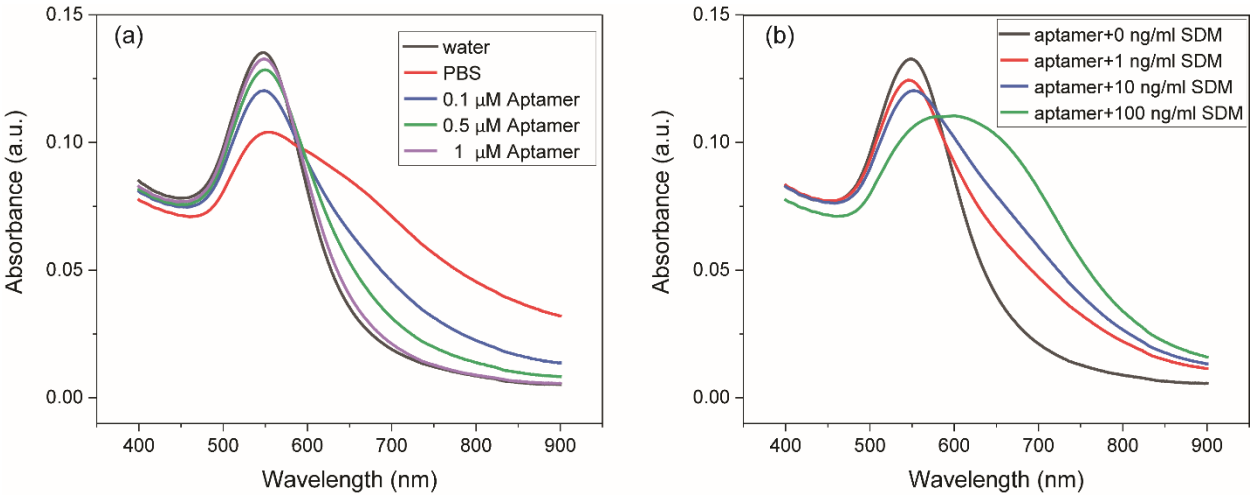

Figure 3.6 (a) UV−Vis spectra of AuNPs in water, PBS and various concentrations of aptamer in PBS; **(b)** UV−Vis spectra of AuNPs solution in 1 μM aptamer (in PBS) and various concentration of sulfadimethoxine (in water).

As shown in **Figure 3.7**, the CL signal increased with increasing concentration of SDM. When SDM concentration changed from 0.01 to 1000 ng/ml, there was a linear relationship between the CL signal and the logarithm of the SDM concentration. The linear regress equation can be expressed as y = 1955.5 x + 34513.7 (y is the intensity of CL signal, x is the logarithm of SDM concentration) with a correlation coefficient of 0.9986 (n = 3, m = 5). The detection limit that is taken to be three times the standard derivation in the blank solution (29302.6 ± 179.5) was found to be 0.004 ng/ml. To evaluate the applicability of the developed method, 50 ng/ml SDM was spiked in water and the recovery was 96.8% (48.42 ng/ml). Compared with other reported work for determination of SDM, this approach has wider linearity range and higher sensitivity [2, 36, 37]. The wider linear range could be attributed to the huge catalytic difference between dispersed AuNPs and aggregated AuNPs. The *m*-carboxyl luminol with higher CL quantum yield further enhanced the CL signal difference [12]. Moreover, the water-soluble *m*-carboxyl luminol can be more uniformly dissolved in the solution, therefore, the signal was more stable with lower standard deviation, which leads to the lower limit of detection.

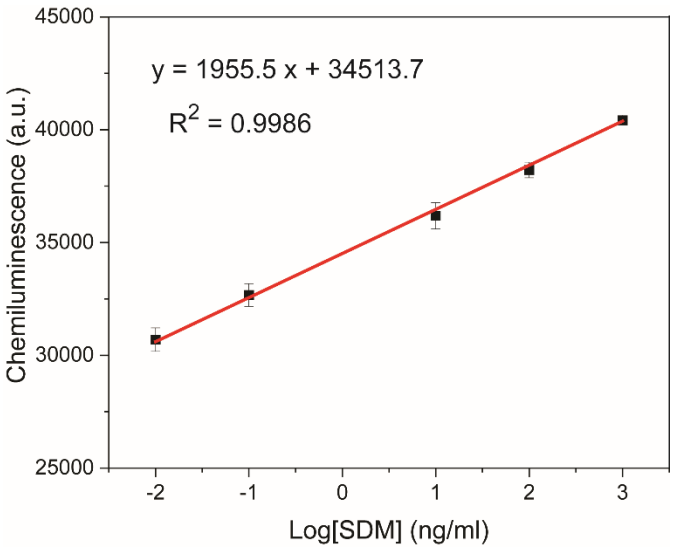

Figure 3.7 The calibration plots of chemiluminescence intensity versus the logarithm of sulfadimethoxine concentration using AuNPs catalyzed chemiluminescence with *m*-carboxy luminol in a homogeneous aptamer-based assay in a flow-based 3D mixer chip, n = 3.

3.4 Conclusions

In this paper, a 3D microfluidic flow-injection platform with AuNPs-catalyzed and *m*-carboxy luminol enhanced chemiluminescence for highly sensitive aptamer-based homogeneous assays was developed. The novel detection platform was used for the specific detection of SDM and yielded a stunning dynamic range over 5 orders of magnitude (0.01 - 1000 ng/ml) and a limit of detection of 4 pg/ml. This new detection concept not only outperforms other methods for SDM detection, but can be suggested as a new flow-injection strategy for aptamer-based rapid and cost efficient analysis in environmental monitoring where antibiotics often occur at concentrations from ng/l to µg/l [38]. The more water-soluble *m*-carboxy luminol was used for the first time for AuNPs-catalyzed CL with high sensitivity and reliable results. As it can be applied in physiological conditions, *m*-carboxy luminol can be used for the detection of analyses in complex matrices with purification systems [39].

Author Contributions

Conceptualization of the project was done by YW and MS. The manuscript was written by YW. Experiments were performed by YW under supervision of MS. MS, reviewed the manuscript,

acquired funding and supervised YW. SR and AJB reviewed the manuscript. All authors have given approval to the final version of the manuscript.

Conflicts of interest

There are no conflicts to declare.

Acknowledgements

We gratefully thank China Scholarship Council (CSC) for the funding. Special thanks to Roland Hoppe from workshop for the fabrication of the PMMA carrier.

3.5 References

1. Zahra, Q.U.A., Z. Luo, R. Ali, M.I. Khan, F. Li, and B. Qiu, *Advances in Gold Nanoparticles-Based Colorimetric Aptasensors for the Detection of Antibiotics: An Overview of the Past Decade.* Nanomaterials, 2021. **11**(4).
2. Chen, X.X., Z.Z. Lin, C.Y. Hong, Q.H. Yao, and Z.Y. Huang, *A dichromatic label-free aptasensor for sulfadimethoxine detection in fish and water based on AuNPs color and fluorescent dyeing of double-stranded DNA with SYBR Green I.* Food Chem., 2020. **309**: p. 125712.
3. Cliquet, P., E. Cox, W. Haasnoot, E. Schacht, and B.M. Goddeeris, *Extraction procedure for sulfachloropyridazine in porcine tissues and detection in a sulfonamide-specific enzyme-linked immunosorbent assay (ELISA).* Anal. Chim. Acta, 2003. **494**(1-2): p. 21-28.
4. Bach, C., V. Boiteux, J. Hemard, A. Colin, C. Rosin, J.F. Munoz, and X. Dauchy, *Simultaneous determination of perfluoroalkyl iodides, perfluoroalkane sulfonamides, fluorotelomer alcohols, fluorotelomer iodides and fluorotelomer acrylates and methacrylates in water and sediments using solid-phase microextraction-gas chromatography/mass spectrometry.* J. Chromatogr. A, 2016. **1448**: p. 98-106.
5. Qin, Y., F. Jatamunua, J. Zhang, Y. Li, Y. Han, N. Zou, J. Shan, Y. Jiang, and C. Pan, *Analysis of sulfonamides, tilmicosin and avermectins residues in typical animal matrices with multi-plug filtration cleanup by liquid chromatography-tandem mass spectrometry detection.* J. Chromatogr. B Analyt. Technol. Biomed. Life Sci., 2017. **1053**: p. 27-33.
6. Li, N., D. Liu, and H. Cui, *Metal-nanoparticle-involved chemiluminescence and its applications in bioassays.* Anal. Bioanal. Chem., 2014. **406**(23): p. 5561-71.
7. Duan, C., H. Cui, Z. Zhang, B. Liu, J. Guo, and W. Wang, *Size-Dependent Inhibition and Enhancement by Gold Nanoparticles of Luminol−Ferricyanide Chemiluminescence.* J. Phys. Chem. C, 2007. **111**(12): p. 4561-4566.

8. Cui, H., J.-Z. Guo, N. Li, and L.-J. Liu, *Gold Nanoparticle Triggered Chemiluminescence between Luminol and AgNO3.* J. Phys. Chem. C, 2008. **112**(30): p. 11319-11323.

9. Karabchevsky, A., A. Mosayyebi, and A.V. Kavokin, *Tuning the chemiluminescence of a luminol flow using plasmonic nanoparticles.* Light Sci. Appl., 2016. **5**(11): p. e16164-e16164.

10. Yeh, Y.-C., B. Creran, and V.M. Rotello, *Gold nanoparticles: preparation, properties, and applications in bionanotechnology.* Nanoscale, 2012. **4**(6): p. 1871-1880.

11. Wang, Y. and M. Seidel, *Integration of 3D Hydrodynamic Focused Microreactor with Microfluidic Chemiluminescence Sensing for Online Synthesis and Catalytical Characterization of Gold Nanoparticles.* Sensors (Basel), 2021. **21**(7).

12. Mayer, M., S. Takegami, M. Neumeier, S. Rink, A. Jacobi von Wangelin, S. Schulte, M. Vollmer, A.G. Griesbeck, A. Duerkop, and A.J. Baeumner, *Electrochemiluminescence Bioassays with a Water-Soluble Luminol Derivative Can Outperform Fluorescence Assays*. Angew. Chem. Int. Ed. Engl., 2018. **57**(2): p. 408-411.

13. Iranifam, M., *Revisiting flow-chemiluminescence techniques: pharmaceutical analysis.* Luminescence, 2013. **28**(6): p. 798-820.

14. Lee, C.-Y. and L.-M. Fu, *Recent advances and applications of micromixers.* Sens. Actuators B Chem., 2018. **259**: p. 677-702.

15. Lee, C.Y., C.L. Chang, Y.N. Wang, and L.M. Fu, *Microfluidic mixing: a review.* Int. J. Mol. Sci., 2011. **12**(5): p. 3263-87.

16. Bayareh, M., M.N. Ashani, and A. Usefian, *Active and passive micromixers: A comprehensive review.* Chem Eng Process, 2020. **147**.

17. Raza, W., S. Hossain, and K.Y. Kim, *A Review of Passive Micromixers with a Comparative Analysis.* Micromachines (Basel), 2020. **11**(5).

18. Lee, C.-Y., W.-T. Wang, C.-C. Liu, and L.-M. Fu, *Passive mixers in microfluidic systems: A review.* Chem. Eng. J., 2016. **288**: p. 146-160.

19. Clark, J., M. Kaufman, and P.S. Fodor, *Mixing Enhancement in Serpentine Micromixers with a Non-Rectangular Cross-Section.* Micromachines (Basel), 2018. **9**(3).

20. Tsai, C.D. and X.Y. Lin, *Experimental Study on Microfluidic Mixing with Different Zigzag Angles.* Micromachines (Basel), 2019. **10**(9).

21. Chen, X. and T. Li, *A novel passive micromixer designed by applying an optimization algorithm to the zigzag microchannel.* Chem. Eng. J., 2017. **313**: p. 1406-1414.

22. Du, Y., Z. Zhang, C. Yim, M. Lin, and X. Cao, *Evaluation of Floor-grooved Micromixers using Concentration-channel Length Profiles.* Micromachines, 2010. **1**(1): p. 19-33.

23. Taheri, R.A., V. Goodarzi, and A. Allahverdi, *Mixing Performance of a Cost-effective Split-and-Recombine 3D Micromixer Fabricated by Xurographic Method.* Micromachines (Basel), 2019. **10**(11).

24. Raza, W., S. Hossain, and K.-Y. Kim, *Effective mixing in a short serpentine split-and-recombination micromixer.* Sens. Actuators B Chem., 2018. **258**: p. 381-392.

25. Chen, X. and Z. Zhao, *Numerical investigation on layout optimization of obstacles in a three-dimensional passive micromixer.* Anal. Chim. Acta, 2017. **964**: p. 142-149.

26. Wang, D., D. Ba, K. Liu, M. Hao, Y. Gao, Z. Wu, and Q. Mei, *A Numerical Research of Herringbone Passive Mixer at Low Reynold Number Regime.* Micromachines (Basel), 2017. **8**(11).

27. Zhang, J. and X. Luo, *Mixing Performance of a 3D Micro T-Mixer with Swirl-Inducing Inlets and Rectangular Constriction.* Micromachines (Basel), 2018. **9**(5).

28. Afzal, A. and K.-Y. Kim, *Passive split and recombination micromixer with convergent–divergent walls.* Chem. Eng. J., 2012. **203**: p. 182-192.

29. Islam, M., R. Natu, and R. Martinez-Duarte, *A study on the limits and advantages of using a desktop cutter plotter to fabricate microfluidic networks.* Microfluid. Nanofluid., 2015. **19**(4): p. 973-985.

30. Yan, J., Y. Huang, C. Zhang, Z. Fang, W. Bai, M. Yan, C. Zhu, and A. Chen, *Aptamer based photometric assay for the antibiotic sulfadimethoxine based on the inhibition and reactivation of the peroxidase-like activity of gold nanoparticles.* Microchim Acta, 2016. **184**(1): p. 59-63.

31. Mehlhorn, A., P. Rahimi, and Y. Joseph, *Aptamer-Based Biosensors for Antibiotic Detection: A Review.* Biosensors (Basel), 2018. **8**(2).

32. Sun, Y. and J. Lu, *Chemiluminescence-based aptasensors for various target analytes.* Luminescence, 2018. **33**(8): p. 1298-1305.

33. Qi, Y. and B. Li, *A sensitive, label-free, aptamer-based biosensor using a gold nanoparticle-initiated chemiluminescence system.* Chemistry (Easton), 2011. **17**(5): p. 1642-8.

34. Song, K.M., E. Jeong, W. Jeon, H. Jo, and C. Ban, *A coordination polymer nanobelt (CPNB)-based aptasensor for sulfadimethoxine.* Biosens. Bioelectron., 2012. **33**(1): p. 113-9.

35. Song, K.-M., M. Cho, H. Jo, K. Min, S.H. Jeon, T. Kim, M.S. Han, J.K. Ku, and C. Ban, *Gold nanoparticle-based colorimetric detection of kanamycin using a DNA aptamer.* Anal. Biochem., 2011. **415**(2): p. 175-181.

36. Bai, Z., Y. Chen, F. Li, Y. Zhou, H. Yin, and S. Ai, *Electrochemical aptasensor for sulfadimethoxine detection based on the triggered cleavage activity of nuclease P1 by aptamer-target complex.* Talanta, 2019. **204**: p. 409-414.

37. Chen, X.X., Z.Z. Lin, C.Y. Hong, H.P. Zhong, Q.H. Yao, and Z.Y. Huang, *Label-Free Fluorescence-Based Aptasensor for the Detection of Sulfadimethoxine in Water and Fish.* Appl. Spectrosc., 2019. **73**(3): p. 294-303.

38. Roose-Amsaleg, C. and A.M. Laverman, *Do antibiotics have environmental side-effects? Impact of synthetic antibiotics on biogeochemical processes.* Environ. Sci. Pollut. Res. Int., 2016. **23**(5): p. 4000-12.

39. Guo, Y., W. Wei, Y. Zhang, Y. Dai, W. Wang, and A. Wang, *Determination of sulfadimethoxine in milk with aptamer-functionalized Fe3 O4 /graphene oxide as magnetic solid-phase extraction adsorbent prior to HPLC.* J. Sep. Sci., 2020. **43**(17): p. 3499-3508.

General conclusion and outlook

This thesis contains three main parts. The first part aims to propose a simple, cheap, fast, and versatile way to fabricate 3D microfluidic chips based on the laminated method. A low-cost cutting plotter was used to cut PMMA sheets and double-sided PSA tapes. Then the layers were assembled manually by a roller with moderate pressure. It is a strategy to develop highly flexible multilayered microfluidic chips without masks, molds, and cleanroom requirements due to the absence of lithographic methods [1].

This fabrication protocol was used to generate a 3D hydrodynamic focusing microreactor for the synthesis of AuNPs. It could be shown that reproducible spherical colloidal AuNPs were synthesized. Compared with a 2D microreactor, the sheath stream can focus the central flow and avoid fouling. The concept of flow-based modulation of size and properties for AuNPs was implemented by changing synthesized parameters. It was an improvement compared to conventional batch synthesis, where the properties of nanoparticles vary from batch to batch. The 3D hydrodynamic focusing microreactor has the potential to be applied in other syntheses and reactions. Also, the microfluidic reactor makes it possible to do online synthesis and characterizing or detection [2]. The proposed fabricating method provides another option for research institutes where specialized microfabrication equipment is unavailable. The fabrication method can be used to create 3D multilayer laminated microfluidic chips. One microfluidic chip can be fabricated in minutes, and the design is easy to be modified. The only needed tool is a cutting plotter. Although limited to the resolution of cutting plotter (25 µm), more sophisticated microanalytical systems are not suitable to fabricated with this method, it still can be applied in the area of diagnostics, environment and food analysis where complex matrices may clog microfluidic channels.

In the second part of this dissertation, for the first time, online synthesis using a 3D hydrodynamic focusing microreactor was combined with microfluidic CL sensing. The catalytic properties of AuNPs continuously produced by a single-phase reaction can be directly characterized by the CL reaction of luminol and NaOCl in a microfluidic channel with a CCD camera. AuNPs were synthesized using glucose as a reducing agent and stabilizer at room temperature. Therefore, the properties of AuNPs were easily controlled by changing the concentration of reagents to obtain the best catalytic activity in enhanced luminol-NaOCl CL reaction. The CL signal was 171 times

enhanced using synthesized AuNPs with optimized parameters. This method provides a good method to obtain the optimal synthesis parameters of AuNPs for specific CL applications. This continuous synthesis method with microreactor has the potential to couple online with other analytical instruments, such as inductively coupled plasma mass spectrometer (ICP-MS) and flow-based UV-Vis spectrometers.

The AuNPs synthesized under optimal conditions were stable for at least one month without adding other stabilizers. However, after adding an amount of salt, AuNPs aggregated with an enhanced catalytic activity which induced higher CL signal. On the contrary, the CL signal was quenched by molecules that can bind on the surface of AuNPs. For example, the CL signal was inhibited by glutathione. A concentration-dependent quantification of glutathione could be shown. The synthesized AuNPs with excellent catalytic activities can replace enzymes and be applied to flow-based CL microarrays [3, 4]. The other option is the labeling of AuNPs with luminol for ultra-sensitive chemical analysis [5]. The property that AuNPs catalyzed CL reaction can be quenched by some molecules with specific functional groups can also be used in analytical applications [6]. The synthesized AuNPs can act as labels which bind with recognizing molecules such as antibodies and aptamers for specific detection [7, 8].

With the need for efficient mixing in a microfluidic platform and the application of specific detection, the AuNPs catalyzed CL sensor system with aptamer was applied in a newly developed 3D mixer in the third part of this thesis. Different mixing patterns were investigated. As a result, a five-layer laminated 3D mixer was developed for CL measurement, and the structure was optimized to achieve better mixing and signal recording. The 3D mixer was an essential part of the microfluidic platform to improve mixing efficiency and save time, and it can also be applied in other flow-based systems.

Furthermore, the performance of standard luminol and its more hydrophilic derivative *m*-carboxy luminol was investigated in the developed 3D mixer, and *m*-carboxy luminol provided a 10-fold signal enhancement and repeatable results. A certain amount of salt caused aggregation of AuNPs with enhanced CL signal, and aptamers interacting with AuNPs and inhibiting the aggregation showed the successful application of aptamers in the platform. Finally, the 3D microfluidic flow-injection platform with AuNP-catalyzed and *m*-carboxy luminol enhanced CL for highly sensitive aptamer-based homogeneous assays was developed. The platform was successfully applied for the

detection of sulfadimethoxine (SDM) with its specific aptamer. A linear relationship between CL signal and the logarithm of SDM concentration was obtained in the range of 0.01 - 1000 ng/ml with the detection limit of 0.004 ng/ml. This new detection concept not only outperforms other methods for SDM detection but can be suggested as a new flow-injection strategy for aptamer-based rapid and cost-efficient analysis in environmental monitoring where antibiotics often occur at concentrations from ng/l to µg/l [9]. The water-soluble *m*-carboxy luminol was used for the first time in AuNPs-catalyzed CL and showed reliable results. This combination of *m*-carboxy luminol and AuNPs-catalyzed CL has a great potential for other aptamer-based sensor systems with high sensitivity and a simple treatment process [10]. As it can be applied in physiological conditions, the platform with *m*-carboxy luminol can also be applied to detect analytes in complex matrices in combination with purification systems like solid phase extraction [11].

References

1. Bemetz, J., A. Wegemann, K. Saatchi, A. Haase, U.O. Hafeli, R. Niessner, B. Gleich, and M. Seidel, *Microfluidic-Based Synthesis of Magnetic Nanoparticles Coupled with Miniaturized NMR for Online Relaxation Studies.* Anal. Chem., 2018. **90**(16): p. 9975-9982.
2. Pahl, M., M. Mayer, M. Schneider, D. Belder, and K.R. Asmis, *Joining Microfluidics with Infrared Photodissociation: Online Monitoring of Isomeric Flow-Reaction Intermediates.* Anal. Chem., 2019. **91**(5): p. 3199-3203.
3. Gopfert, L., M. Elsner, and M. Seidel, *Isothermal haRPA detection of blaCTX-M in bacterial isolates from water samples and comparison with qPCR.* Anal. Methods, 2021. **13**(4): p. 552-557.
4. Meyer, V.K., C.V. Chatelle, W. Weber, R. Niessner, and M. Seidel, *Flow-based regenerable chemiluminescence receptor assay for the detection of tetracyclines.* Anal. Bioanal. Chem., 2020. **412**(14): p. 3467-3476.
5. Syed, L.U., L.Z. Swisher, H. Huff, C. Rochford, F. Wang, J. Liu, J. Wu, M. Richter, S. Balivada, D. Troyer, and J. Li, *Luminol-labeled gold nanoparticles for ultrasensitive chemiluminescence-based chemical analyses.* Analyst, 2013. **138**(19): p. 5600-9.
6. Yang, D., Y. He, Y. Sui, and F. Chen, *Determination of catechol in water based on gold nanoclusters-catalyzed chemiluminescence.* J. Lumin., 2017. **187**: p. 186-192.
7. Huang, Y., L. Gao, and H. Cui, *Assembly of Multifunctionalized Gold Nanoparticles with Chemiluminescent, Catalytic, and Immune Activity for Label-Free Immunoassays.* ACS Appl. Mater. Interfaces, 2018. **10**(20): p. 17040-17046.

8. Yao, L.-Y., X.-Q. Yu, Y.-J. Zhao, and A.-P. Fan, *An aptamer-based chemiluminescence method for ultrasensitive detection of platelet-derived growth factor by cascade amplification combining rolling circle amplification with hydroxylamine-enlarged gold nanoparticles.* Anal. Methods, 2015. **7**(20): p. 8786-8792.

9. Roose-Amsaleg, C. and A.M. Laverman, *Do antibiotics have environmental side-effects? Impact of synthetic antibiotics on biogeochemical processes.* Environ. Sci. Pollut. Res. Int., 2016. **23**(5): p. 4000-12.

10. Shaban, S.M. and D.H. Kim, *Recent Advances in Aptamer Sensors.* Sensors (Basel), 2021. **21**(3).

11. Guo, Y., W. Wei, Y. Zhang, Y. Dai, W. Wang, and A. Wang, *Determination of sulfadimethoxine in milk with aptamer-functionalized Fe3 O4 /graphene oxide as magnetic solid-phase extraction adsorbent prior to HPLC.* J. Sep. Sci., 2020. **43**(17): p. 3499-3508.

Appendix

Appendix A1 Supplementary material for Chapter 1

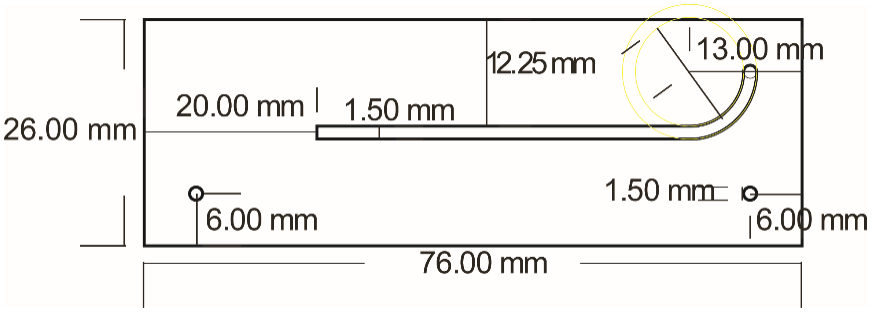

Figure S1.1 Main dimensions of the microreactor.

The effect of flow rates on the focus stream

There were two sheath flows, and the flow rates were the same. The sum of these two flow rates was defined as flow rate (FR) of sheath flow. By variation of both flow rates of sheath flow and central flow, the profile of the focused stream could be adjusted. The flow profile was made visible by using blue dye for the central stream and water for the sheath streams. The profiles of focus streams for varied flow rates are shown in **Figure S2.1**. With the same flow rate ratio between sheath streams and central stream (**Figure S2.1 a** and **c**), the central stream was slightly focused for a stream flow rate of 5 µl/s and it was focused to a line by a stream flow rate of 50 µl/s. For the same central flow rate of 0.5 µl/s (**Figure S2.1 a** and **b**), the one with higher sheath flow rate was more focused. It can be concluded that increasing the flow rate of the sheath stream made the central stream more focused. Also, higher flow rates of both streams with the same flow rate ratio led to a narrow focus stream. The microfluidic reactor can withstand a maximum total flow rate of 300 µl/s which is applicable to most applications [1].

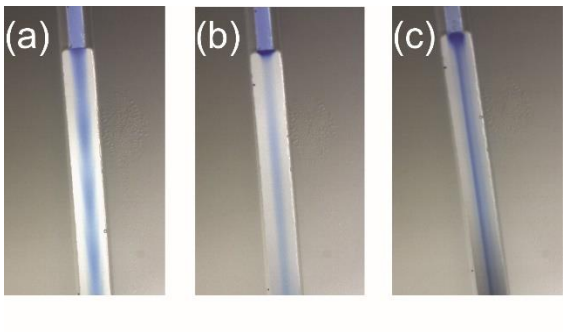

Figure S1.2 The profile of the focus stream with different flow rates: **(a)** central stream 0.5 µl/s, sheath streams 5 µl/s; **(b)** central stream 0.5 µl/s, sheath streams 20 µl/s; **(c)** central stream 5 µl/s, sheath stream 50 µl/s.

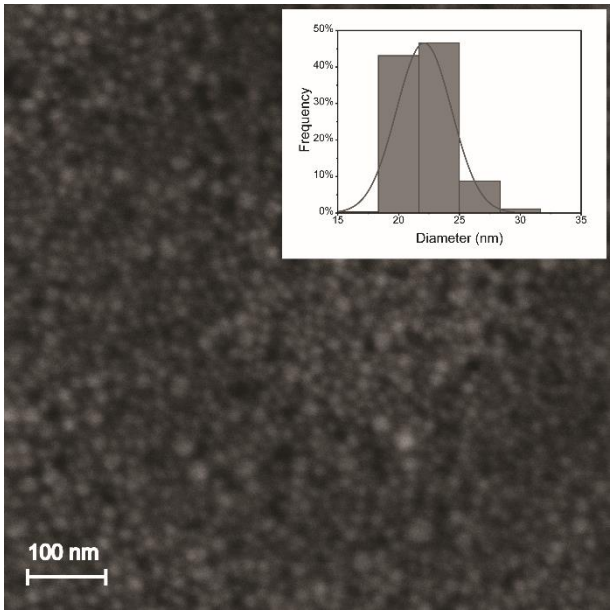

Figure S1.3 SEM image of AuNPs synthesized at pH = 8.46 with 20 mM AA, 1 mM $HAuCl_4$, 1% PVP and FR 10-3. Histograms with the respective particle size distributions and the percentage are included as inset.

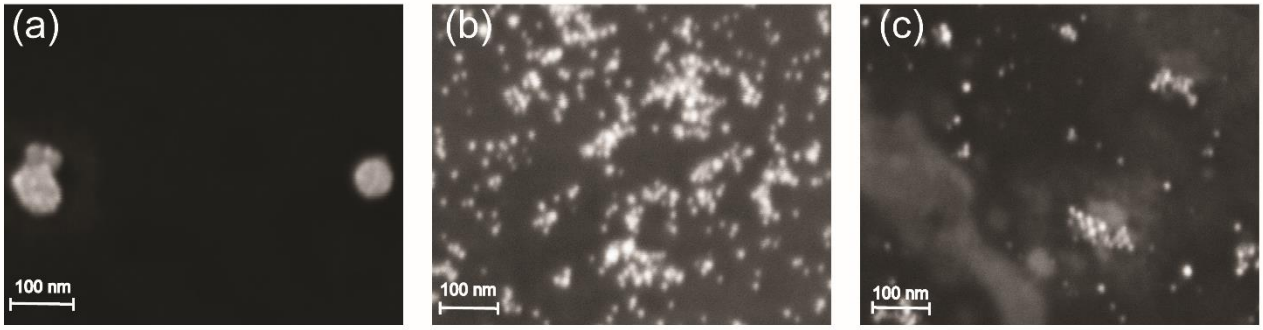

Figure S1.4 SEM images of AuNPs synthesized with 20 mM AA, 1 mM $HAuCl_4$, 1% PVP and FR 10-5 at different pH. (a) pH 4.30, (b) pH 9.34, (c) pH 11.30.

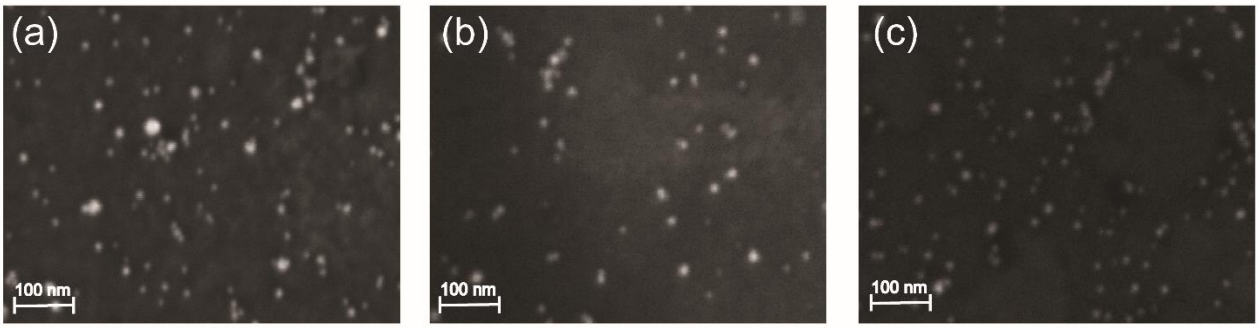

Figure S1.5 SEM images of AuNPs synthesized with 20 mM AA (pH 9.34), 1 mM $HAuCl_4$, 1% PVP and different FR. (a) FR10-4, (b) FR 10-8, (c) FR 10-16.

Reference

1. Mark, D., S. Haeberle, G. Roth, F. von Stetten, and R. Zengerle, *Microfluidic lab-on-a-chip platforms: requirements, characteristics and applications.* Chem. Soc. Rev., 2010. **39**(3): p. 1153-82.

Appendix A2 Supplementary material for Chapter 2

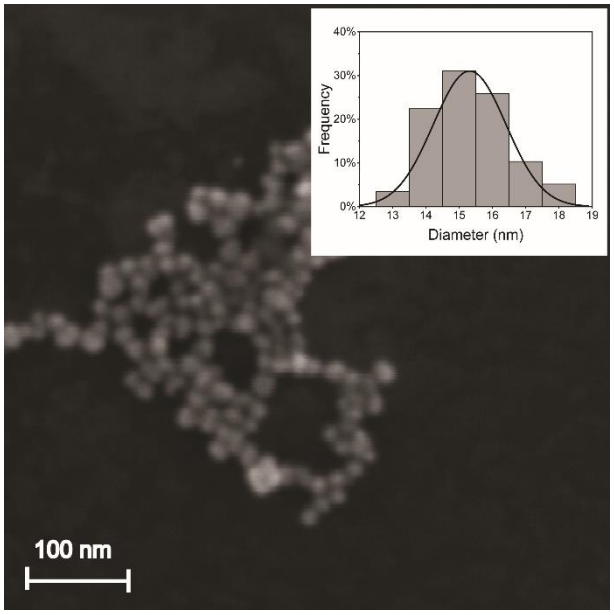

Figure S2.1 SEM images of synthesized AuNPs with optimal synthesis conditions. Histograms with the respective particle size distributions and the percentage are included as inset.

Appendix A3 Supplementary material for Chapter 3

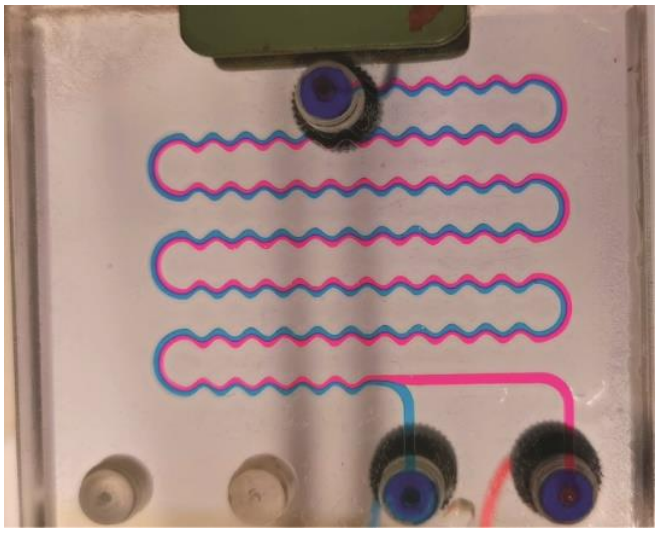

Figure S3.1 Image of 2D mixing chip with dyes showing flow profile.

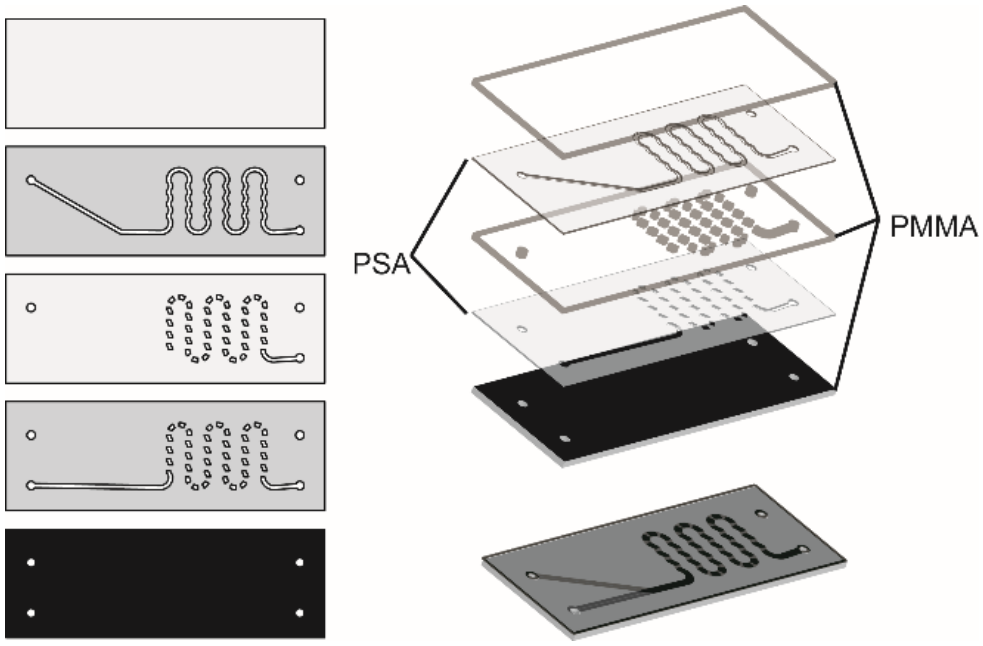

Figure S3.2 Structure of 3D micromixer for chemiluminescence.

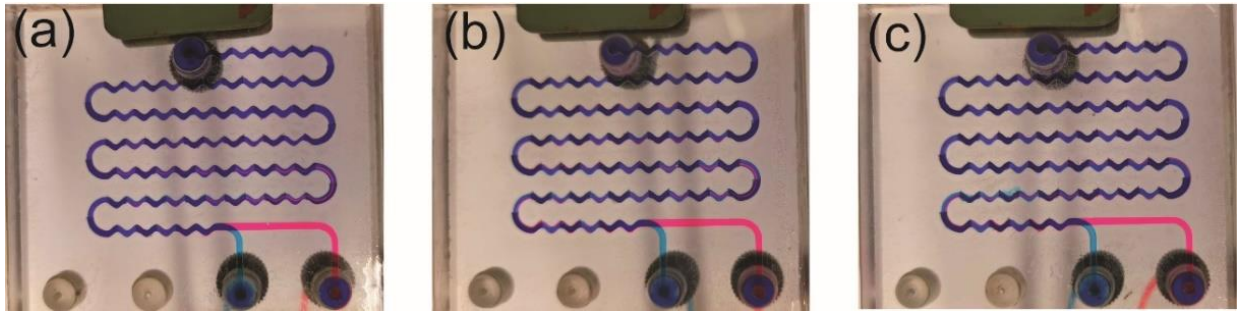

Figure S3.3 Images of 3D mixer with different thickness of central PMMA layer: (**a**) 0.08 mm; (**b**) 0.17 mm; (**c**) 0.25 mm.

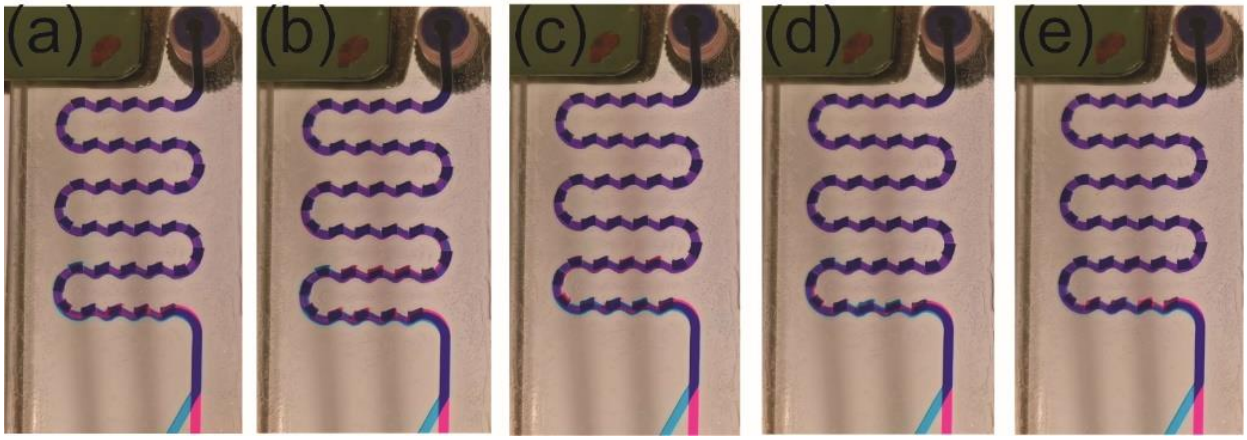

Figure S3.4 Mixing with different flow rate: (**a**) 5 ml/h; (**b**) 10 ml/h; (**c**) 20 ml/h; (**d**) 30 ml/h; (**e**) 40 ml/h.

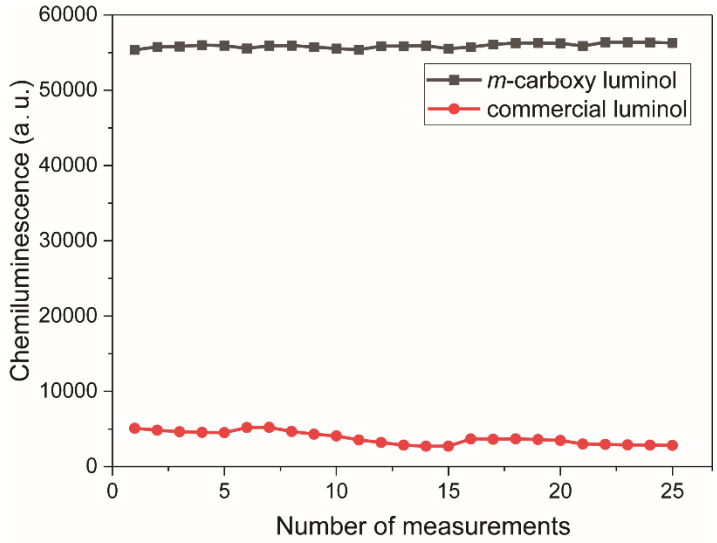

Figure S3.5 Comparison of chemiluminescence signal in 3D mixer for commercial luminol and m-carboxy luminol. The concentration of both luminophores was 0.5 mM (pH 9.6) mixed with 1% NaOCl. The measurement was repeated 25-times, respectively.

Pictures were recorded by CCD camera when different concentrations of SDM were mixed with 1 μM aptamer in PBS, synthesized AuNPs, and CL reagents. The results were shown in **Figure S3.6**. Since the dispersed AuNPs have excellent catalytic activity under the optimal synthesis parameters, the mixture without SDM also generates strong light signals of about 30,000 a.u.. Therefore, the naked eye cannot distinguish the difference in signal strength because all signals were very high. Signals were subtracted by 30,000 a.u. to make the difference easy to distinguish. As the signal was an average value, there were still some white pixels whose value exceed 30,000 a.u. left. The left signals were doubled to enhance the difference. In this case, it can be seen that the CL signal increases with the increase of the SDM concentration. For further analysis with software, values of original pictures were used.

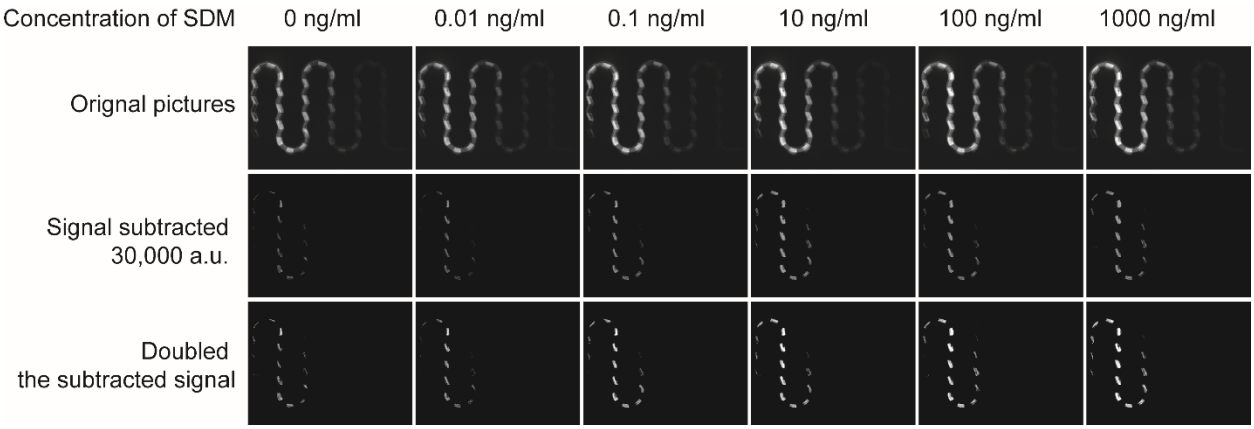

Figure S3.6 Pictures recorded by the camera with different concentrations of SDM (0 ng/ml to 1000 ng/ml).

Abbreviations

AuNPs	Gold nanoparticles
CL	Chemiluminescence
SEM	Scanning electron microscope
SPR	Surface plasmon resonance
PMMA	Poly (methyl methacrylate)
PVP	Polyvinylpyrrolidone
LSP	Localized surface plasmon
SERS	Surfaced enhanced Raman scattering
AA	Ascorbic acid
CTAB	Cetrimonium bromide
PEG	Polyethylene glycol
UV/Vis	Ultraviolet/Visible light
DLS	Dynamic light scattering
PDI	Polydispersity index
PTFE	Polytetrafluorethylen
NaOCl	Sodium Hypochlorite
$NaBH_4$	Sodium borohydride
TOAB	Tetraoctylammonium bromide

9-BBN	9-borabicyclo[3.3.1]nonane
PTS	Poly[2-(3-thienyl)ethyloxy-4-butylsulfonate] sodium salt
PAA	Poly(acrylic acid)
DMSO	Dimethyl sulfoxide
mPEG-SH	Thiolated polyethylene glycol
TCPO	(2,4,6-trichlorophenyl) oxalate
CRP	C-reactive protein
SDM	Sulfadimethoxine
SBA	Sulfadimethoxine binding aptamer
PBS	Phosphate buffered saline